Integrated Navigation Architecture Analysis for Moon and Mars Exploration

by

Thomas Chabot

Diplôme d'Ingénieur de l'Ecole Centrale des Arts et Manufactures, 2003

Submitted to the Department of Aeronautics and Astronautics
in partial fulfillment of the requirements for the degree of

Master of Science in Aeronautics and Astronautics

at the

MASSACHUSETTS INSTITUTE OF TECHNOLOGY

June 2005

Author .....
Department of ~~Aeronautics~~ and Astronautics
June 2005

Certified by.....
Jonathan P. How
Associate Professor
Thesis Supervisor

Accepted by .....
Jaime Peraire
Professor of Aeronautics and Astronautics
Chair, Committee on Graduate Students

Integrated Navigation Architecture Analysis for Moon and Mars Exploration

by

Thomas Chabot

Submitted to the Department of Aeronautics and Astronautics
on June 2005, in partial fulfillment of the
requirements for the degree of
Master of Science in Aeronautics and Astronautics

Abstract

The new solar system exploration objectives announced in January 2004 have the goal of sending humans back to the Moon by the year 2020 in preparation for human exploration of Mars. Advanced, but cost effective, surface navigation and communication capabilities are required to support these new exploration objectives. In response to this need, a set of three Navigation/Communication architectures have been designed: *Minimalist*, *Simple*, and *Performance*, as well as several augmentation options. The design and refinement of these architectures was performed using numerous models and tools developed for this work. A unique feature of the analysis in this thesis was that the architectures considered combine different navigation assets (onboard, on-surface and on-orbit). The three main Navigation/Communication architectures were then evaluated and compared using several metrics, such as navigation coverage, accuracy and operability, communication metrics, and mass. Based on this analysis we recommend the initial deployment of the *Simple* architecture for surface exploration of the Moon and Mars with a gradual accretion of assets and possibly transition to the *Performance* architecture. A specific combination of onboard and vision-based sensors is recommended as the fundamental navigation equipment.

In addition to this navigation study, a control-based analysis of formation flying dynamic models around the libration point L_2 of the Sun-Earth system is also presented. The objective of this research was to assess the quality of different dynamical models of the relative motion of two spacecraft in orbit around Sun-Earth L_2. This was done using open-loop simulations to investigate the intrinsic fidelity of each model and closed-loop simulations to evaluate the impact of modeling errors on fuel costs. The conclusion from this analysis is that the more sophisticated models give appreciable better closed-loop performance, and that the difference appears to be sufficient to justify the additional effort required to implement them on-line.

Thesis Supervisor: Jonathan P. How
Title: Associate Professor

Acknowledgments

First I would like to thank my advisor, Prof. Jonathan How, for his constant drive for intellectual rigor and his helpful insights and advice. The company of my labmates at the Aerospace Controls Lab was also very much appreciated, especially during the last nights spent writing this thesis.

I would like to thank my project fellows of the information team Steve, François, Brendan and Gokhan for these cheerful Fridays evenings. I would like especially to thank Gokhan for his constant help throughout this year, from the start of the CE&R project to the completion of this thesis.

I would like to thank my family back in France for their love and support during these past two years, even though the ocean's presence made my trips back home too unfrequent.

Finally I would like to thank all the people that made my stay at MIT and in Boston such an unforgettable experience, and especially the French community. So, in random order (I swear) and maybe with some unintended (I swear again) omissions, I thank Jean-Marie, Amandine, Serge, Antoine, Jeff, Rick, Pierre, Riadh, Guillaume, Adrien, J-B, Théo, Olivier, Henry, François, Célia, François, Jérome, Camille, Claire, Greg, Jeff, and all the other members of the French crew that made of Boston their second home, either for a few months or a few years.

This research was funded in part under NASA Contract P.O.# DL-H-551000 *Concept Exploration and Refinement*, NASA Grant NAG5-10440 *Agent Based Software for the Autonomous Control of Formation Flying Spacecraft*, and NASA Glenn Research Center Grant NAG3-2839 *Decentralized Relative Navigation Algorithms.*

Contents

List of Figures

List of Tables

Chapter 1

Introduction

1.1 Context of the Research: the CE&R Project

In January 2004, President Bush presented a new vision for space exploration. As stated in [1], "the fundamental goal of this vision is to advance U.S. scientific, security, and economic interests through a robust space exploration program. In support of this goal, the United States will:

- Implement a sustained and affordable human and robotic program to explore the solar system and beyond;
- Extend human presence across the solar system, starting with a human return to the Moon by the year 2020, in preparation for human exploration of Mars and other destinations;
- Develop the innovative technologies, knowledge, and infrastructures both to explore and to support decisions about the destinations for human exploration;
- Promote international and commercial participation in exploration to further U.S. scientific, security, and economic interests."

In response to this new vision, the National Aeronautics and Space Administration (NASA) released the Concept Exploration and Refinement (CE&R) Broad Agency Announcement and a team comprised of MIT faculty, Draper Laboratory technical Staff, and students received a contract to do the necessary studies to support this new

space vision. Due to funding restrictions, the development of separate space exploration systems for both the Moon and Mars is not possible. Therefore a "Mars-back" approach to lunar exploration was adopted that first designed a Martian exploration system and then applied/modified it to explore the Moon [2]. The MIT/Draper Lab group was divided into four teams: Value delivery, Transportation, Surface Exploration, and Information. The work presented in this thesis was done as part of the Information and Surface Exploration teams.

1.2 Research Objectives

The exploration of the surface of the Moon and Mars will likely involve long-range traverses from the main base station [6]. Depending on the specific activity (e.g. base setup, scientific exploration, drilling, etc.), different levels of positioning accuracy will need to be available to the astronauts. The astronauts need also to be able to communicate to the main base station and to Earth. So the main objective of this research (as part of the CE&R project) was to design a set of Nav/Comm architectures that will support these exploration requirements. A unique architecture doing both navigation and communication is being looked for, as it is a way to minimize the total number of assets (and therefore their mass). Communication issues (studied by other team members) have been considered while designing the navigation architectures, and the most important points and results of the communication analysis will also be discussed in this thesis. Once developed, the Nav/Comm architectures were evaluated using various metrics: navigation coverage, accuracy and operability. Other factors, such as communication metrics and mass were analyzed by other team members . The design and evaluation of the Nav/Comm architectures were accomplished by developing models and tools for the design and analysis of the navigation infrastructure, doing trade-off studies, and then refining the various components. Throughout the study, emphasis has been put on the integration of on-orbit, on-surface, and onboard navigation assets.

1.3 Previous Work and Main Contribution

Most of the previous work about navigation for planetary surface exploration dealt separately with the different elements that will constitute the navigation architectures presented in this thesis: namely onboard sensors (inertial, celestial, odometry sensors, vision sensors), on-surface assets (surface beacons), and on-orbit assets (Nav/Comm satellites). These different types of assets will be described in more detail in Chapter 2. For the inertial sensors, much of the work focused on drift reduction of inertial sensors through error estimation [21, 22]. Some researchers also used a combination of on-board relative sensors with absolute measurements, such as sun sensor [12] or GPS [4] measurements. Many recent papers focus on the use of vision [8, 9, 10, 16, 17, 18] and combined inertial and vision-based measurements [13, 14, 15]. The exploration of the Moon using surface beacons has been investigated [25], but this work was done before the invention of GPS . Most of recent works focus indeed on the use of GPS-based surface beacons and pseudolites, either stationary on the ground [31] or mobile [32]. A number of navigation constellation studies have been done, either for the Moon [26, 30] or for Mars [27, 28, 29].

As most of the previous studies focused on one specific navigation element, the main contribution of the work presented in this thesis is the integration of these different navigation assets in a set of complete navigation architectures. These architectures also integrate communication needs, as mentioned in section 1.2.

1.4 Thesis Outline

The first chapter discusses the navigation top-level metrics, as well as the requirements and the navigation architectures designed to satisfy these requirements at different levels of performance and cost. Chapter 3 presents several analysis tools that have been developed to evaluate and refine these architectures. Chapter 4 discusses tools for the integration of different navigation techniques and sensors, as well as the main results of our analysis. In addition to this CE&R navigation study, a control-based

analysis of formation flying dynamic models around the Libration point L_2 of the Sun-Earth system is presented in Chapter 5. This analysis was done prior to the main work of this thesis.

Chapter 2

Navigation Metrics, Requirements and Architectures

In this chapter are first described the navigation (and briefly communication) metrics that have been used to evaluate the different Nav/Comm architectures that are proposed. Then the Nav/Comm requirements stated by the Surface Exploration team are described, and the Nav/Comm architectures designed to fulfill these requirements are presented.

2.1 Top-Level Metrics

In this section the main top-level metrics are discussed. Top-level metrics are the ones being used to evaluate and compare with each other the various architectures that have been developed throughout this work and are described in Section 2.3.

2.1.1 Accuracy

The accuracy metric is often defined as the degree of accordance of the calculated position to its actual value. As applied to surface navigation applications, it is assumed that the accuracy can be considered to be the root mean square of the error covariance. If the error has zero mean (which means that the position error is unbiased),

the error covariance is

$$\mathbf{P} = E[(\mathbf{x} - \hat{\mathbf{x}})(\mathbf{x} - \hat{\mathbf{x}})^T] \tag{2.1}$$

and

$$RMS = \sqrt{\sigma_{xx}^2 + \sigma_{yy}^2 + \sigma_{zz}^2} = \sqrt{P_{11} + P_{22} + P_{33}} \tag{2.2}$$

Accuracy is given in meters.

2.1.2 Coverage

The coverage is considered as being the surface area where navigation is possible to some degree. "To some degree" refers to the time a user on the surface of the planet will have to wait on average to get a position fix to a specified level of accuracy. This metric is particularly relevant to architectures which contain navigation satellites or surface beacons. This definition also leaves come degree of flexibility which allows for different degrees of coverage. As will be explained in more details in section 3.1.3, two different coverage metrics will be defined in the constellation analysis, corresponding to two different waiting times:

- $Coverage_1$: surface area where a navigation fix is possible in a time less than 1 minute (this allows for real-time or quasi-real-time navigation).
- $Coverage_2$: surface area where a navigation fix is possible in a time less than 1 hour (this corresponds to a surface area where real-time or quasi-real-time navigation are not possible, but where a navigation fix is still available after some limited wait).

These coverage metrics will be expressed as percentages of the whole surface area of the planet.

2.1.3 Operability

This metric is a measure of the ease of operation of each navigation architecture and of the effort spent by the astronauts navigating. For instance, the use of navigation

satellites can have a good operability when a navigation fix is readily available, but also a medium or bad operability if a lack of visible satellites at the time of operation requires a long waiting time. Surface beacons that may require a significant setup by the astronauts are considered to have a medium operability. On the other hand, automatic devices that are able to give position information with no user setup have good operability.

2.1.4 Communication metrics

The communication metrics considered in this study are:

- Data rate: this is the data rate, from Earth to the Moon or Mars, and from the Moon or Mars to Earth. It is being measured in Megabits per second (Mbps).
- Communication Coverage: this is the surface area where rover to base communication is possible.
- Communication Availability: this metric is the percentage of time that a communication Surface-Earth is available, either directly or through a satellite.
- Maximum Gap Time: this metric is defined as the longest surface-Earth communication black-out.

2.2 Surface Operations Requirements

The surface operations requirements are developed by the Surface Exploration team of the MIT/Draper Lab group. The set of missions that are currently being designed have very different purposes: science, human and robotic exploration, outpost setup. These very different types of surface missions lead to a wide range of requirements regarding the surface navigation architecture.

The navigation and communication requirements are roughly the same for the Moon and Mars, although the location of the base station differ. They apply to the followings of the navigation and communication metrics.

2.2.1 Navigation

For the Moon the base station is recommended by the Surface Exploration team to be placed at the South Pole, mostly for Mars-back (see section 1.1) considerations.

- Coverage: a navigation fix should be available in a $\sim$ 500km radius around the main base station on the Moon or on Mars, to allow for long-range traverses from the base station. For Mars, the base station is recommended by the Surface Exploration team to be placed on the equatorial region, whereas for the Moon the preferred location is in the South Pole region. As the line-of-sight is $\approx$ 1.8km on the Moon and $\approx$ 2.6km on Mars for a one meter high rover or antenna, these coverage requirements definitely require beyond line-of-sight capabilities.

- Accuracy: for scientific purposes themselves, the span of accuracy requirements can be quite wide as is shown in Figure 2-1

For other activities such as human and robotic physical exploration, the accuracy requirements are less stringent, with $\approx$ 100m position accuracy.

2.2.2 Communication

- Communication Coverage: the communication coverage requirement is the same as for the navigation, and corresponds to a communication coverage area of a $\approx$ 500km radius from the main base station, with 100% availability.

- Data rate: from the Moon or Mars to Earth, the data rate requirements expressed by the Surface Exploration team is of at least 10 Mbps. It corresponds to live video data rate. The data rate requirement for communication from the Earth to the Moon or Mars is of 1Mbps, and corresponds to vocal commands.

2.3 Navigation Architectures

The recommendations formulated to NASA by the Information team are expressed in a set of various navigation architectures. Each architecture is a set of various onboard,

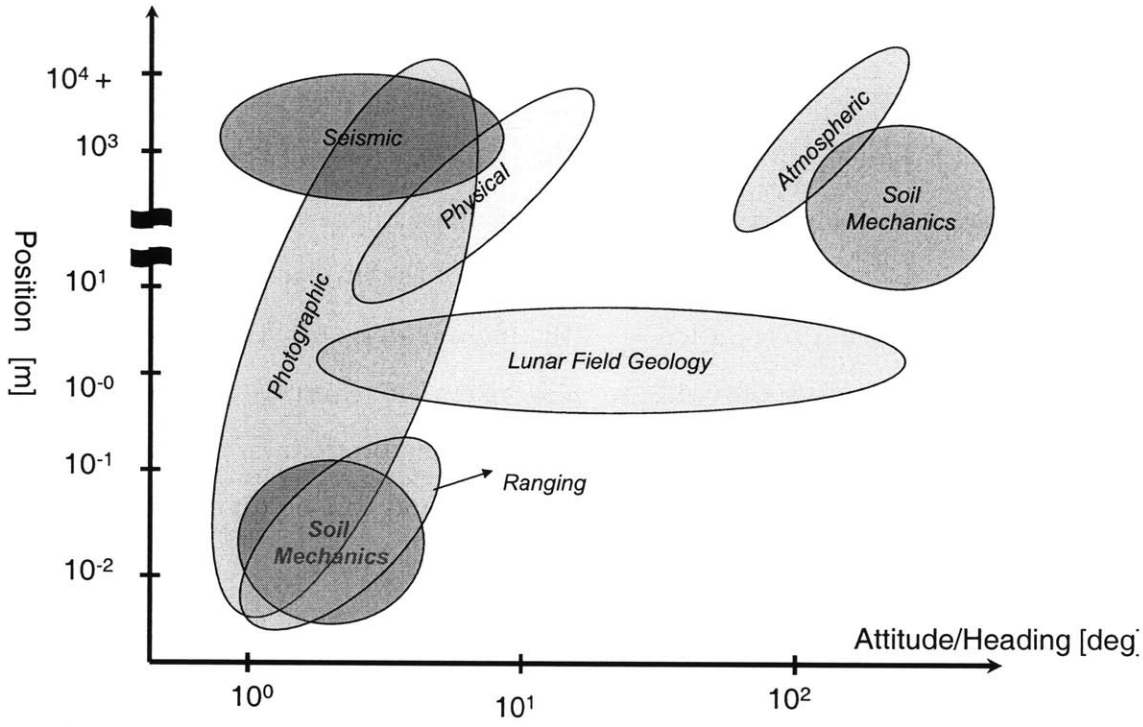

Figure 2-1: Typical Scientific Navigation Requirements, from [7]

on-surface and on-orbit elements. The rationale that led our team to choose this particular set of architectures will be presented in this section, as well as a description of the three main architectures (called *Minimalist*, *Simple*, and *Performance*) that constitute one of our main recommendations to NASA.

2.3.1 Navigation architecture elements

Most navigation sensors and techniques used for rover applications have been considered in the Information team work. This subsection will present these sensors, which have been classified in three different groups: onboard, on-surface, and on-orbit. Note that magnetic compasses are not taken into account, as no global magnetic field exists on the Moon and on Mars.

Onboard sensors

Inertial sensors Inertial sensors measure internal state variables of the vehicle, such as acceleration and rotation rates. The main components of Inertial Navigation Systems (INS) are accelerometers and gyroscopes. Accelerometers measure the acceleration of the vehicle with respect to an inertial reference frame. As described in [24], a simplified single-axis accelerometer is basically a spring mass system with a displacement measurement sensor. A measure of the displacement of the mass will give a measure of the acceleration that the mass undergoes. Three perpendicularly mounted spring-mass systems will give a complete 3-axis acceleration measurement. Gyroscopes provide an output proportional to the rotational velocity of the vehicle. Gyroscopes are based on different principles and can be divided in three main categories: mechanical, piezoelectric and optical gyroscopes.

The main advantages of these inertial sensors is that they are self-contained and can be sealed from the environment. They have been used for decades in aerospace applications and inertial navigation is a well-known method. Their main drawback comes from the integration process that is required to get position and attitude information. Indeed, these sensors are often corrupted by noise and drift. Under the assumption that the drift can be approximated by a constant bias b, a single integration of a gyroscope's output gives:

$$\theta_m = \int \dot{\theta} + b + v \; dt \; = \; \theta + bt + \int v dt \tag{2.3}$$

In addition to the rotation angle θ there are two additional terms, one of which growing constantly with time. Similarly, any bias in the accelerometer output will result in an error in position which will grow as the square of time, due to the double integration process.

Odometry sensors The term *Dead-reckoning* designates techniques where the actual position (and velocity, heading, etc.) is deduced from the position (and velocity, heading, etc.) at a former time using velocity data (and/or acceleration, rotation

rate, steering angle, etc.). A way to navigate with dead-reckoning is to use odometry sensors, such as encoders and potentiometers, which are the most common sensors used to measure the velocity or the position of a rotating device, such as a wheel or a steering shaft.

Odometry sensors share much of the advantages and disadvantages of inertial sensors. They are also self-contained, and give position and heading estimates. In addition to that, they are often considered as a low-cost solution. A major issue is that the position error will grow until some external fix is provided. Another problem is that these sensors are unable to detect wheel slip.

Celestial sensors Celestial sensors, such as star and sun sensors, can also be used to provide the user with an absolute position fix. The positioning methods used for mobile robot navigation come from marine navigation and usually require the user to measure the altitude of two or more celestial bodies, which can be the Sun, the Earth, or stars. One method used is the Two-Star Sight Method [25]. The user measures the altitude of two celestial bodies above the horizon, which combined with the precise knowledge of the date and time gives the user location, as the intersection of two circles of position (see Figure 2-2).

Another pair of measurements allows for the removal of the ambiguity between the two possible solutions. Although these devices constitute a low-cost and well-known technique for planetary navigation, they suffer multiple drawbacks. First of all, the position accuracy achievable via celestial positioning is very poor compared to other absolute positioning methods, on the order of 20km [8, 9]. In addition to that, although star sensors are always usable on the Moon due to the lack of atmosphere, this is not the case on Mars, where atmospheric effects and day/night alternation may considerably diminish the performance and availability of a navigation solution based on celestial sensors.

However, in addition to positioning capabilities, celestial sensors are also able to give absolute heading information, and can be a good aid to relative navigation devices, such as inertial sensors and odometers, as shown in [11] for instance.

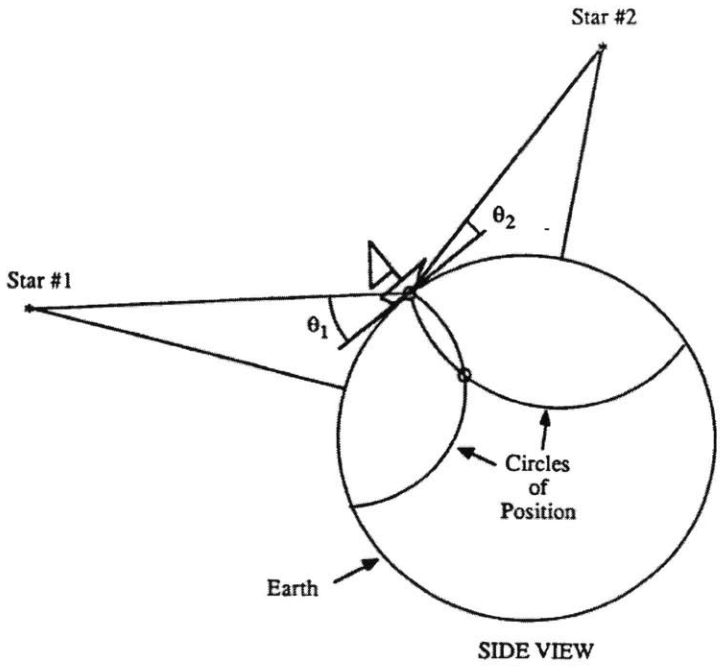

Figure 2-2: Two-star method of celestial navigation, from [25]

Vision sensors Navigation using vision sensors usually uses map-based positioning as the positioning method. Map-based positioning (or map-matching) is a method in which the sensors onboard the rover help build a map which is then compared to a global map already stored. This comparison allows the robot to compute its absolute position and orientation. The procedure usually followed is described in Figure 2-3.

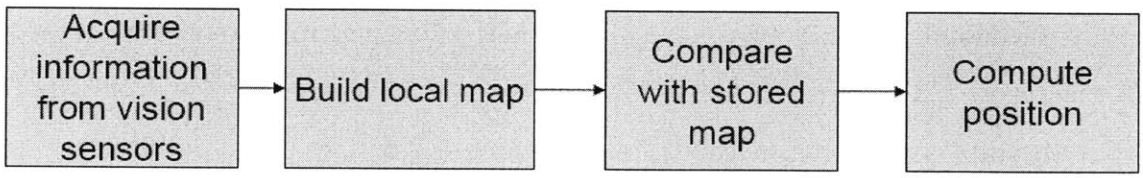

Figure 2-3: Procedure for map-based positioning, adapted from [23]

The sensors used for map-matching are laser range-finders and cameras (ultrasonic range sensors being better suited to very short range applications – 1 to 10 meters [24]).

One of the main advantages of vision-based positioning is that is allows for global surface navigation as long as accurate maps are available without the need for an

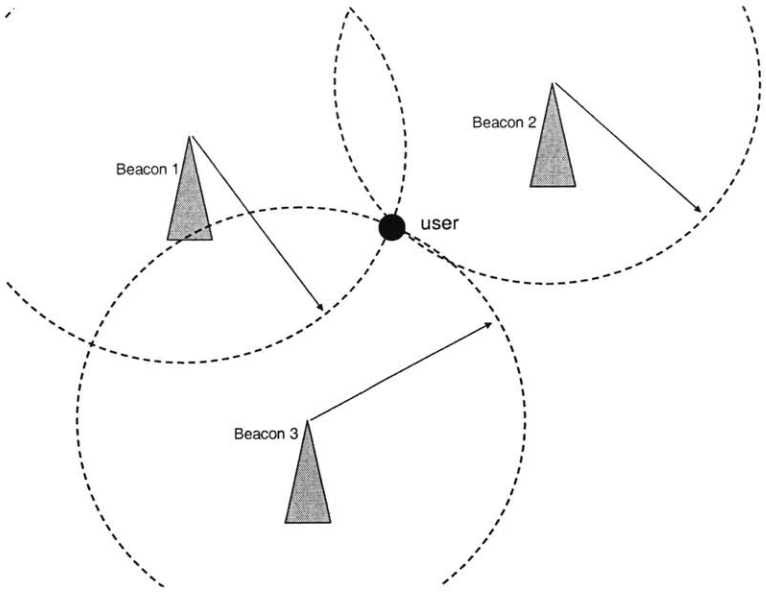

Figure 2-4: Trilateration method

external infrastructure (such as beacons or satellites). Furthermore, it is also a way to improve already existing maps. On the other hand, it requires a large amount of processing capabilities due to the huge amount of information provided by vision cameras. It is also dependent on the accuracy of the existing elevation maps, and on the quantity and visibility of distinctive landscape features. Finally, vision-based positioning is a relatively new navigation method and there have been relatively few tests in real-world experiments.

Surface devices

Active beacons have already been widely used for terrestrial positioning applications. Although laser and ultrasonic transmitters can be used for beacon navigation, they are most useful for short range and indoor applications. Consequently only radio-frequency (RF) beacons will be considered. One of the most used methods for beacon positioning is *trilateration* (see Figure 2-4), where the user's position is determined from the ranges from at least three beacons.

Another method is called *hyperbolic positioning.* Here the measurement is the difference of times of arrival of signals coming from two synchronized emitters (see [3] for a short introduction). Each measurement from a pair of beacons gives a hyperbolic

line-of-position (LOP), and the intersection of two or more LOP gives the user's position. This method has been used for LORAN (LOng-RAnge Navigation) since World War II and Omega, which was the first worldwide radionavigation system in the 1970s.

Also to be taken into consideration are positioning beacons similar to the VHF Omnidirectional Range (VOR) navigation system used for air navigation on Earth. VOR provides the user with its heading with respect to a reference direction (which is the magnetic North on Earth). Augmented with a Distance Measurement Equipment (DME), which is a transponder allowing for 2-way ranging with the interrogating aircraft, one such station gives complete 2D positioning (though with limited accuracy).

Most of today's research about beacon positioning is considering the use of Global Positioning System (GPS) transmitters combined with trilateration methods (see [31] for instance). This is a way to reach very high accuracy (cm level) in a local area (limited by line-of-sight). In addition to the infrastructure that needs to be deployed, one drawback of this navigation technique is that the coverage is limited to the area covered by the beacon network. Another disadvantage is that there is a need for careful initialization of the network (the positioning accuracy being limited to the accuracy by which the locations of the beacons are known).

On-orbit devices

Another possible navigation solution is the deployment of a navigation constellation (which could also be used for communication purposes) of satellites in orbit around the Moon or Mars. For Earth navigation the GPS system provides multiple users with precise (meter-level) position and timing information on most of the Earth's surface. As a consequence, some research has been done to study the possible deployment of a similar system on the Moon or on Mars. For the Moon, a 10 to 15 navigation satellite constellation using 2-way ranging has been proposed in [26]. For navigation on Mars, NASA's Jet Propulsion Laboratory is currently designing a constellation to provide communication relay capabilities as well as navigation capabilities. Several designs are considered, using both 1-way and 2-way ranging measurements [27, 28, 29].

This type of infrastructure would provide future explorers on the Moon and Mars with capabilities similar to the ones offered on Earth by GPS (global coverage and absolute positioning). Nevertheless, a lower number of satellites (for cost reasons) would reduce the overall performance in terms of coverage and accuracy. In spite of its cost, the use of such orbital assets can also be considered as a way to provide an already existing onboard navigation system with absolute navigation fixes at regular times.

2.3.2 Architecture selection rationale

A navigation architecture is being defined in our study as the arrangement of the elements that will provide any user on the surface of the Moon or Mars with navigation capabilities.

The navigation requirements have been expressed by the Surface Exploration team (see section 2.2), for both navigation and communication. Taking into account these requirements, various architectures have been designed from the combination of the different onboard, on-surface and on-orbit navigation elements. Communication studies were developed in parallel and used in the navigation architecture design process. Considering the fact that communication assets such as surface beacons or orbiting satellites, as well as other non-dedicated assets can be provided with navigation capabilities to augment the navigation architectures, this approach has been considered to be more effective towards our goal of a non-redundant integrated navigation/communication architecture.

Performance analysis tools have been developed and led to a downselect of these architecture across both design requirements (see section 2.2) and the metrics described in section 2.1. This process is summarized in Figure 2-5.

Through this process, the design space have been narrowed to the three architectures that are described in the following section. The rationale followed in this downselect is to design a set of three architectures that span the design space, while meeting the navigation and communication requirements. In addition to reaching the extremes of the design space in terms of performance as well of cost, this set

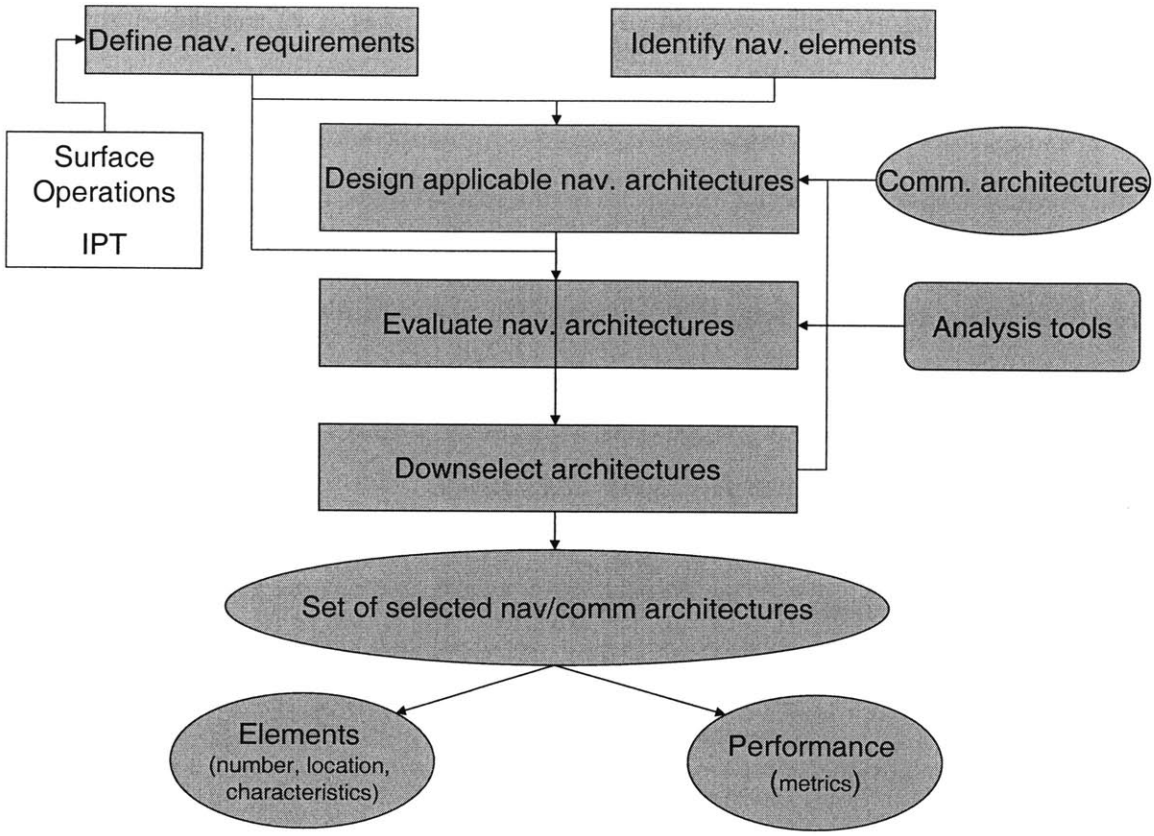

Figure 2-5: Navigation architecture development process

of three architectures also enables a gradual accretion of assets over time as better performance is required on the one hand, and funding becomes available on the other hand.

2.3.3 Architectures description

Minimalist The *Minimalist* architecture is the simplest adequate architecture navigation architecture, with low navigation and communication performance but low cost too. It is based on onboard sensors: visual navigation, one sun sensor, inertial measurement unit and odometers for the navigation part, without the aid of any dedicated navigation/communication satellite. In addition to this onboard equipment, one VOR-like beacon at the base station provides with absolute positioning and communication link inside a line-of-sight circle around the base station.

Simple The *Simple* architecture is based on the basic architecture, augmented by one dedicated nav/comm satellite. It is designed to allow good communication availability, and a navigation performance similar to that of the *Minimalist* architecture, but with the possibility of absolute position fixes in a sizable area around the base (beyond line-of-sight).

Performance The *Performance* architecture is once again based on the *Minimalist* architecture, but is augmented by a three to four satellite constellation for "Earth-like" navigation and communication performances (excellent communication availability and real-time navigation) over continental areas.

These architectures are based on the same onboard equipment. It is possible to transition from *Minimalist* to *Performance* over a campaign as additional satellites are deployed. The precise description of the Nav/Comm equipment and constellations will be determined in Chapter 4.

2.3.4 Architecture augmentation options

In addition to these core architectures, some architectural options aimed at augmenting these architectures have been considered. They are not part of any architecture, but rather additional assets improving the performance of any architecture when added. For any of the three architectures, two options have been considered:

- Surface beacons for both communication and navigation. In addition to providing with communication links, these ranging beacons allow the precise positioning capability required for specific scientific needs.
- Using a non-dedicated asset. A non-dedicated asset is a vehicle used for transportation left in orbit around the Moon or Mars. For such an asset, the following orbital parameters have been considered
  - For the Mars equatorial mission, the non-dedicated asset is assumed to be on an equatorial ($i = 0°$) circular ($e = 0$) orbit at an altitude $h = 500$km,

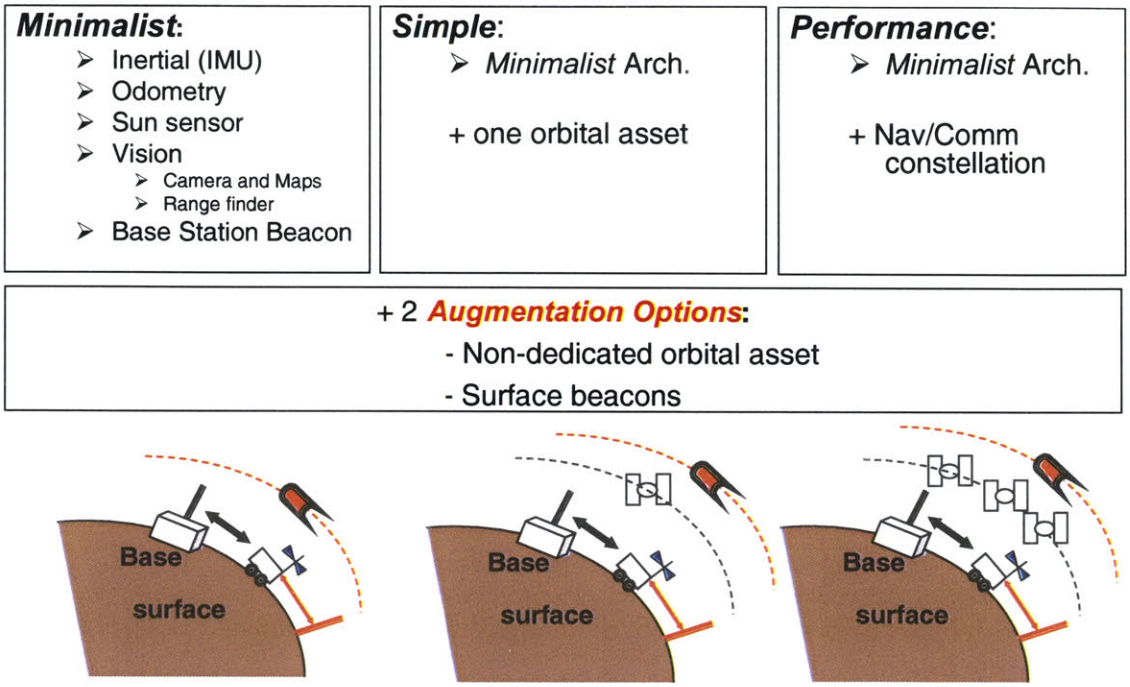

Figure 2-6: Navigation/Communication architectures description

– For the Moon polar (South Pole) mission, the non-dedicated asset is assumed to be on a polar ($i = 90°$) circular ($e = 0$) orbit at an altitude $h = 100$km.

The three architectures as well as the two augmentation options are summarized in Figure 2-6.

Chapter 3

Navigation Architectures Analysis

In Chapter 2, various navigation architectures were developed by combining onboard, emplaced, and on-orbit navigation elements. These designs were tailored to meet the requirements expressed by the surface operational requirements for Moon and Mars mission concepts. This chapter presents analysis tools that have been developed to evaluate and refine these architectures. Specifically, we describe the measurement models of navigation elements, the estimation processes and the metrics associated with the performance of the architectures.

3.1 On-Orbit Assets Analysis

The studies done by the Surface Exploration team of the MIT/Draper Lab group suggest that the envisioned surface operations on both the Moon and Mars will require beyond line-of-sight navigation (and communication) coverage with a 100m absolute position accuracy [7].

For instance, exploration traverses are planned to be as long as 500km [6], whereas the Line-Of-Sight distance is much shorter (5.7km on the Moon and 7.8km on Mars for 4m high antennas). Thus, a GPS like system with orbital assets provides a convenient means of absolute position information and the ability to reset the drift inherent to relative navigation techniques.

In this section, we describe the basic measurement process from dual use Nav/Comm

satellites, and compare various constellation design on the merit of the coverage and the absolute position accuracy requirements.

3.1.1 Assumptions

Concerning the on-orbit assets studies, the following assumptions are made:

Constellation assets assumptions: This set of assumptions concerns the types and number of on-orbit assets that have been taken into account in this study.

- Satellites having both navigation and communication capabilities have been considered.
- The number of Nav/Comm satellites is limited to four for both the Moon and Mars. Indeed, four satellites is the minimum number of satellites allowing to instantaneously solve for position and time (in the special case when all four satellites are simultaneously visible). So this is the number of satellites that allows for real-time navigation while minimizing the total mass to be placed in lunar or martian orbit.
- In addition to satellites orbiting the Moon or Mars, satellites orbiting the Lagrangian points of the Earth-Moon system for the Moon have been taken into account, because of their convenient location (see Chapter 5 for an introduction to Lagrangian points).

Orbital mechanics assumptions: A certain number of simplifying assumptions have been made about the dynamics of the Nav/Comm satellites, in order to make the problem more easily tractable.

- The satellites' motion is assumed to be purely Keplerian so that orbital perturbations, either due to the celestial body's non-homogeneous and non-spherical shape, or to the gravitational influence of other bodies such as the Earth or the Sun or other planets, or to the solar radiation pressure, or to any atmospheric drag are neglected. In particular, the effect of the J_2 term of the planet's

gravitational constant has not been taken into account. This is clearly an approximation, especially for the moon, but it facilitates much simpler analysis at this stage of the program. More detailed future analysis could consider the impact of the orbital perturbations on the constellation geometry and/or the fuel costs to remain in the appropriate configuration.

- Periodic (*halo*) or quasi-periodic (*Lissajous*) orbits around the Lagrangian points L_1 and L_2 of the Earth-Moon system are considered as a possible location for Nav/Comm satellites for the exploration of the Moon. In this case, the halo orbits have been approximated by a circular orbit lying in a plane perpendicular to the Earth-Moon line, centered about L_1. The radius of this orbit is of 10 Moon radii. The period of the satellites on this circular orbit is the one of the actual halo orbit of the same amplitude.
- The inclination of the equatorial plane with respect to the ecliptic plane has been neglected in our analysis.

Navigation assumptions: Here are listed the assumptions relative to the navigation method itself. Most of them closely match the ones used in [27].

- Our analysis uses the trilateration method for the navigation. Both 2–way and 1–way ranging have been considered.
- The measurement uncertainty (standard deviation) is of 1 meter for both 1–way and 2–way ranging. This assumption follows the one used in some of the Mars network studies [27].
- The uncertainty on the location of the Nav/Comm satellite on its orbit is considered to be of 2m along the radial direction, 7m along track, and 7m cross track. As before, this assumption is based on previous Mars network studies [27]. Radial, along track and cross track directions are shown on Figure 3-1.
- Due to the presence of atmosphere, reliefs, mountains and any visual obstacle, a minimum elevation angle must be defined for direct visibility of a satellite from the user. It has been fixed to 5° for the Moon and 15° on Mars (because of the

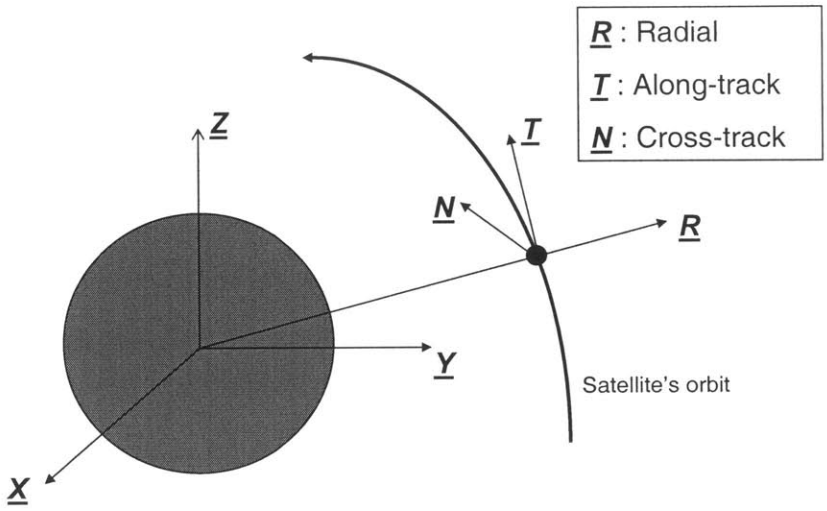

Figure 3-1: Radial, along-track and cross-track directions

presence of an atmosphere, which limits direct visibility in directions which are close to the horizon).

3.1.2 Principles of satellite navigation

In this section are presented the basic principles of satellite navigation. To evaluate a Nav/Comm constellation along the metrics described in Chapter 2, three intermediate metrics specific to satellite navigation need to be defined: the Dilution-of-Precision, the range accuracy, and the Mean Response Time.

Dilution-of-Precision

The Dilution-of-Precision (DOP) is often used in navigation analysis when the measurements available are ranges between the user and beacons, or satellites. Given some simplifying assumptions that will be described in this section, DOP enables a simple evaluation of the accuracy reached with a given constellation, and is also a way to characterize the goodness of the user-satellite geometry. Its derivation is based on the linearization of the measurement equations, which are given in Eq. 3.1. Each

measurement available to the used is called a *pseudorange.* The difference between range and pseudorange is shown on Figure 3-2. Pseudorange is the apparent measured range, and it differs from the actual range between the user and the satellite because of the following effects:

- When using 1–way ranging similar to GPS on Earth, the measurement made by the receiver is the difference between the signal reception time and the signal transmission time as carried in the signal. The user clock and the satellite clock being *a priori* not synchronized, there is a user clock bias that needs to be determined [3].
- When the signal is propagating through an atmosphere (Mars case), the ionosphere and the troposphere both introduce delays in the signal transmission. Although the Martian atmosphere is still only partially known, the assumption is made that these additional delays will be accurately modeled by the time the Martian exploration starts.
- The position of the satellite on its orbit is uncertain, which introduces another error.
- There are other disturbing effects, such as multipath and receiver noise.

So the pseudorange measured by the user from satellite k at time t is given by:

$$\rho_k(t) = r_k(t, t-\tau) + c[\delta t_u(t) - \delta t_k(t-\tau)] + I_k(t) + T_k(t) + \varepsilon_k(t) \qquad (3.1)$$

where c is the speed of light, τ is the signal transit time, $r_k(t, t-\tau)$ is the actual range between the user at time t and the satellite at time $t-\tau$. $\delta t_u(t)$ and $\delta t_k(t-\tau)$ are the clock user and satellite biases (with respect to some reference time scale similar to GPS Time (GPST) on Earth, see [3] for instance) at times t and $t-\tau$, respectively. $I_k(t)$ and $T_k(t)$ are the ionospheric and tropospheric delays, and $\varepsilon_k(t)$ are the other errors (mostly satellite position error). Some of these errors can be compensated for: the ionospheric and tropospheric delays, the satellite clock bias, and the multipath and receiver noise can be reduced too. This leads to the following simpler equation

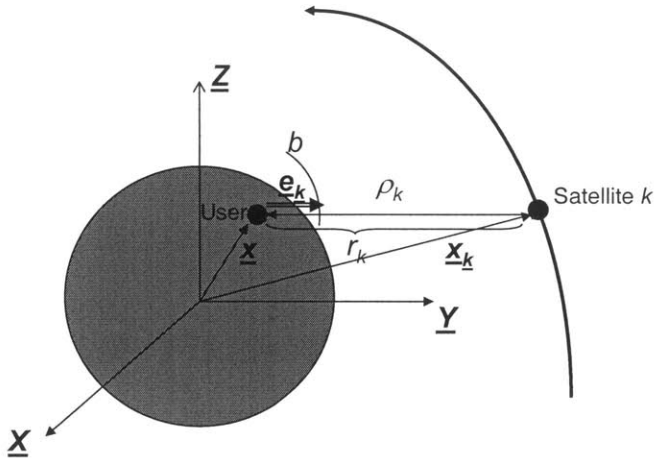

Figure 3-2: Range and corrected pseudorange

involving the *corrected pseudorange* ρ_k^c

$$\rho_k^c = r_k + c\delta t_u + \tilde{\varepsilon}_k \tag{3.2}$$

where the time t has been removed for simplicity and $\tilde{\varepsilon}_k$ represents the residual errors. Using the position vectors of the user $\mathbf{x}_u$ and of the satellite k $\mathbf{x}_k$, and replacing the clock bias term $c\delta t_u$ by b,

$$\rho_k^c = \|\mathbf{x}_k - \mathbf{x}_u\| + b + \tilde{\varepsilon}_k \tag{3.3}$$

If 1–way ranging is used, the clock bias b needs to be solved for, so there are a total of four unknowns for the user (three spatial and b). Therefore at least four measurements are needed, each corresponding to the nonlinear equation Eq. 3.3. If 2–way ranging is used, only three measurements are needed, as the user clock bias does not appear. The derivation that follows is done in the first case (1–way ranging), which is more complicated, and the result will be simply applied to the second case (2–way ranging).

The following development will lead to a simple expression for the accuracy of a satellite navigation system. The assumption is made that there is a first estimate of the user position $\hat{\mathbf{x}}_{u0}$ and of the user clock bias $\hat{b}_0$. The corresponding pseudorange

is expressed

$$\rho_{k0} = \|\mathbf{x}_k - \hat{\mathbf{x}}_{u0}\| + \hat{b}_0 \tag{3.4}$$

Any measurement given by a pseudorange ρ_k^c will lead to corrections $\delta\hat{\mathbf{x}}$ and $\delta\hat{b}$ that must be applied to the previous initial estimates. Assuming small corrections, the non-linear pseudorange equation can be linearized:

$$\begin{aligned}
\delta\rho_k &= \rho_k^c - \rho_{k0} \\
&= \|\mathbf{x}_k - (\hat{\mathbf{x}}_{u0} + \delta\hat{\mathbf{x}})\| + (\hat{b}_0 + \delta\hat{b}) + \tilde{\varepsilon}_k - (\|\mathbf{x}_k - \hat{\mathbf{x}}_{u0}\| + \hat{b}_0) \\
&= -\tfrac{\mathbf{x}_k - \hat{\mathbf{x}}_{u0}}{\|\mathbf{x}_k - \hat{\mathbf{x}}_{u0}\|} \cdot \delta\hat{\mathbf{x}} + \delta\hat{b} + \tilde{\varepsilon}_k + o(\delta\hat{\mathbf{x}}) \\
&= -\mathbf{e}_k \cdot \delta\hat{\mathbf{x}} + \delta\hat{b} + \tilde{\varepsilon}_k + o(\delta\hat{\mathbf{x}})
\end{aligned} \tag{3.5}$$

where $\mathbf{e}_k$ is the unit line-of-sight vector from the user to the satellite k, as shown in Figure 3-2.

Contrary to GPS used for navigation on Earth, whose space segment is comprised of 29 satellites (as of 1st March 2001), the number of Nav/Comm satellites that will orbit the Moon or Mars will be very limited. As a result, three or more satellites will not be visible simultaneously most of the time (if ever), so the ranging measurements required to obtain a position fix will not be available simultaneously. Consequently the user will need to accumulate measurements, either from the same satellite as it moves along its orbit or from new satellites as they appear above the horizon. Each new measurement can be used to improve the positioning accuracy, provided that we can model the user's motion between measurements. The following assumes the simplest case, where the user is stationary on the surface.

Combining N measurements, either coming simultaneously from different satellites, or from the same or different satellites at different times Eq. 3.5 can be rewritten

as

$$\boldsymbol{\delta\rho} = \begin{bmatrix} \delta\rho_1 \\ \delta\rho_2 \\ \vdots \\ \delta\rho_N \end{bmatrix} = \begin{bmatrix} -\mathbf{e}_1^T & 1 \\ -\mathbf{e}_2^T & 1 \\ \vdots & \vdots \\ -\mathbf{e}_N^T & 1 \end{bmatrix} \begin{bmatrix} \delta\hat{\mathbf{x}} \\ \delta\hat{b} \end{bmatrix} + \begin{bmatrix} \tilde{\varepsilon}_1 \\ \tilde{\varepsilon}_2 \\ \vdots \\ \tilde{\varepsilon}_N \end{bmatrix} \tag{3.6}$$

$$\Rightarrow \boldsymbol{\delta\rho} = \mathbf{H} \begin{bmatrix} \delta\hat{\mathbf{x}} \\ \delta\hat{b} \end{bmatrix} + \tilde{\boldsymbol{\varepsilon}} \tag{3.7}$$

with

$$\mathbf{H} = \begin{bmatrix} -\mathbf{e}_1^T & 1 \\ -\mathbf{e}_2^T & 1 \\ \vdots & \vdots \\ -\mathbf{e}_N^T & 1 \end{bmatrix} \tag{3.8}$$

Defining the augmented state vector $\delta\mathbf{y}$ as

$$\boldsymbol{\delta\mathbf{y}} = \begin{bmatrix} \delta\hat{\mathbf{x}} \\ \delta\hat{b} \end{bmatrix} \tag{3.9}$$

means that Eq. 3.7 can be rewritten as

$$\boldsymbol{\delta\rho} = \mathbf{H}\boldsymbol{\delta\mathbf{y}} + \tilde{\boldsymbol{\varepsilon}} \tag{3.10}$$

If N is less than 4, Eq. 3.10 cannot be solved directly. If $N = 4$, this system can be solved directly, provided that the $\mathbf{H}$ matrix is full-rank. More generally, N is greater that 4, and a solution for $\delta\mathbf{y}$ can be found using a weighted least-squares estimate. The objective is to find $\delta\hat{\mathbf{y}}$ that will maximize the conditional probability of $\boldsymbol{\delta\rho}$ given $\delta\hat{\mathbf{y}}$, which is equivalent to minimizing the following cost function

$$J = \frac{1}{2}(\boldsymbol{\delta\rho} - \mathbf{H}\boldsymbol{\delta\mathbf{y}})^T\mathbf{R}^{-1}(\boldsymbol{\delta\rho} - \mathbf{H}\boldsymbol{\delta\mathbf{y}}) \tag{3.11}$$

where $\mathbf{R}$ is the covariance of the zero-mean noise vector $\tilde{\varepsilon}$

$$\mathbf{R} = E[(\tilde{\varepsilon} - \bar{\tilde{\varepsilon}})(\tilde{\varepsilon} - \bar{\tilde{\varepsilon}})^T] = E(\tilde{\varepsilon}\tilde{\varepsilon}^T) \tag{3.12}$$

The solution to this minimization problem is

$$\begin{aligned} \delta\hat{\mathbf{y}} &= (\mathbf{H^T R^{-1} H})^{-1}\mathbf{H^T R^{-1}}\delta\boldsymbol{\rho} && (3.13) \\ &= \mathbf{H}^{\dagger}\delta\boldsymbol{\rho} && (3.14) \end{aligned}$$

where

$$\mathbf{H}^{\dagger} = (\mathbf{H^T R^{-1} H})^{-1}\mathbf{H^T R^{-1}} \tag{3.15}$$

is the *pseudo-inverse* of $\mathbf{H}$ for the above weighted least-squares problem. The new estimate $\hat{\mathbf{y}}$ is then

$$\hat{\mathbf{y}} = \hat{\mathbf{y}}_0 + \mathbf{H}^{\dagger}\delta\boldsymbol{\rho} \tag{3.16}$$

and the covariance $\mathbf{P}$ of this new estimate is given as a function of the covariance $\mathbf{P_0}$ of the first estimate $\hat{\mathbf{y}}_0$ and the noise covariance $\mathbf{R}$

$$\mathbf{P} = [\mathbf{P_0}^{-1} + \mathbf{H^T R^{-1} H}]^{-1} \tag{3.17}$$

If the first estimate $\hat{\mathbf{y}}_0$ is assumed to be arbitrarily chosen, i.e. there is no *a priori* knowledge of the user's state, then $\mathbf{P_0} = \infty\mathbf{I}$ and Eq. 3.17 reduces to

$$\mathbf{P} = [\mathbf{H^T R^{-1} H}]^{-1} \tag{3.18}$$

In the case where all measurements have the same error distributions, i.e. all the satellites have the same constant error distribution, a simplified statistical model of the measurement error $\tilde{\varepsilon}$ can be used. The measurement errors from the different satellites are now assumed to be:

- Zero-mean,
- Uncorrelated,

- Of the same distribution.

So the simplified model chosen for $\tilde{\varepsilon}$ is

$$E(\tilde{\varepsilon}) = \mathbf{0} \tag{3.19}$$

$$\mathbf{R} = E(\tilde{\varepsilon}\tilde{\varepsilon}^{T}) = \sigma_r^2 \boldsymbol{I} \tag{3.20}$$

And from Eq. 3.18, the covariance of the estimate error is

$$\mathbf{P} = \sigma_r^2 (\mathbf{H^T H})^{-1} \tag{3.21}$$

With $\mathbf{G} = (\mathbf{H^T H})^{-1}$, this leads to

$$\begin{cases} \sigma_x^2 = \sigma_r^2 G_{11} \\ \sigma_y^2 = \sigma_r^2 G_{22} \\ \sigma_z^2 = \sigma_r^2 G_{33} \\ \sigma_b^2 = \sigma_r^2 G_{44} \end{cases} \tag{3.22}$$

The root-mean-square of the position error being the sum of the precedent values, this leads to the definition of the *Position Dilution-Of-Precision* (*PDOP*):

$$RMS = \sqrt{\sigma_x^2 + \sigma_y^2 + \sigma_z^2} = \sigma_r \sqrt{G_{11} + G_{22} + G_{33}} = \sigma_r PDOP \tag{3.23}$$

with

$$PDOP = \sqrt{G_{11} + G_{22} + G_{33}} \tag{3.24}$$

Similarly can be defined the *Time Dilution-Of-Precision* (*PDOP*):

$$TDOP = \sqrt{G_{44}} \tag{3.25}$$

Table 3.1: Orbit errors

Direction	σ
Radial (R)	2m
Along track (T)	7m
Cross track (N)	7m

and the *Geometric Dilution-Of-Precision*

$$GDOP = \sqrt{G_{11} + G_{22} + G_{33} + G_{44}} = \sqrt{\texttt{Trace}(\mathbf{G})} \tag{3.26}$$

Most of our analysis will be based on the *PDOP*. In the following, *PDOP* will be used to refer to the *instantaneous* value obtained by a set of simultaneous measurements, as opposed to the *integrated PDOP*, called $PDOP_i$, which will correspond to the value of *PDOP* as new satellite measurements are integrated in the measurement matrix $\mathbf{H}$ over time.

The *DOP* metric can be interpreted as the influence of the user-satellite geometry on the navigation accuracy.

Range accuracy

As discussed in Section 3.1.2, the range measurement is subject to many error sources, which will be modeled as follows

- The main source of error is assumed to be due to the uncertainty of the satellite on its orbit. This is the slant range error σ_ρ
- other measurement errors (such as receiver noise) are modeled by a white, zero-mean, Gaussian noise with standard deviation σ_m

Table 3.1 lists the orbit errors that were chosen to be consistent with the Martian gravity field MGS75B developed from data from Mars Global Surveyor [27].

The total slant range error $\varepsilon_{\rho k}$ from satellite k is equal to the projection of the position error of satellite k along the line-of-sight vector $\mathbf{e}_k$:

$$\varepsilon_{\rho k} = \boldsymbol{\varepsilon}_k \cdot \mathbf{e}_k \tag{3.27}$$

Taking the components of $\mathbf{e}_k$ in the $(\mathbf{R}, \mathbf{T}, \mathbf{N})$ reference frame (which is described in Figure 3-1), and using the radial, along track and cross track error standard deviations [27], this gives for the variance of $\varepsilon_{\rho k}$:

$$\sigma_{\rho k}^2 = (\mathbf{e}_k \cdot \mathbf{R})^2 \sigma_R^2 + (\mathbf{e}_k \cdot \mathbf{T})^2 \sigma_T^2 + (\mathbf{e}_k \cdot \mathbf{N})^2 \sigma_N^2 \tag{3.28}$$

Both 1–way and 2–way other measurement errors are modeled by a white gaussian noise with standard deviation $\sigma_m = 1\text{m}$. So assuming uncorrelated errors, the total ranging accuracy from satellite k has a standard deviation

$$\sigma_r^2 = \sigma_{\rho k}^2 + \sigma_m^2 \tag{3.29}$$

Mean response time

The Mean Response Time (MRT) is defined as the time a user on surface has to wait before they obtain a "good enough" navigation fix. This metric is based on the assumption that a navigation fix will generally not be available in real-time. Indeed, because of the limited number of Nav/Comm satellites, three or four satellites will not be visible simultaneously most of the time, and the three to four ranging measurements required (depending on whether time is an extra unknown or no) to get a position fix will not be available simultaneously. Consequently the user will need to accumulate measurements, either from the same satellite as it moves along its orbit or from new satellites as they appear above the horizon. Each new measurement will augment the $\mathbf{H}$ matrix with an additional Line-Of-Sight vector, which will in turn decrease the value of $PDOP_i$. And the MRT is defined as the time the user must wait so that $PDOP_i < 5$.

3.1.3 Final metrics

As stated in Chapter 2, the different Nav/Comm architectures will be evaluated and compared along a set of navigation and communication metrics. The navigation metrics considered are the navigation accuracy, the navigation coverage, and the

navigation operability. In this section is shown how the metrics specific to satellite constellation, i.e. the DOP, the ranging accuracy and the MRT, are used to compute the final navigation metrics which have just been listed.

Accuracy

In general, and as described in section 3.1.2, measurement errors associated with different satellites have different standard deviations. In this case, the measurement error covariance is of the form

$$\mathbf{R} = \mathtt{Cov}(\tilde{\varepsilon}) = \mathtt{diag}(\sigma_1^2, \sigma_2^2, ..., \sigma_N^2) \tag{3.30}$$

for N measurements. The position error covariance matrix is then

$$\mathbf{P} = Cov \begin{bmatrix} \hat{\mathbf{x}} \\ \hat{b} \end{bmatrix} = \left(\mathbf{H}^{\mathbf{T}}\mathbf{R}^{-1}\mathbf{H}\right)^{-1} \tag{3.31}$$

And as described in Chapter 2, the position accuracy is then

$$RMS = \sqrt{P_{11} + P_{22} + P_{33}}; \tag{3.32}$$

An assuming that all measurements have the same uncertainty

$$RMS = \sigma_r PDOP_{(i)} \tag{3.33}$$

However, the variation in the user-satellite geometry has the strongest impact on changes on the accuracy of the navigation fix (as compared to variation in ranging accuracies over time or over different satellites). Consequently, the calculation of the $PDOP$ and $PDOP_i$ metrics provides a lot of insight on the overall performance of the constellation.

Coverage

As discussed in Section 3.1.2, a navigation fix will typically not be immediately available from the navigation constellation because there are only a few Nav/Comm satellites orbiting the planet. Nevertheless, providing that the user can wait a certain time, a navigation fix can be made available on most of the surface of the planet by accumulating measurements. Consequently, the *coverage* depends on this waiting time period. For example, the surface area where a navigation fix is immediately available will be much smaller than the surface area where a navigation fix will be available after a waiting period of one hour. Consequently two similar metrics have been defined to evaluate the coverage performance of the navigation constellations, corresponding to two different key values for the waiting time MRT:

- $Coverage_1$: surface area where a navigation fix is possible in a time less than 1 minute. This waiting time is small enough not to significantly disturb exploration activities and allows for real-time or quasi-real-time navigation.

- $Coverage_2$: surface area where a navigation fix is possible in a time less than 1 hour. This longer waiting time corresponds to a surface area where real-time or quasi-real-time navigation are not possible. Nevertheless, a navigation fix is still available after a wait that is long, but still possible in practice. For instance, one can imagine the astronauts doing some scientific (e.g. samples collection) or exploration (e.g. outpost setup) while staying essentially at the same place and therefore acquiring a position fix meanwhile.

The coverage will be given as percentage of the total surface area of the planet, approximated by a sphere:

$$Coverage_i = \frac{A_i}{4\pi R_m^2} \quad i = 1, 2 \tag{3.34}$$

where A_i is the surface area where a navigation fix is possible in a time less than the corresponding waiting time, and R_m is the radius of the planet.

Operability

This metric is a measure of the ease of operation of each navigation architecture and of the effort spent by the astronauts navigating. In the special case of navigation using a Nav/Comm satellite constellation, this definition translates to the time the user has to wait before getting a position fix. As for the coverage, the operability metric relies on the MRT intermediate metric. Nevertheless, the geographic area is not taken into account here, as only the MRT at the main place of exploration (e.g. at the South pole for polar lunar exploration) is considered.

3.1.4 Tools developed

A Constellation analysis tool has been developed for communication and navigation. This tool evaluates the navigation and communication metrics of a Nav/Comm satellites constellation.

Tool Inputs

The inputs of this tool are:

- A description of the constellation in terms of number of satellites, satellites location (lunar or martian orbit, libration point orbit), and constellation orbital parameters. The constellation description is given with NLO, which is the Number of satellites in Libration point Orbit, and with the matrix:

$$\mathbf{MOS} = \begin{bmatrix} i_1 & a_1 & e_1 & \Omega_1 & \omega_1 & N_1 & \varphi_1 \\ i_2 & a_2 & e_2 & \Omega_2 & \omega_2 & N_2 & \varphi_2 \\ \vdots & \vdots & \vdots & \vdots & \vdots & \vdots & \vdots \\ i_{N_o} & a_{N_o} & e_{N_o} & \Omega_{N_o} & \omega_{N_o} & N_{N_o} & \varphi_{N_o} \end{bmatrix} \tag{3.35}$$

  where N_o is the number of different orbits, i_k, a_k, e_k, Ω_k, ω_k are respectively the inclination, the semimajor axis, the eccentricity, the right ascension of the ascending node, and the argument of perigee of the kth orbit. N_k is the number of satellites on the kth orbit and φ_k is the initial phasing of the first satellite

on the kth orbit. All satellites on a given orbit are assumed to be regularly spaced, for both Moon/Mars and libration point orbits, i.e. their initial mean anomalies are evenly spaced on the orbit (see Eq. 3.38). This is justified by the need to have a navigation performance as stable as possible over time.

- The location of the user, given in a $(latitude, longitude)$ format
- Navigation parameters, such as the orbit uncertainties described in section 3.1.2 as well as the minimum elevation angle for a satellite to be seen by the user.

Orbit propagation

The Nav/Comm satellites trajectories are then computed using a Keplerian orbit propagator. All computations are first made in an inertial $(\mathbf{e_x}, \mathbf{e_y}, \mathbf{e_z})$ reference frame. All variables given in the rotating Planet-fixed reference frame will have the subscript R. First the *mean anomaly* M of satellite k on orbit n_o is computed as follows:

$$M = M_0 + nt \tag{3.36}$$

assuming $t_0 = 0$, where n is the mean motion of the satellite and is given by

$$n = \sqrt{\frac{GM}{a^3}} \tag{3.37}$$

where GM equals the planet's gravitational constant: $GM = 1.54 \times 10^8 \text{km}^3/\text{min}^2$ for Mars and $GM = 1.77 \times 10^7$ km^3/min^2 for the Moon. M_0 is the satellite's initial mean anomaly

$$M_0 = \frac{2\pi}{N_{n_o}} + \varphi_{n_o} \tag{3.38}$$

assuming that all satellites on the same orbit have regularly spaced initial mean anomalies. The *eccentric anomaly* E can be computed using Kepler's equation 3.39

$$E - e \sin E = M \tag{3.39}$$

which is solved for E in an iterative fashion employing Newton's method. Then the unit vectors $\mathbf{P}$ and $\mathbf{Q}$ are computed. $\mathbf{P}$ is the unit vector pointing towards the perigee, and $\mathbf{Q}$ is the unit vector perpendicular to $\mathbf{P}$, and corresponding to a true anomaly $\nu = \frac{\pi}{2}$, as shown in Figure 3-3.

$\mathbf{P}$ and $\mathbf{Q}$ are given as follows [45]

$$\mathbf{P} = \begin{bmatrix} \cos\omega\cos\Omega - \sin\omega\cos i\sin\Omega \\ \cos\omega\sin\Omega + \sin\omega\cos i\cos\Omega \\ \sin\omega\sin i \end{bmatrix} \tag{3.40}$$

and

$$\mathbf{Q} = \begin{bmatrix} -\sin\omega\cos\Omega - \cos\omega\cos i\sin\Omega \\ -\sin\omega\sin\Omega + \cos\omega\cos i\cos\Omega \\ \cos\omega\sin i \end{bmatrix} \tag{3.41}$$

Now the satellite position and velocity vectors can be computed from the ellipse geometry shown in Figure 3-4.

$$\begin{aligned} \mathbf{r} &= x_e\,\mathbf{P} + y_e\,\mathbf{Q} \\ &= r\cos\nu\,\mathbf{P} + r\sin\nu\,\mathbf{Q} \\ &= a(\cos E - e)\,\mathbf{P} + a\sqrt{1-e^2}\sin E\,\mathbf{Q} \end{aligned} \tag{3.42}$$

with

$$r = a(1 - e\cos E) \tag{3.43}$$

Similarly, the velocity vector is given by:

$$\dot{\mathbf{r}} = \frac{\sqrt{GMa}}{r}(-\sin E\,\mathbf{P} + \sqrt{1-e^2}\cos E\,\mathbf{Q}) \tag{3.44}$$

The trajectories being obtained first in the inertial reference frame, they can be then computed in a Planed-fixed reference frame, using the rotation matrix

$$\mathbf{r}_R = \mathbf{R}_\theta\mathbf{r} \tag{3.45}$$

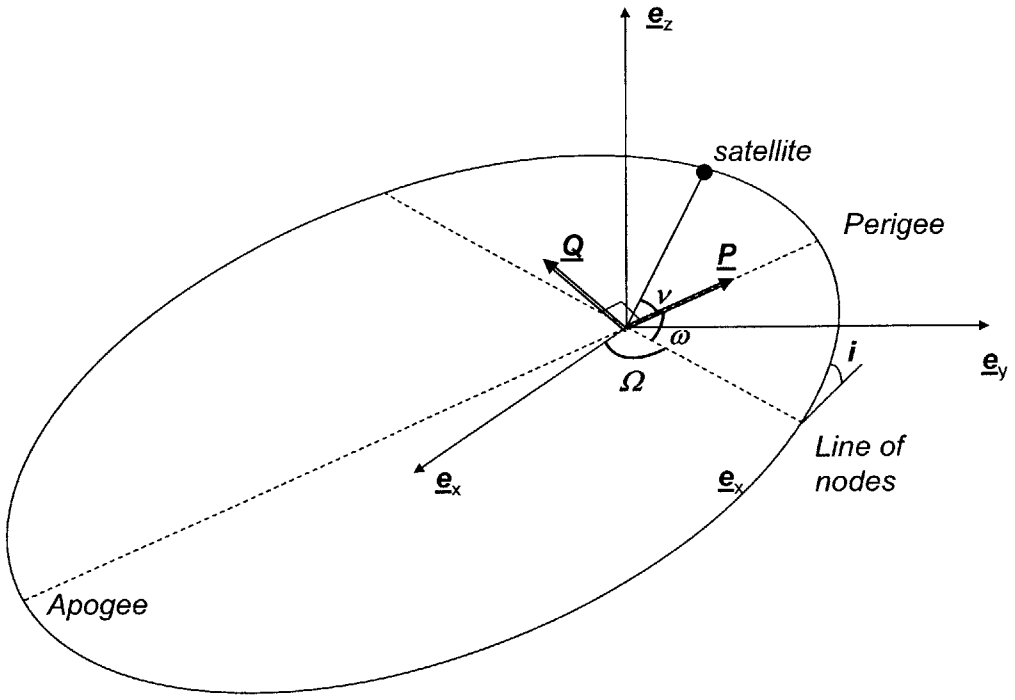

Figure 3-3: Orbital elements

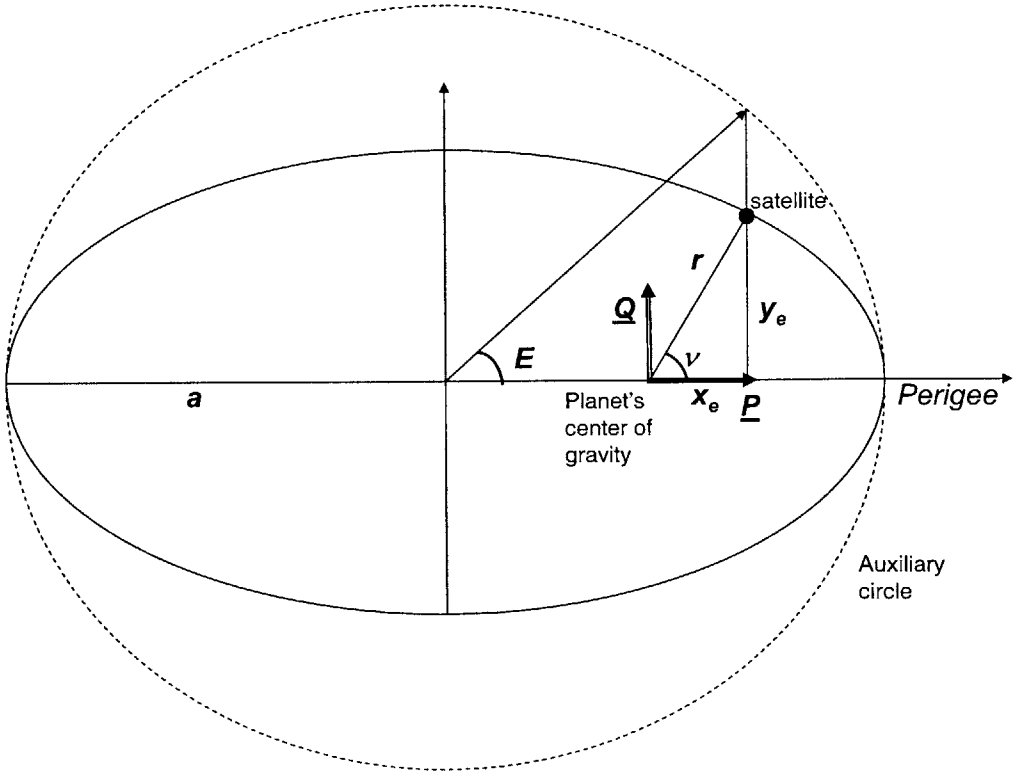

Figure 3-4: Ellipse geometry and orbital elements

with

$$\mathbf{R}_\theta = \begin{bmatrix} \cos\Omega_0 t & sin\Omega_0 t & 0 \\ -\sin\Omega_0 t & cos\Omega_0 t & 0 \\ 0 & 0 & 1 \end{bmatrix} \tag{3.46}$$

where Ω_0 is the planet's sidereal frequency. For Mars, $\Omega_0 = 7.1 \times 10^{-5}\text{s}^{-1}$, and for the Moon, $\Omega_0 = 2.7 \times 10^{-6}\text{s}^{-1}$.

For the satellites in libration point orbit in the Moon case, the trajectories are computed using the simplifying assumptions described in 3.1.1. The satellites are assumed to be on a halo orbit of the Earth-Moon system. This halo orbit is approximated by a circle whose plane is perpendicular with the Earth-Moon axis. First the angular position of the satellite k on this circle is obtained

$$\theta_k(t) = \frac{2\pi}{T}t + (k-1)\frac{2\pi}{NLO} \tag{3.47}$$

and the position vector of the satellite k can then be computed, *in the Moon-fixed reference frame.* Indeed, the libration points and the halo orbits around them are fixed with respect to the Earth's and the Moon's center of masses. The Moon itself begin fixed with respect to these points, the halo orbits are fixed in the Moon-fixed reference frame. The position vector of satellite k is then given by

$$\mathbf{r_R} = \begin{bmatrix} x_{L_1} \\ R_{halo}\cos\theta_k(t) \\ R_{halo}\sin\theta_k(t) \end{bmatrix} \tag{3.48}$$

as shown in Figure 3-5. R_{halo} is chosen to be equal to ten Moon radii (or 17,374km), as in [30], as it is a large enough value to ensure visibility at the South Pole. x_{L_1} is the distance from the center of the Moon to L_1 (58,777km).

The position vector in the inertial reference frame is obtained using the rotation matrix $\mathbf{R}_\theta$

$$\mathbf{r} = \mathbf{R}_\theta{}^{-1}\mathbf{r_R} \tag{3.49}$$

and note that only L_1 and L_2 are considered.

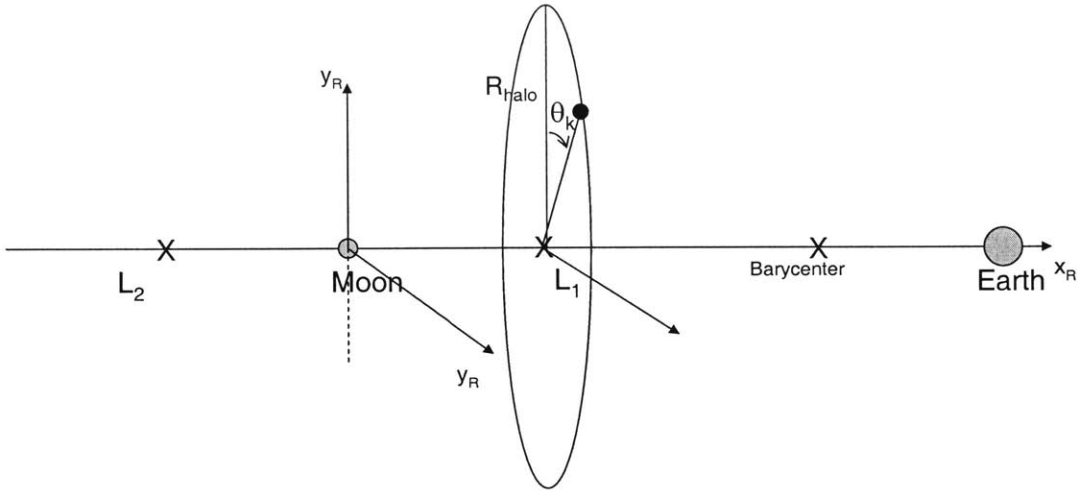

Figure 3-5: Libration point orbit geometry

Metrics computation and outputs

At each time and for each satellite, the line-of-sight vector is computed. This enables to determine if the satellite is visible or not. If the elevation angle β as shown in Figure 3-6 is greater than the minimum elevation angle β_{min}, the satellite is considered to be visible from the user.

If the satellite k is visible from the user, the radial, along track and across track vectors are computed, and the total measurement error is obtained from the combination of the slant range and ranging errors, as shown in Eq. 3.28 and Eq. 3.29. The line-of-sight vector $\mathbf{e_k}$ is then added to the measurement matrix $\mathbf{H}$ and $PDOP_i$ is calculated according to 3.23. When the integrated $PDOP_i$ gets below 5, the augmentation process is stopped, the time required to obtain this value for $PDOP_i$ is stored as Response Time, and $\mathbf{H}$ is reset to zero. At the end of the simulation, the Mean Response Time is then obtained as the average of all Response Times. The average accuracy obtained through the simulation is also given according to Eq. 3.32.

The simulation can be repeated for a part or the whole surface of the planet. Then $(latitude, longitude)$ maps of the surface of the planet are generated, showing contour plots of equal MRT. The coverage metrics are computed using Eq. 3.34.

In summary, the outputs of the constellation analysis tool are:

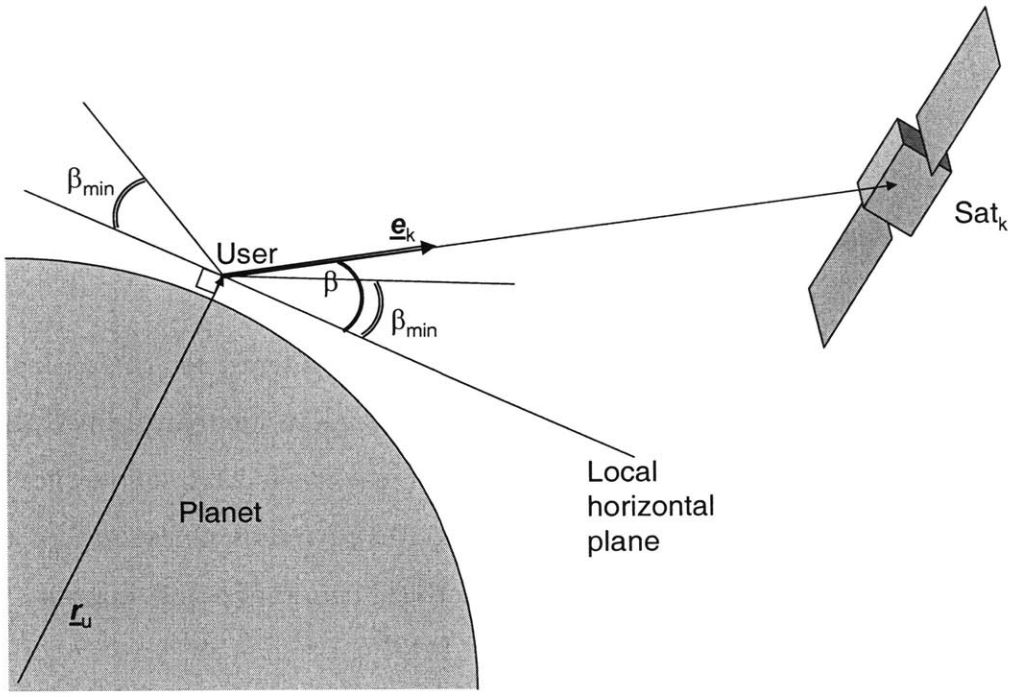

Figure 3-6: Minimum elevation angle

- Constellation visibility (number of satellites visible) over time
- Instantaneous and Integrated PDOP over time
- Accuracy over time
- Mean Response Time and Mean Accuracy
- Coverage maps
- Coverage metrics ($Coverage_i$)

3.1.5 Constellation design process

The whole option space of orbits suitable for navigation and communication applications has been divided in different orbit classes. The choice of these orbit classes has been made according to the recommended locations for surface exploration: the South Pole for the Moon, and the equatorial region for Mars.

Orbit classes

Three classes of orbits have been defined, for both the Moon and Mars.

- Moon orbit classes:
  - Circular (C): circular ($e = 0$) orbits, with altitudes ranging from 100km to 10,000km, and inclination ranging from $i = 45°$ to $i = 90°$ (polar orbit).
  - Elliptic (E): these orbits are all the eccentric orbits, with inclination ranging from $i = 45°$ to $i = 90°$ (polar orbit).
  - Libration Point Orbit (L): as no specific interest for the dark side of the Moon has been shown by the Surface Exploration team, only L_1 halo orbits have been considered. As explained in section 3.1.4, halo orbits have been approximated by circular trajectories of radius equivalent to ten Moon radii (which corresponds to an orbital period of $\simeq 291$ hours).
- Mars orbit classes:
  - Circular (C): circular ($e = 0$) orbits, with altitudes ranging from 500km to 10,000km, and inclination ranging from $i = 0°$ (equatorial orbit) to $i = 45°$.
  - Elliptic (E): these orbits are all the eccentric orbits, with inclination ranging from $i = 0°$ (equatorial orbit) to $i = 45°$.
  - Synchronous (S): Mars-synchronous orbits are all orbits with the same semimajor axis as the Mars-stationary orbit. According to Kepler's third law, this semimajor axis a_* is given by

$$a_* = \left(\frac{GM_{Mars}}{n^2}\right)^{\frac{1}{3}} = 20,428\text{km} \tag{3.50}$$

    where GM_{Mars} is Mars gravitational constant and n is Mars rotation rate. This class of orbits includes Mars-stationary orbits for $i = 0°$ and $e = 0$, whose groundtrack is a point on the equator of the planet. For non-zero inclination or eccentricity, these orbits do not stay all the time above the same point anymore, but *on average* only. Their ground tracks become closed loops around this point. By staying above the same region around

Table 3.2: Orbit classes

Moon	Mars
Circular (C)	Circular (C)
Elliptic (E)	Elliptic (E)
Libration Point Orbit (L)	Mars-synchronous (S)

the martian equator while still moving, this class of orbits shows properties quite suited to equatorial navigation.

The orbit classes are summarized in Table 3.2.

On Figures 3-7 and 3-8 are shown examples of each of the three classes of orbits considered in the lunar case, in the Moon-fixed and inertial reference frames respectively. The thick curve represents a high-inclination ($i = 80°$) circular orbit with a semimajor axis $a = R_m + 10,000\text{km} = 11,737\text{km}$ (R_m being the radius of the Moon). The thin curve represents a Molniya orbit ($i = 65°$, $a = R_m + 10,000\text{km} = 11,737\text{km}$, $e = 0.7$). Lastly, the dashed curve represents a halo orbit around L_1.

On Figures 3-9 and 3-10 are shown examples of each of the three classes of orbits considered in the Mars case, in the Mars-fixed and inertial reference frames respectively. The thick curve represents a medium-inclination ($i = 45°$) circular orbit with a semimajor axis $a = R_M + 5,000\text{km} = 8,397\text{km}$ (R_M being the radius of Mars). The thin curve represents a Molniya orbit ($i = 65°$, $a = R_M + 10,000\text{km} = 13,397\text{km}$, $e = 0.7$). Lastly, the dashed curve represents a slightly eccentric Mars-synchronous orbit ($i = 15°$, $a = 20,428\text{km}$, $e = 0.1$).

Constellation design

The objective is to design the constellation with the best combined Nav/Comm performance, subject to the following constraints:

- For the Moon, the most plausible place of exploration will be the South Pole region.
- For Mars, the most plausible place of exploration will be the equatorial region.

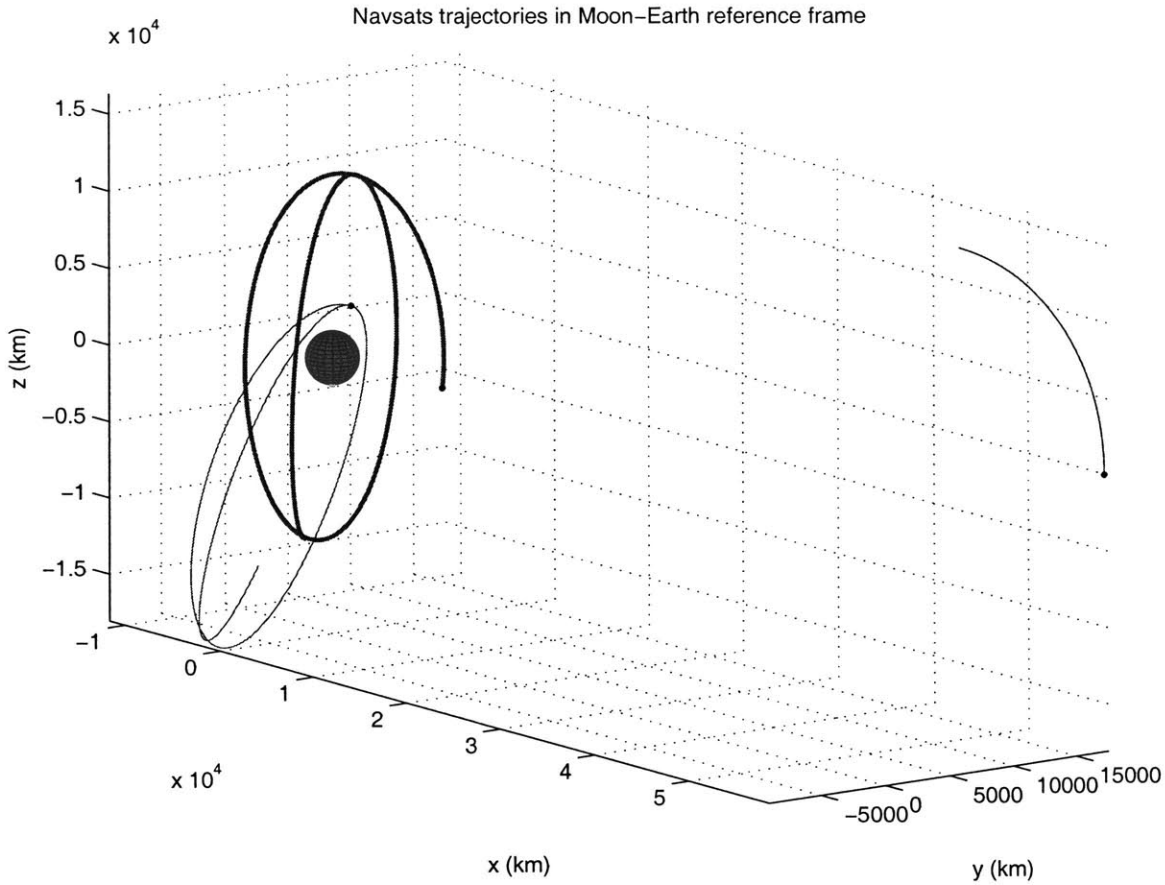

Figure 3-7: Orbits considered for the Moon - Moon-fixed reference frame

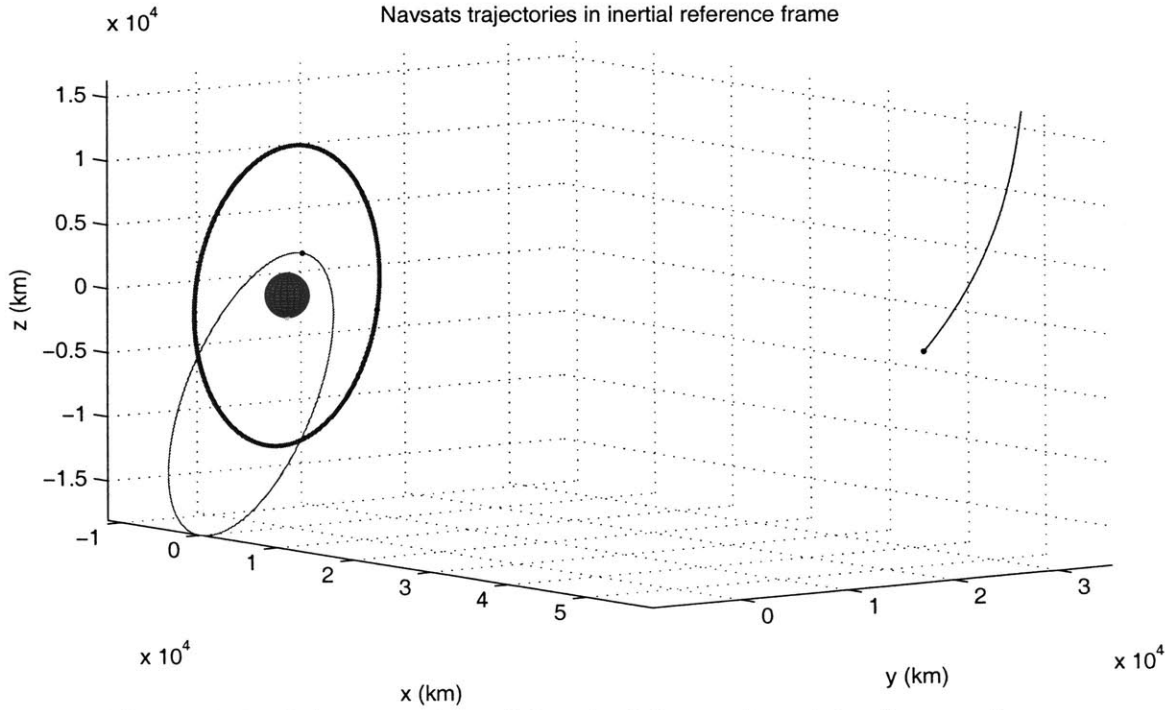

Figure 3-8: Orbits considered for the Moon - Inertial reference frame

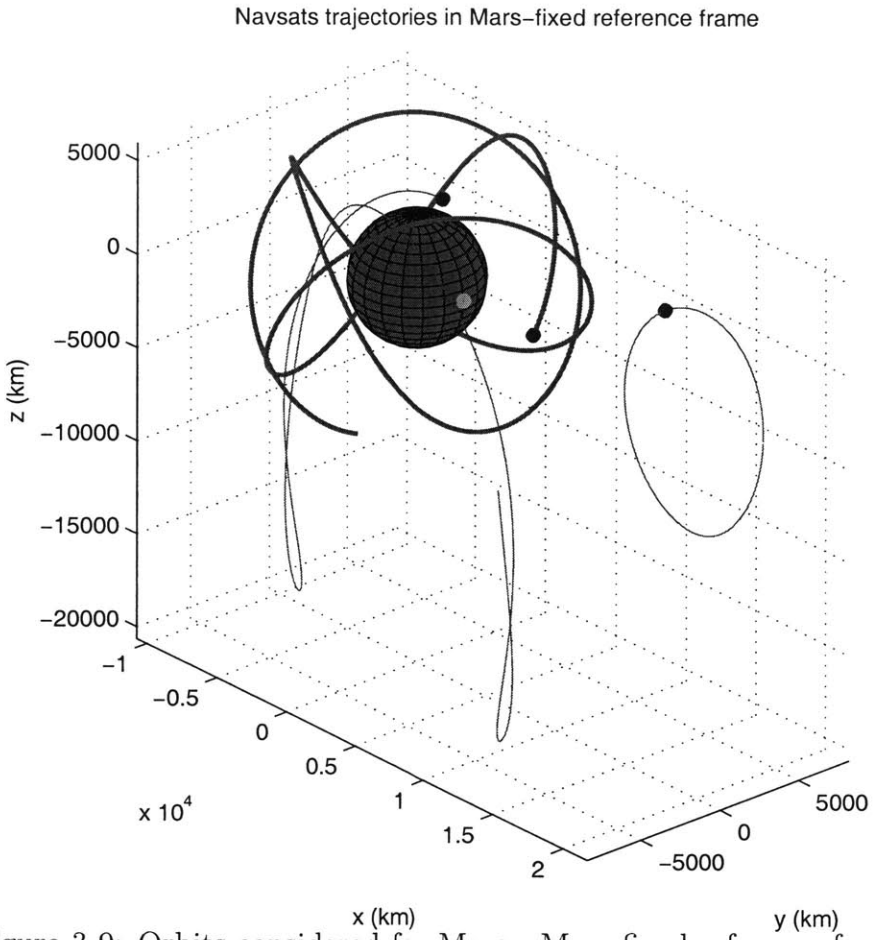

Figure 3-9: Orbits considered for Mars - Mars-fixed reference frame

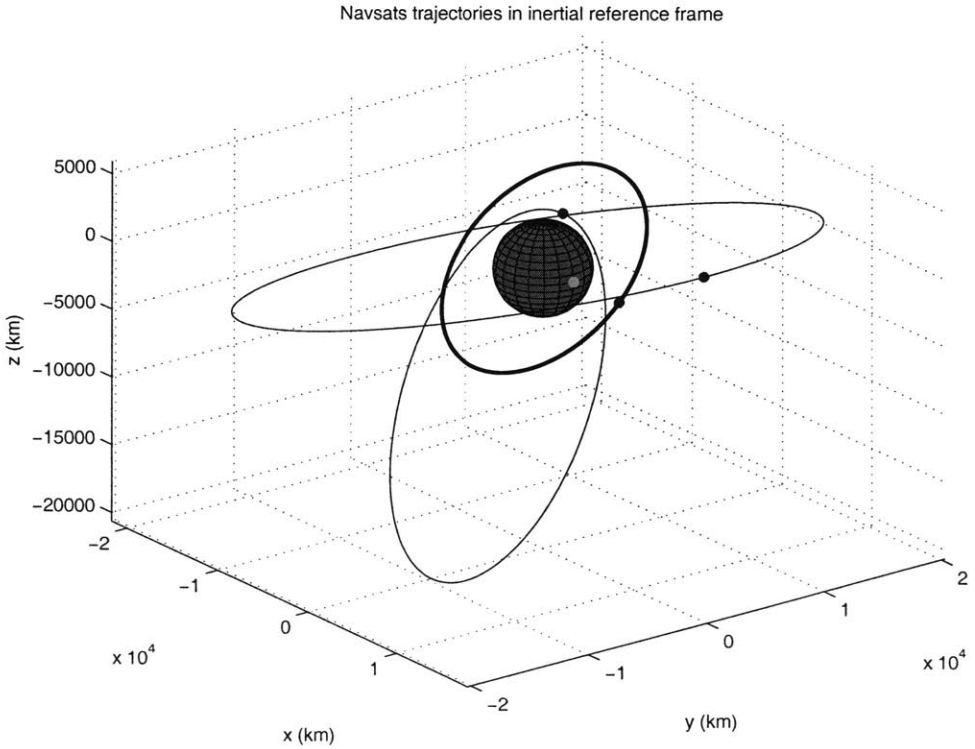

Figure 3-10: Orbits considered for Mars - Inertial reference frame

- The constellation size is limited to four satellites (Performance architecture, see section 3.1.1).

These preferred locations drove the design of the Nav/Comm constellations. For the Moon, the Nav/Comm performances should be the best in a continental region around the South Pole. Therefore only high-inclination orbits ($i \geq 45°$) have been taken into account. In addition to that, any circular orbit will provide equivalent coverage of the North and South poles, for symmetry reasons, which is considered as suboptimal. On the opposite, a highly eccentric orbit whose apogee is chosen to be placed above the South Pole should provide the required performance. Indeed, due to Kepler's second law, any satellite traveling on such an orbit will spend most of the time above the South Pole, and the southern polar region should therefore benefit of a good coverage. These high-eccentricity, high-inclination orbits are know as *Molniya* orbits and were used by the Soviet Union to provide with good communication coverage over high-latitude regions. So it is expected that a constellation made of four satellites on at least two different Molniya orbits should provide with the best Nav/Comm performance over the South Pole region.

For Mars, the Nav/Comm performances should be best above the equatorial region. So low-inclination ($i \leq 45°$) orbits are to be preferred. In addition to that, the exploration is more likely to take place on an area of continental size of the equatorial region, around a place of interest for instance, rather than on the whole equatorial region. So instead of a continuous coverage of the equator, a better coverage of a smaller yet still sizable (continental) area is being looked for. Mars-stationary satellites (analogous to geostationary satellites) have the nice property to stay above the same location on the ground. But though this is a nice property for communication purposes, it is not so suited to navigation. Indeed, for a user on the ground, such satellites are fixed in the sky, so they cannot provide with different ranging measurements over time, and consequently do not improve much the positioning accuracy (as $PDOP_i$ is constant). On the contrary, *Mars-synchronous orbits* as described in section 3.1.5 have an apparent motion (though with limited amplitude) as seen from a user on the ground, and at the same time stay *on average* above the same location on

Table 3.3: Moon Constellations

Const. Name	Description	MRT (min)
Moon1a	1C	979
Moon1b	4C	37.2
Moon2a	4E	0.412
Moon2b	6E	0
Moon3a	1L	5156
Moon3b	4L	555
Moon3c	6L	17.5
Moon4	3C3E	0
Moon5	4E2L	0.152

the ground. So a constellation made of three to four navigation satellites on different Mars-synchronous orbits is expected to give the best navigation performance.

Design Evaluation and Downselect

Despite the previous qualitative considerations, all the orbit classes mentioned in Section 3.1.5 need to be taken into account in the design of a first set of constellations that will be evaluated quantitatively. So numerous combinations of different orbits coming from both the two types of orbits highlighted before and from any of the three classes described in Section 3.1.5 have been elaborated. Some of them are briefly presented in Table 3.3, along with their performance in terms of MRT (which is a key intermediate metric in terms of coverage and operability) at the South Pole. The description of these constellations is given in the form $n_C C n_E E n_L L$, with n_C, n_E and n_L being the number of satellites in Circular, Elliptic and Libration point orbits respectively. Though the total number of satellites will not exceed four in our final design, there are up to six satellites here in order to gain some insight about the impact of additional satellites on performance.

The circular orbits have a semimajor axis $a = R_m + 10,000\text{km} = 11,737\text{km}$ for the Moon, and $a = R_m + 5,000\text{km} = 8,397\text{km}$ for Mars, and inclination $i = 45°$. The elliptic orbits are Molniya orbits, with a semimajor axis $a = R_{m/M} + 10,000\text{km}$, an eccentricity $e = 0.7$ and and inclination $i = 65°$. These particular choices of orbital elements are based on a manual optimization process. These results are based on

Table 3.4: Mars Constellations

Const. Name	Description	MRT (min)
Mars1a	1C	507
Mars1b	2C	237
Mars1c	4C	24
Mars2a	2E	431
Mars2b	4E	200
Mars3	2C2E	47.3
Mars4	3S	0

2–way ranging, but simulations based on 1–way ranging simply show a slightly larger MRT and do not change how each constellation compare with the others.

As expected from section 3.1.5, it appears from Table 3.3 that the constellations composed of Molniya orbits (Moon2a, Moon2b, Moon4 and Moon6) for the Moon and Mars-synchronous orbits (Mars4) for Mars have much better navigation performance than the constellations composed of circular or libration point orbits. Therefore our constellations will be composed of Molniya orbits for the lunar South Pole and Mars-synchronous orbits for Mars, as expected from the design considerations presented in section 3.1.5.

In addition to these navigation considerations, the Communication analysis [6] came to the following conclusions:

- For the Moon, a single satellite in a Molniya orbit provides the necessary communication performances, as indicated by the following communication metrics evaluations:
  - Communication coverage is continental
  - Communication availability is about 80%
- For Mars, a single satellite in a Mars-synchronous orbit fulfills the communication requirements too:
  - Communication coverage is continental
  - Communication availability is about 95%

As these single-satellite architectures provide some limited navigation performance (as will be detailed in Chapter 4) , they will form the core of our so-called *Simple* architecture. Augmented to form full constellations, they will form our *Performance* architecture. Here is the result of the constellation design process:

Simple architecture For the Moon polar (South Pole) mission, the nav/comm satellite is chosen to be on a *Molniya*-like orbit ($a = R_m + 10,000$km, $i = 65°$ and $e = 0.7$). And for the Mars equatorial mission, the Nav/Comm satellite is chosen to be on a circular ($e = 0$) Mars-synchronous ($h = 17,000$km) on slightly inclined ($i = 15°$) orbit.

Performance architecture For the Mars equatorial mission, the constellation is chosen to be composed of three Mars-synchronous satellites ($h = 17,000$km) on a slightly elliptical ($e = 0.1$) and inclined ($i = 15°$) orbit. For the Moon polar (South Pole) mission, the constellation is chosen to be composed of four satellites on two orbital planes with *Molnyia*-like orbits ($a = R_m + 10,000$km, $i = 65°$ and $e = 0.7$).

3.2 On-Surface Assets Analysis

Though on-orbit Nav/Comm satellites are necessary to do beyond line-of-sight exploration, they constitute a heavy and expensive infrastructure, and might not give the accuracy required for some demanding scientific activities (see Chapter 1). In addition to providing easily with local navigation around the base, on-surface beacons do have the capability to support this type of high accuracy requirements. They also constitute a support to onboard relative navigation devices, such as odometers and inertial sensors, as will be described in Chapter 4. As for the Nav/Comm constellations, a number of assumptions have been made to perform the required analysis.

3.2.1 Assumptions

To simplify the analysis, a certain number of assumptions have been made concerning the surface beacons. The main assumptions used are the following:

- Surface beacons characteristics assumptions:
  - Only active beacons have been considered,
  - This analysis is limited to two different kinds of active surface beacons: ranging beacons and ranging/heading beacons. This two types of beacons will be discussed in more details below, in Section 3.2.2.
  - The beacon network is assumed to be initialized, i.e. all positions of the beacons of the network are assumed to be known with infinite accuracy.
- Environment assumptions:
  - The terrain surrounding the beacons is assumed to be flat, i.e. there is no mountains or rocks likely to obstruct the antenna signals. Consequently a rover traveling in the area enclosed in a disk of radius the line-of-sight distance around any beacon can communicate with the beacon at any time.
  - The impact of the presence or not of an atmosphere on signal transmission is neglected.

3.2.2 Types of beacons

Two different types of surface beacons have been considered, corresponding to different purposes: ranging beacons for precise local navigation, and ranging/heading beacons for Line-Of-Sight coverage around the base station.

Ranging beacons

The ranging beacons are considered to be GPS transceivers (or *pseudolites*) with the following parameters:

- Height: 4m. This choice allows for a large line-of-sight distance (5.7km on the Moon and 7.8km on Mars) for a one-meter high rover antenna, while still being relatively light and easy to deploy.

- Ranging accuracy: $\sigma_b = 3$cm. This value is consistent with recent research on pseudolites networks [31, 32].

VOR/DME-like beacons

The ranging/heading beacons are considered to be analog to Very High Frequency Omnidirectional Range (VOR) stations coupled with Distance Measuring Equipment (DME) commonly used for aerial navigation on Earth. DME is a radar system which determines slant range between the user and the beacon by using 2–way ranging.

The following characteristics have been assumed:

- Heading accuracy: 1°. This value is consistent with actual VOR stations accuracy

- Ranging accuracy: the typical ranging accuracy of DME systems is about 0.2 nautical miles, or $\sim$ 300m.

The advantage of these beacons is that only one is theoretically enough to determine the user's location. But their accuracy is limited and cannot satisfy most of scientific accuracy requirements. Therefore they are mostly thought as a way to provide absolute navigation fixes in a line-of-sight circle around the base station. Consequently, all of our architectures will have such a beacon at the base station location, which will give some (but limited, for both accuracy and coverage) absolute navigation capabilities around the base station.

3.2.3 Dilution-Of-Precision and accuracy analysis

The analysis of beacon networks performances is very similar to the one performed with satellite constellations. In the ranging beacons case, the measurement is the

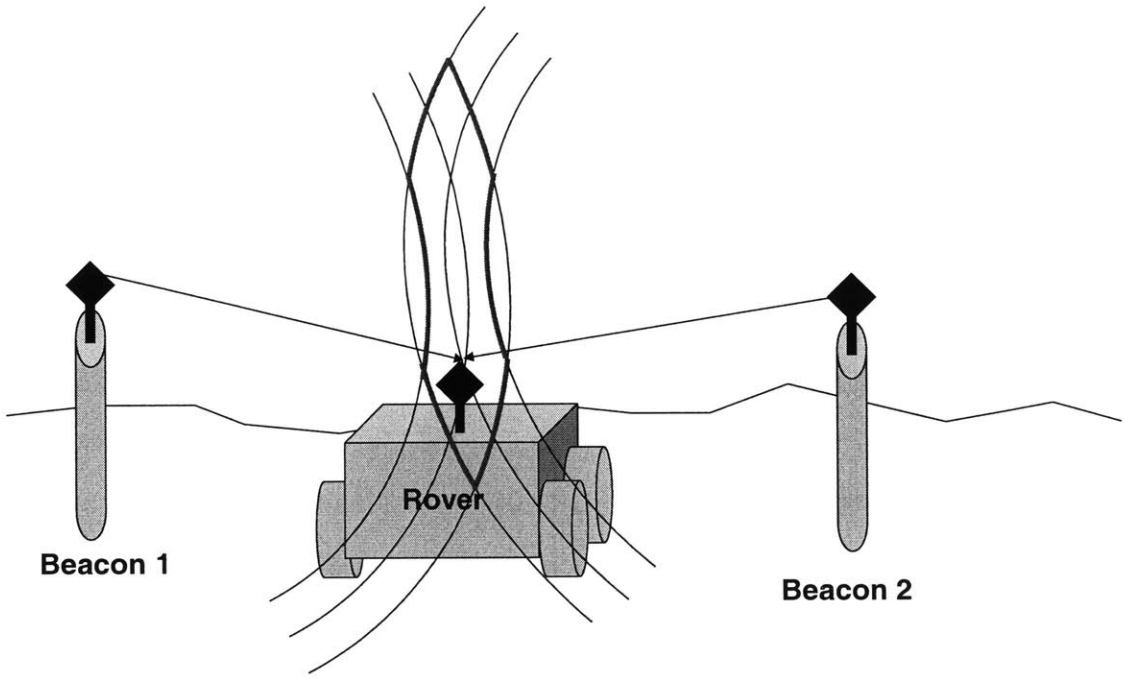

Figure 3-11: Illustration of bad vertical geometry

same as in the satellite constellation study, and therefore a very similar analysis based on the evaluation of the Dilution-of-Precision is possible.

As discussed in the assumptions section 3.2.1, the beacon network is assumed to be *a priori* perfectly known. The user is located somewhere in the vicinity of the beacon network. Then for each beacon in the network, its visibility from the user is determined (i.e. its distance to the user is compared to the line-of-sight distance). For each visible beacon a unit line-of-sight vector is computed, which augments the measurement matrix $\mathbf{H}$. Then the $PDOP$ is computed in the same way as in the constellation analysis (see Eq. 3.24). All beacons having the same height, the geometric configuration in the vertical direction is very poor as shown in Figure 3-11, so it is sensible to separate the horizontal and vertical Dilution-Of-Precision, which are defined as

- Horizontal Dilution-Of-Precision: $HDOP = \sqrt{G_{11} + G_{22}}$
- Vertical Dilution-Of-Precision: $VDOP = \sqrt{G_{33}}$

Assuming a total measurement uncertainty characterized by a standard deviation

$\sigma_b = 3$cm, it is then possible to estimate the horizontal positioning accuracy achieved by the beacon network using the usual DOP formula

$$RMS = \sqrt{\sigma_x^2 + \sigma_y^2} = \sigma_b HDOP \tag{3.51}$$

Notice that in contrary to the satellite constellation case, the beacons are fixed on the ground, which has two consequences: first no time-integration of the $PDOP$ is possible (there is no $PDOP_i$ metric), and second three beacons need to be visible at any time to compute a navigation fix.

3.2.4 Traverse analysis

Typical exploration traverses will be 50km or less long. The objective of this analysis is to design a network of ranging beacons to support precise navigation requirements along such a path.

The line-of-sight distance for a user antenna at height h_u and a beacon antenna at height h_b is obtained with the formula

$$LOS = \sqrt{h_b^2 + 2h_b R_{m/M}} + \sqrt{h_u^2 + 2h_u R_{m/M}} \tag{3.52}$$

which follows from geometric considerations based on Figure 3-12. $R_{m/M}$ is the radius of the Moon (subscript m) or Mars (subscript M).

For a given traverse length, a simple beacon network can be designed. First, at least three beacons need to be visible at any location along the traverse. So the beacon network will consist of a set of elementary beacon triangles. As some angular separation between the beacons is necessary to get a good enough position accuracy, the triangles will be chosen equilateral. Furthermore, this configuration also allows for some transversal travel.

Another design parameters if the size of the elementary triangle. This size will be related to the Line-Of-Sight distance. If r_t is the "radius" of the elementary triangle, understood at the distance from the intersection of its angle bisectors to any of its

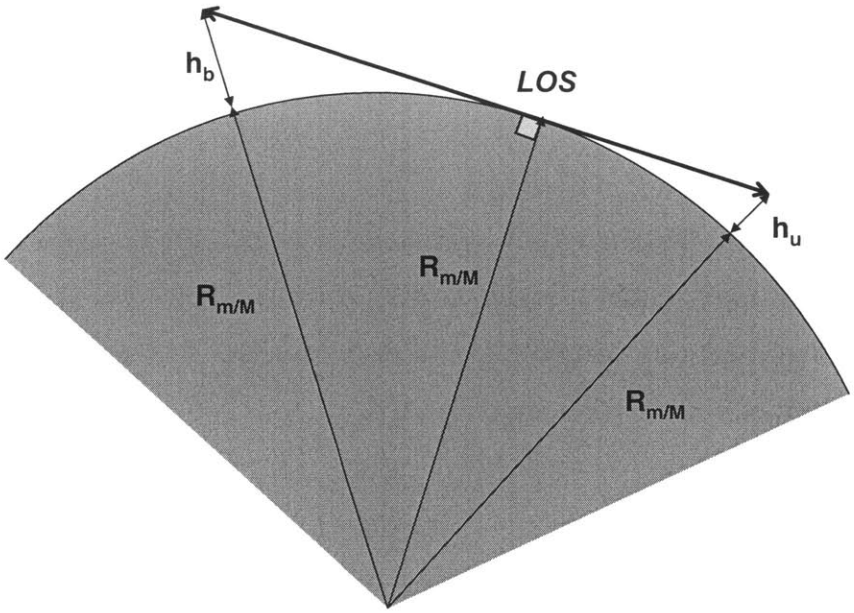

Figure 3-12: Line-of-sight distance

vertices as shown in Figure 3-13, then for $r_t^* = \frac{LOS}{\sqrt{3}}$, all the area included inside the triangle will be covered by the three beacons. But it is necessary to have a continuous coverage from one elementary triangle to another, so the actual value for r_t needs to be taken slightly less than r_t^*. A value of $r_t = 0.7r_t^*$ gives a minimum total number of beacons while keeping a continuous coverage and providing with some limited transversal coverage.

Typical exploration traverses on the surface of the Moon and Mars will be 50km or less long [6]. The beacon network process outlined above gives a set of six consecutive triangles, for a total of 18 beacons. The predicted accuracy achievable using this network on the (x, y) plane is shown on Figure 3-14, and always stays below 10cm. The dark area surrounding the network corresponds to regions where less than three beacons are visible, and therefore no navigation fix using only beacons is possible.

Note however, that using ranging beacons for linear traverse paths has many drawbacks. First, a lot of infrastructure (18 beacons in the previous example) is required. From a network setup point of view, this is inefficient in terms of distance traveled (mostly because of the triangular shape which is nevertheless unavoidable)

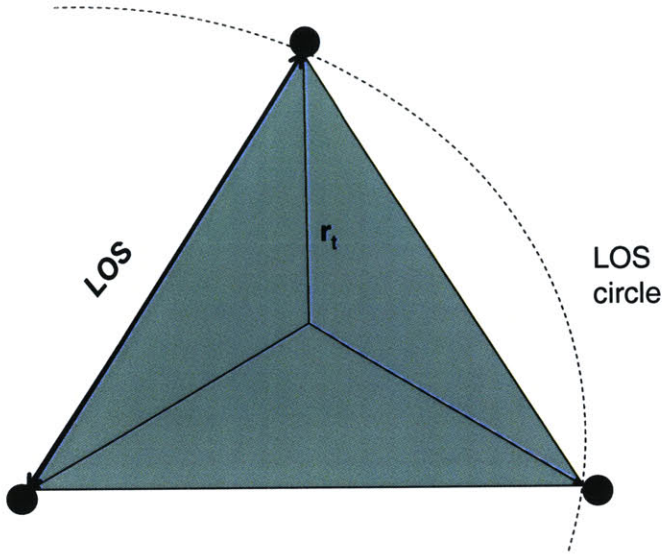

Figure 3-13: Elementary triangle

and in terms of time spent by the astronauts for the whole setup process. As a consequence, the use of ranging beacons network should be focused on local exploration in a small area (with dimensions of the same order of magnitude as the Line-Of-Sight distance) rather than on traverse paths. For such applications, the previous analysis also shows that very high accuracies can be reached ($\leq$ 10cm), which satisfies most of the scientific requirements (see Figure 3-14).

3.3 Onboard Sensors

For the on-orbit and on-surface navigation assets have been presented analysis methods for the evaluation of navigation metrics. In the case of onboard sensors, a similar approach will be followed as the different onboard sensors (vision-based excepted) will be integrated in a filter as will be explained in Chapter 4. In this section are presented the sensors models and the corresponding measurement equations that will be integrated in the navigation filter.

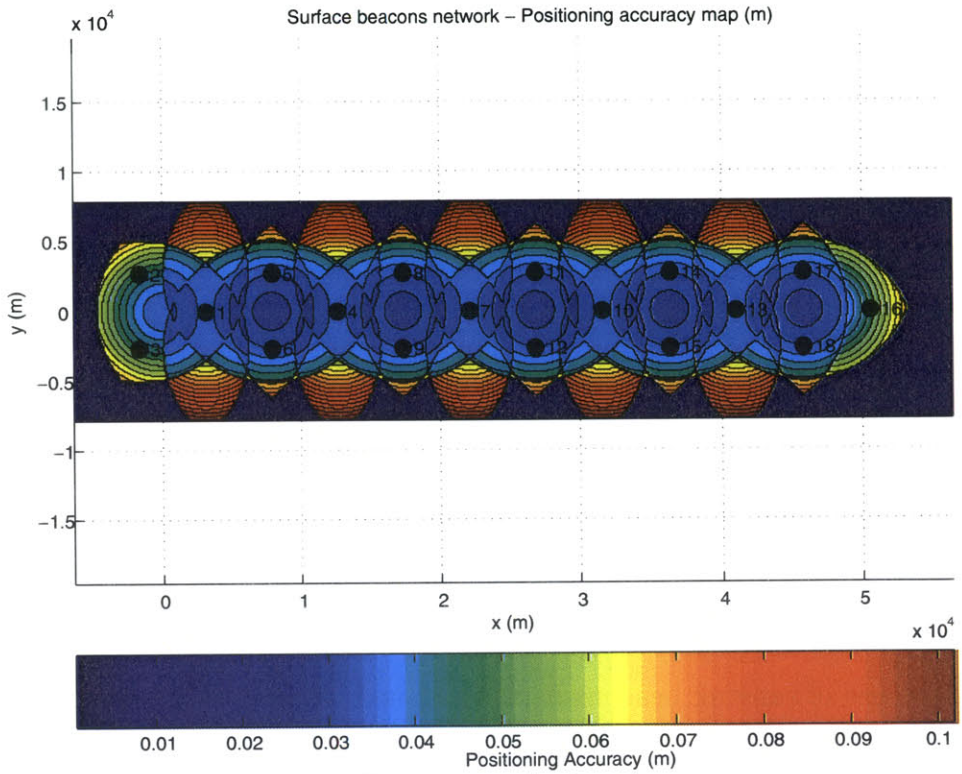

Figure 3-14: Traverse analysis - Accuracy map

3.3.1 Inertial sensors

The Inertial Navigation System (INS) that has been considered in our study has three orthogonally-mounted rate gyroscopes, a triaxial accelerometer and two inclinometers. The measurements from the INS are the three angular rates and the three acceleration components, given in the rover reference frame (defined on Figure 3-15). The three angles are θ, ψ, ϕ around the x, y, and z axis respectively. The corresponding angular rates are $\dot{\theta}$, $\dot{\psi}$, and $\dot{\phi}$. The three acceleration components given in the rover reference frame are obtained from the acceleration components in the external, inertial frame a_x, a_y and $a_z(= g)$, using the transformation matrix

$$\mathbf{a_R} = \mathbf{R^T a_I} \tag{3.53}$$

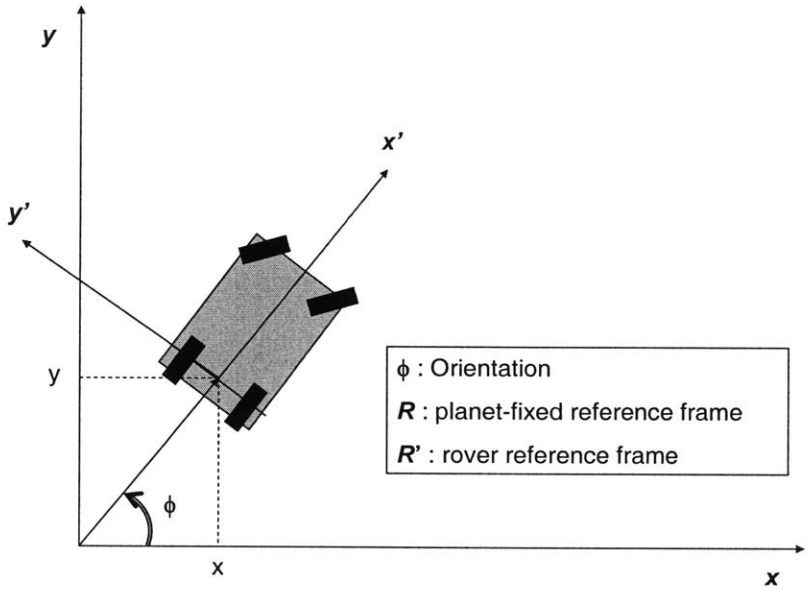

Figure 3-15: Rover reference frame

where $\mathbf{R}$ the transformation matrix from the planet-fixed reference frame to the rover reference frame

$$\mathbf{R} = \begin{bmatrix} \cos\phi & -\sin\phi & 0 \\ \sin\phi & \cos\phi & 0 \\ 0 & 0 & 1 \end{bmatrix} \begin{bmatrix} \cos\psi & 0 & \sin\psi \\ 0 & 1 & 0 \\ -\sin\psi & 0 & \cos\psi \end{bmatrix} \begin{bmatrix} 1 & 0 & 0 \\ 0 & \cos\theta & -\sin\theta \\ 0 & \sin\theta & \cos\theta \end{bmatrix} \tag{3.54}$$

so that

$$\mathbf{a_R} = \begin{bmatrix} \cos\psi\cos\phi\ a_x + \cos\psi\sin\phi\ a_y - \sin\psi\ a_z \\ (\sin\theta\sin\psi\cos\phi - \cos\theta\sin\phi)\ a_x + (\sin\theta\sin\psi\sin\phi + \cos\theta\cos\phi)\ a_y + \sin\theta\cos\psi\ a_z \\ (\cos\theta\sin\psi\cos\phi + \sin\theta\sin\phi)\ a_x + (\cos\theta\sin\psi\sin\phi - \sin\theta\cos\phi)\ a_y + \cos\theta\cos\psi\ a_z \end{bmatrix} \tag{3.55}$$

Table 3.5: Drift model parameters

Sensor	C_1	C_2	T	σ_v
Gyro	0.153°/s	−0.264°/s	5.64 min	0.24°/s
Acc-x	6.6cm/s^2	−148.7cm/s^2	16.3 min	5cm/s^2
Acc-y	2.7cm/s^2	−92.4cm/s^2	4.45 min	5cm/s^2
Acc-z	21.2cm/s^2	−56.9cm/s^2	138.5 min	5cm/s^2

All inertial measurements are corrupted by a bias ϵ and an assumed white, zero-mean noise vector $\mathbf{v}$, so that the final measurement vector is

$$\mathbf{z} = \begin{bmatrix} \dot{\theta} \\ \dot{\psi} \\ \dot{\phi} \\ \cos\psi\cos\phi\ a_x + \cos\psi\sin\phi\ a_y - \sin\psi\ a_z \\ (\sin\theta\sin\psi\cos\phi - \cos\theta\sin\phi)\ a_x + (\sin\theta\sin\psi\sin\phi + \cos\theta\cos\phi)\ a_y + \sin\theta\cos\psi\ a_z \\ (\cos\theta\sin\psi\cos\phi + \sin\theta\sin\phi)\ a_x + (\cos\theta\sin\psi\sin\phi - \sin\theta\cos\phi)\ a_y + \cos\theta\cos\psi\ a_z \end{bmatrix} + \begin{bmatrix} \epsilon_{\dot{\theta}} \\ \epsilon_{\dot{\psi}} \\ \epsilon_{\dot{\phi}} \\ \epsilon_{a_x} \\ \epsilon_{a_y} \\ \epsilon_{a_z} \end{bmatrix} + \begin{bmatrix} v_1 \\ v_2 \\ v_3 \\ v_4 \\ v_5 \\ v_6 \end{bmatrix} \tag{3.56}$$

For each measurement, the bias error is approximated by a model of the form (from the Levenberg-Marquardt iterative least-squares method as shown in [21, 22])

$$\epsilon(t) = C_1(1 - e^{-t/T}) + C_2 \tag{3.57}$$

Table 3.5 lists the parameters of this drift model [21, 22]. These measurement and error models will be used in Chapter 4 in an integrated navigation system, along with other types of onboard (celestial) and off-board (surface beacons, navigation satellites) navigation assets.

3.3.2 Celestial navigation

Celestial sensors can be grouped in two types: star sensors and sun sensors. They can provide an absolute positioning capability, but the accuracy is typically very poor compared to other absolute positioning methods (i.e., on the order of 20km) [8, 9]. So these sensors will be considered in our study as absolute heading sensors only. This type of measurement is usually provided on Earth by magnetic devices such as compass, but the lack of a strong magnetic field on both the Moon and Mars prohibits the use of such a sensor. Star trackers usually require a narrow field-of-view, which may not be suited to a rover motion on a rough motion [11]. In addition, they will not provide any information during the daytime, at least on Mars. So only sun sensors will be considered here, as a absolute heading sensor.

The sun sensor considered in our analysis is fully described in Refs. [12, 20]. This sun sensor is called the Wide Angle Sun Sensor (WAAS) and was developed by Lockheed Martin. It has a 160° field-of-view, and provides heading information (the vehicle's orientation as shown in Figure 4-2) by using pitch and roll information given by an accelerometer and the time of the day. The picture information from the sun sensor is converted into an orientation angle through a calibration table. The time required to access this table limits the frequency at which the sun sensor measurements are available. While typical odometry sensors are available at a $f_o =$ 50Hz frequency, the sun sensor input rate is assumed to less than $f_{SS} =$ 10Hz [12]. The measurement equation from the sun sensor is

$$z = \phi + v_{SS} \tag{3.58}$$

where v_{SS} is a white Gaussian noise, with a standard deviation $\sigma_{SS} = 0.31$rad [12].

3.3.3 Vision-based navigation

Cozman and Krotkov [10] used a feature-based approach to deduce position estimates from panoramas taken by a camera mounted on a rover. Mountains and peaks appearing in the panoramas are first detected, and position and heading estimates are

then generated by matching the peaks to a Digital Elevation Map (DEM) of the surrounding area. Real tests on Earth gave positioning accuracies below 100m with DEMs resolution of 30m. Provided that the DEMs that will be available for the Moon and Mars at the time of exploration will have at least this resolution (30m) and that they will cover the areas of interest for surface exploration, which seems likely, absolute positioning with accuracies better than 100m can be expected from such navigation techniques.

As a consequence, in our analysis the assumption has been made that absolute positioning with this accuracy is obtained by a camera mounted on a rover. This vision/landmark detection system is the only way to get absolute positioning with reasonable accuracy (less than 1km, which is much better than with celestial devices) beyond the line-of-sight, without necessitating the extra infrastructure implied by the use of surface beacons and navigation satellites. Consequently vision cameras will constitute one of the most important components of our Minimalist architecture (which is intended to be based on onboard sensors only). It will also be one element of our Simple and Performance architectures as a backup and an aid to the absolute positioning provided by the navigation satellites present in these two heavier architectures.

Measurement and error models (see Eq. 3.56, Eq. 3.58) as well as analysis methods (see sections 3.1.4 and 3.2.3) have been developed for the different kinds of navigation assets and sensors that are the elements of our three different navigation architectures. These models and tool will be integrated in Chapter 4 in order to perform analysis of a full navigation equipment.

Chapter 4

Navigation Analysis Integration and Results

The models and tools developed in Chapter 3 are now going to be integrated in order to perform the analysis of a full navigation equipment. The first section of this chapter describes the integration tools that were developed to combine measurements from different types of assets. Then the evaluations of the three Nav/Comm architectures and their augmentation options are presented in the second section.

4.1 Navigation Analysis Integration Tools

4.1.1 Integration of surface beacons and navigation satellites

One of the disadvantages of ranging beacon networks is their very bad vertical accuracy, as explained in section 3.2.3. One possibility to improve this vertical accuracy when required is to use the ranging measurement coming from a Nav/Comm satellite. Surface beacons and navigation satellites provide the user with the same kind of measurements, i.e. ranging measurements. Consequently measurements from these two types of assets can be easily combined in the same *PDOP* metric (see section 3.1.2 for a description of the *PDOP* metric). The following simulation illustrates this method using one navigation satellite in an equatorial circular orbit around Mars simultane-

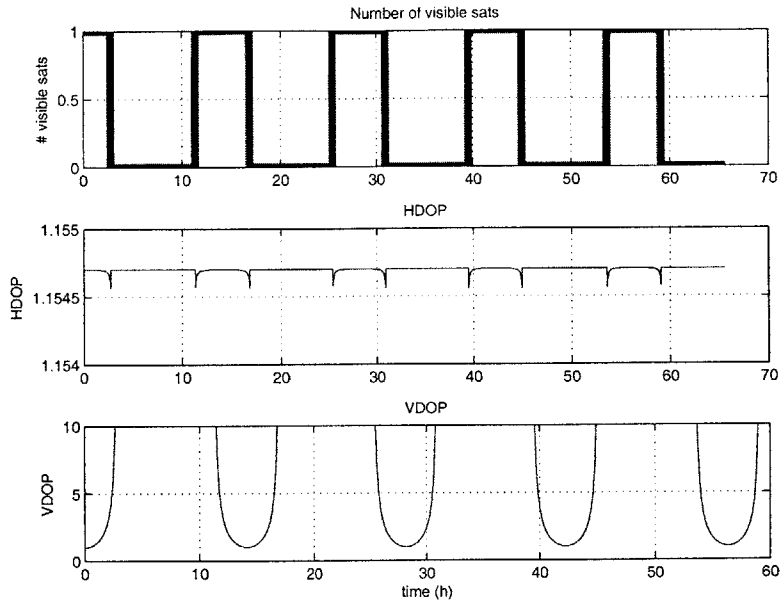

Figure 4-1: Combined $PDOP$ for surface beacons and navigation satellites

ously with a beacon network made of three surface beacons in an equilateral triangle configuration. The length of each side of the triangle is approximatively 2250 m. This configuration allows the three beacons to be visible from any point inside the triangle. The satellite orbits Mars at an altitude $h = 5,000$ km. The user is located on the equator, at the center of the beacon network.

Figure 4-1 shows when the navigation satellite is visible from the user, as well as the Horizontal ($HDOP$) and Vertical ($VDOP$) Dilution-Of-Precision. The impact of the navigation satellite on the $HDOP$ is minimal as expected, but very important on the $VDOP$. As soon as the navigation satellite appears above the horizon, the $VDOP$ quickly decreases until it reaches 1, and then grows again.

4.1.2 Integration of onboard sensors with external assets

The integrated analysis of onboard sensors of different types such as inertial devices (accelerometers and gyros), odometers, celestial sensors with external measurements coming either from surface beacons or navigation satellites requires the development of a filter to combine, in the best possible way, these different types of measurements. First, a kinematic model of a standard four-wheeled rover is needed to be incorporated in the filter.

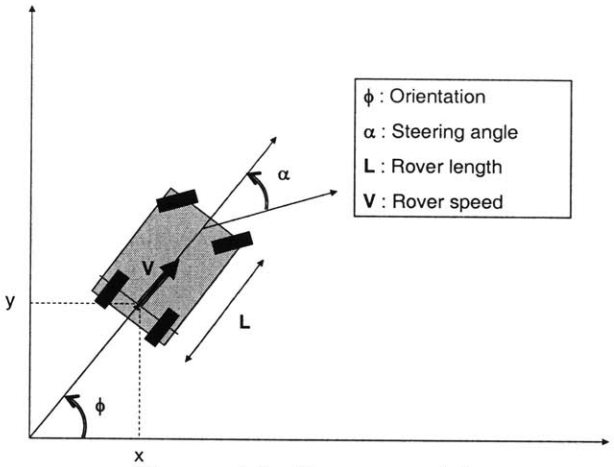

Figure 4-2: Rover model

Rover model

The geometric description of the rover is shown on Figure 4-2. The (x,y) position of the rover is taken at the middle of the rear wheel axis. ϕ is the orientation of the rover with respect to a reference direction. α is the steering angle of the front wheels. L is the length of the rover, and V is its speed. For simplicity, the angular speed of the wheels as well as the steering angle are assumed to be piecewise constant. The rover model described in Figure 4-2 has the following equations of motion

$$\begin{cases} \dot{x} = V\cos\phi \\ \dot{y} = V\sin\phi \\ \dot{\phi} = \frac{V}{L}\tan\alpha \end{cases} \tag{4.1}$$

Extended Kalman Filter

The model described above will be implemented in an extended Kalman filter, which is theoretically described in this section (see [4] for a more detailed derivation). Discrete time dynamics have been considered in the following derivation.

Linear case: In the special case of linear measurement and state equations (see Eq. 4.2 and 4.3), the *optimal* filter (i.e. which minimizes the mean-square estimation

error) is the *Kalman filter*.

$$\mathbf{x}_{k+1} = \mathbf{\Phi}_k \mathbf{x}_k + \mathbf{w}_k \tag{4.2}$$

$$\mathbf{z}_k = \mathbf{H}_k \mathbf{x}_k + \mathbf{v}_k \tag{4.3}$$

where $\mathbf{x}_k$ is the state vector, $\mathbf{\Phi}_k$ is the state transition matrix, $\mathbf{z}_k$ is the measurement vector, $\mathbf{H}_k$ is the measurement matrix, $\mathbf{w}_k$ is the process noise and $\mathbf{v}_k$ is the measurement noise. $\mathbf{w}_k$ and $\mathbf{v}_k$ are assumed to be white sequences having zero cross-correlation. The covariance matrices of $\mathbf{w}_k$ and $\mathbf{v}_k$ are assumed to be known and given by

$$E[\mathbf{w}_k \mathbf{w}_i^T] = \begin{cases} \mathbf{Q}_k, & i = k \\ 0, & i \neq k \end{cases} \tag{4.4}$$

and

$$E[\mathbf{v}_k \mathbf{v}_i^T] = \begin{cases} \mathbf{R}_k, & i = k \\ 0, & i \neq k \end{cases} \tag{4.5}$$

Starting from an estimate $\hat{\mathbf{x}}_k^-$ of the state vector and the error covariance matrix $\mathbf{P}_k^- = E[(\mathbf{x}_k - \hat{\mathbf{x}}_k^-)(\mathbf{x}_k - \hat{\mathbf{x}}_k^-)^T]$ at time t_k, the Kalman filter computes their values at time t_{k+1} in two steps: one *update* step and one *propagation* step.

The update step modifies the value of the estimate taking into account the difference between the actual measurement vector $\mathbf{z}_k$ and the expected measurement vector $\mathbf{H}_k \hat{\mathbf{x}}_k^-$ as follows

$$\hat{\mathbf{x}}_k = \hat{\mathbf{x}}_k^- + \mathbf{K}_k(\mathbf{z}_k - \mathbf{H}_k \hat{\mathbf{x}}_k^-) \tag{4.6}$$

and

$$\begin{aligned} \mathbf{P}_k &= (\mathbf{I} - \mathbf{K}_k \mathbf{H}_k)\mathbf{P}_k^-(\mathbf{I} - \mathbf{K}_k \mathbf{H}_k)^T + \mathbf{K}_k \mathbf{R}_k \mathbf{K}_k^T \\ &= \mathbf{P}_k^- - \mathbf{K}_k(\mathbf{H}_k \mathbf{P}_k^- \mathbf{H}_k^T + \mathbf{R}_k)\mathbf{K}_k^T \\ &= (\mathbf{I} - \mathbf{K}_k \mathbf{H}_k)\mathbf{P}_k^- \end{aligned} \tag{4.7}$$

where $\mathbf{K}_k$ is the Kalman gain, given by

$$\mathbf{K}_k = \mathbf{P}_k^- \mathbf{H}_k^T (\mathbf{H}_k \mathbf{P}_k^- \mathbf{H}_k^T + \mathbf{R}_k)^{-1} \tag{4.8}$$

Now that the measurements at time t_k are taken into account, the propagation step projects the values of the state estimate and the error covariance matrix at time t_{k+1}.

$$\hat{\mathbf{x}}_{k+1}^- = \mathbf{\Phi}_k \hat{\mathbf{x}}_k \tag{4.9}$$

and

$$\mathbf{P}_{k+1}^- = \mathbf{\Phi}_k \mathbf{P}_k \mathbf{\Phi}_k^T + \mathbf{Q}_k \tag{4.10}$$

Nonlinear case: In many navigation problems, the state dynamics and/or the measurement equations are nonlinear. In order to use the estimate and covariance propagations derived in the previous chapter, one needs to linearize the navigation problem. Two approaches can be followed: the linearization can take place either about some fixed, nominal trajectory (this is the *linearized Kalman filter*), or about a trajectory that is permanently updated as new estimates are computed (this is the *extended Kalman filter*). Each of these alternatives has its own pros and cons, and in this analysis the choice has been made to use the extended Kalman filter . Assuming nonlinear state and measurement equations

$$\mathbf{x}_{k+1} = \mathbf{f}_k(\mathbf{x}_k) + \mathbf{w}_k \tag{4.11}$$

$$\mathbf{z}_k = \mathbf{h}_k(\mathbf{x}_k) + \mathbf{v}_k \tag{4.12}$$

With $\hat{\mathbf{z}}_k^- = \mathbf{h}_k(\hat{\mathbf{x}}_k^-)$, the same state update equation as in the linear case is used (see [4] for details)

$$\hat{\mathbf{x}}_k = \hat{\mathbf{x}}_k^- + \mathbf{K}_k(\mathbf{z}_k - \hat{\mathbf{z}}_k^-) \tag{4.13}$$

the Kalman gain $\mathbf{K}_k$ being defined as before (see Eq. 4.8). The state propagation equation is then

$$\hat{\mathbf{x}}_{k+1}^- = \mathbf{f}_k(\hat{\mathbf{x}}_k) \tag{4.14}$$

And the error covariance update and propagation equations are the same as in the linear case (Eq. 4.7 and Eq. 4.10), with the state transition and measurement matrices

coming from the nonlinear model linearized about the current best estimate:

$$\mathbf{\Phi}_k = \left(\frac{\partial \mathbf{f}}{\partial \mathbf{x}}\right)_{\mathbf{x}=\hat{\mathbf{x}}_k} \tag{4.15}$$

and

$$\mathbf{H}_k = \left(\frac{\partial \mathbf{h}}{\partial \mathbf{x}}\right)_{\mathbf{x}=\hat{\mathbf{x}}_k^-} \tag{4.16}$$

4.1.3 Exploration scenarios

Different mission scenarios with different navigation architectures have been set up in order to test the different combinations of onboard and off-board devices. The values for the different variables and parameters used in the simulations are detailed in Appendix A.

Scenario 1 – complete Inertial Measurement Unit (IMU) and surface beacons for a fixed rover: This scenario investigates the combination of a complete IMU with surface beacons. More specifically, the inertial sensors composing the IMU are subject to drifting errors. Ranging beacons are a way to reset periodically these errors to an acceptable level. An important issue is the maximum time between two updates. If it is too short (for instance, on the order of minutes), the required density of the beacon network may be too high, which would forbid the option of an inertial onboard navigation system assisted by surface beacons for long traverses. If this time is long enough (for instance, on the order of hours or days), it would give a requirement on the density of the beacon network.

In the following simulations a rover is stationary at the center of a surface beacons network made up of three beacons, placed at an equilateral triangle vertices. The length of the triangle's sides is approximately 2250m. The rover is equipped with a full inertial measurement unit as described in section 3.3.1 and ranging measurement updates from the beacons. The measurement equations from section 3.3.1 and for the ranging beacons, as well as the inertial sensors models described in section 3.3.1 are implemented in an Extended Kalman Filter (described in section 4.1.2). Figure 4-3

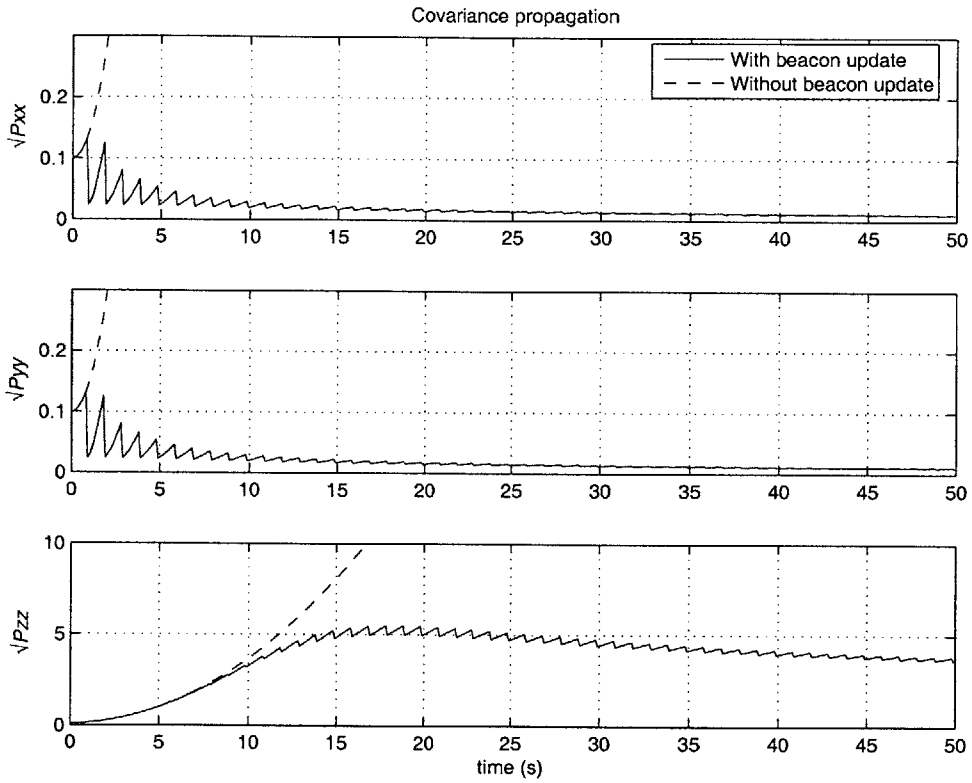

Figure 4-3: Rover position covariance propagation

shows the evolution of the position covariance components.

The dashed lines show the evolution of the covariance without any update from the surface beacon network, whereas the solid line corresponds to a beacon update rate of 1Hz. The covariance of the position error grows very quickly without any update ($\approx$ 100m in less than one minute), so any beacon network aimed at supporting the position given from an inertial-only navigation system should be continuous along the traverse to reset the inertial drift, which greatly penalizes this type of solution.

Scenario 2 – combination of inertial sensors, odometers with a sun sensor
Odometers (such as wheel encoders measuring the rover's velocity and potentiometer measuring the steering angle of the vehicle) are commonly used on mobile robots. The orientation of the vehicle is a very important component of the state vector as a constant error in this component leads to increasing errors in the vehicle's position (see Eq. 4.1). One way to augment the measurements capturing the orientation is to have an inertial gyro onboard. The combination of odometers and a gyro is indeed

Table 4.1: Sensor noises standard deviations

Sensor	Standard deviation	Value
Encoders	σ_V	2 cm/s
Potentiometer	σ_α	0.31 rad
Gyro	$\sigma_{\dot{\phi}}$	0.0031 rad/s
Sun sensor	σ_ϕ	0.31 rad

very common (this is the navigation onboard sensor suite used on the Lunar Roving Vehicle [5]). In this scenario is investigated the option of adding an absolute heading sensor such as a sun sensor, as suggested in [11, 12].

Using the rover model and the notation defined in Ref. 4.1.2, the measurement equations coming from the wheel encoders, the steering angle potentiometer and the gyro are

$$\mathbf{z} = \begin{bmatrix} V \\ \alpha \\ \dot{\phi} \end{bmatrix} + \begin{bmatrix} v_V \\ v_\alpha \\ v_{\dot{\phi}} \end{bmatrix} \tag{4.17}$$

where v_V, v_α, and $v_{\dot{\phi}}$ are white-noise processes, with standard deviations σ_V, σ_α and $\sigma_{\dot{\phi}}$. When the sun sensor measurement is used, a fourth component is added to the measurement vector $\mathbf{z}$

$$z_4 = \phi + v_\phi \tag{4.18}$$

The numerical values chosen for the noises standard deviations are consistent with [12] and listed in Table 4.1. The values chosen for σ_V corresponds to 2% of the nominal value ($V = 1$m/s). The values chosen for σ_α, σ_ϕ and $\sigma_{\dot{\phi}}$ corresponds to at least 15% of standard mid-range values (90°, 90° and 1°/s respectively), which correspond to low quality sensors. The use of higher quality sensors should not change the conclusions of this section anyway.

The previous measurement equations Eq. 4.17 and 4.18 as well as the rover model described in Eq. 4.1 are implemented in the Extended Kalman Filter described in section 4.1.2. On Figure 4-4 are shown the estimated and actual trajectories performed by a rover moving along a circular path with a speed $V = 1$ m/s and a constant steering angle $\alpha = 1°$, for an onboard sensor suite including or not a sun sensor. The

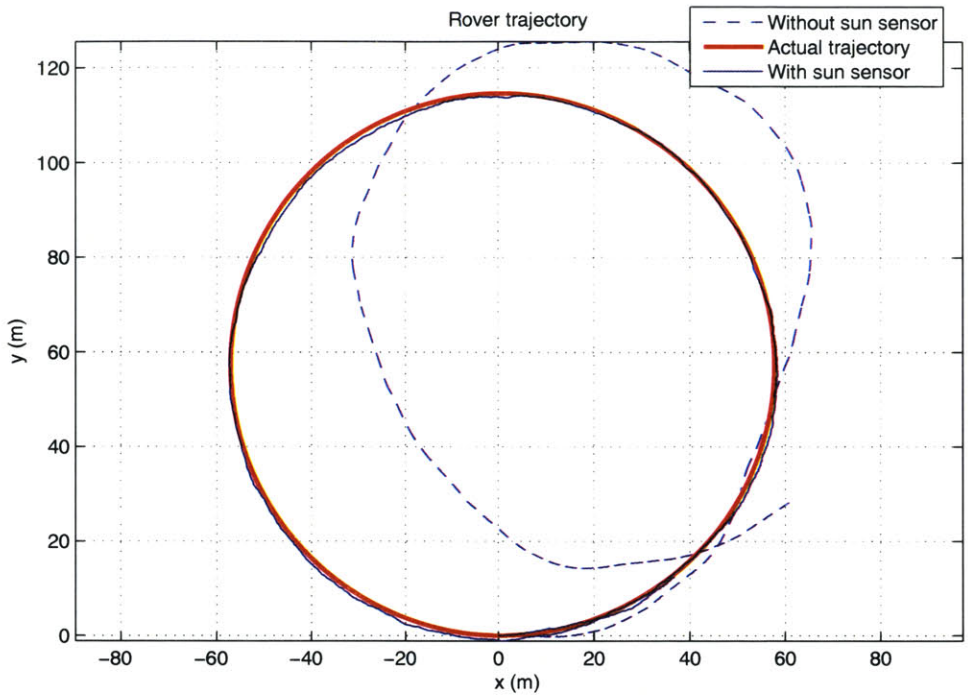

Figure 4-4: Actual and estimated rover trajectory with and without the Sun Sensor

measurement rate coming from the wheel encoders, the potentiometer and the gyro is 50 Hz, whereas the measurement rate coming from the sun sensor is only 10 Hz.

Figures 4-4, 4-5, and 4-6 show that the addition of an absolute heading sensor is essential to improve the accuracy of the onboard navigation system. Indeed, the absolute heading sensor helps to reduce periodically (the update rate from the sun sensor is here five times smaller than the update rates from the other sensors) the error in the orientation angle ϕ (the corresponding covariance matrix component stabilizes to a constant value with a sun sensor), which in turns improves the positioning accuracy.

A note about time knowledge In this study the assumption has been made that time is known to a reasonable level. Making the assumption that a time reference is available at least at the base station (which can be done by time transfer from Earth for instance), clock errors on vehicles are assumed to be computable. For instance, the clock offset and drift can be estimated via simultaneous 1–way and 2–way ranging from a time reference station, or satellite, as explained in [28].

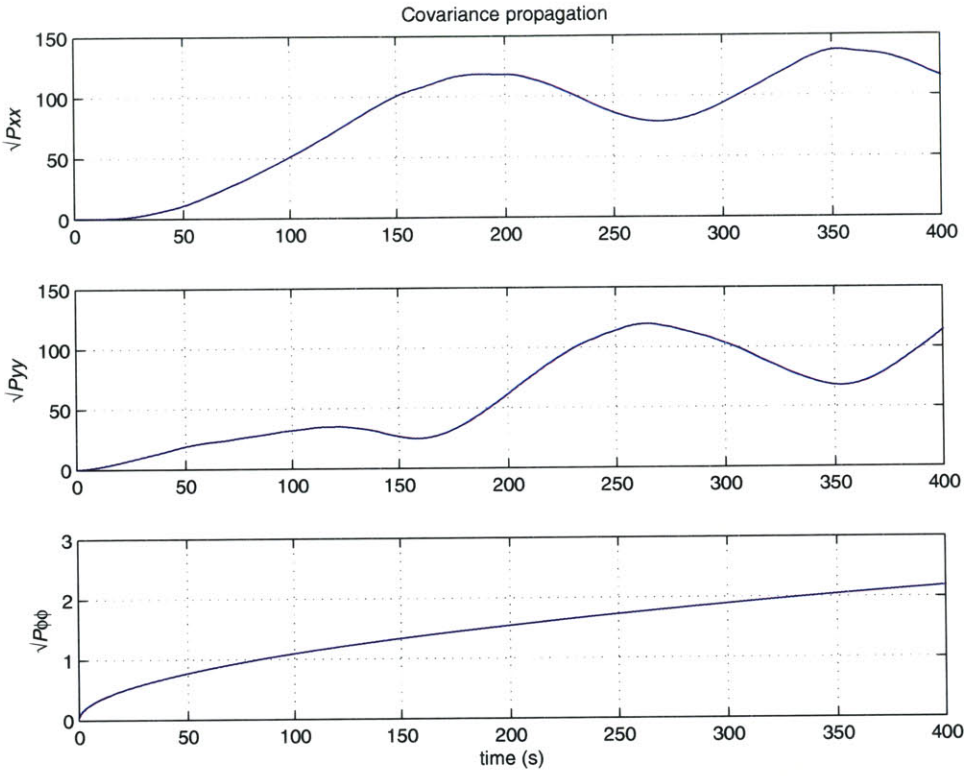

Figure 4-5: Covariance propagation, without Sun Sensor

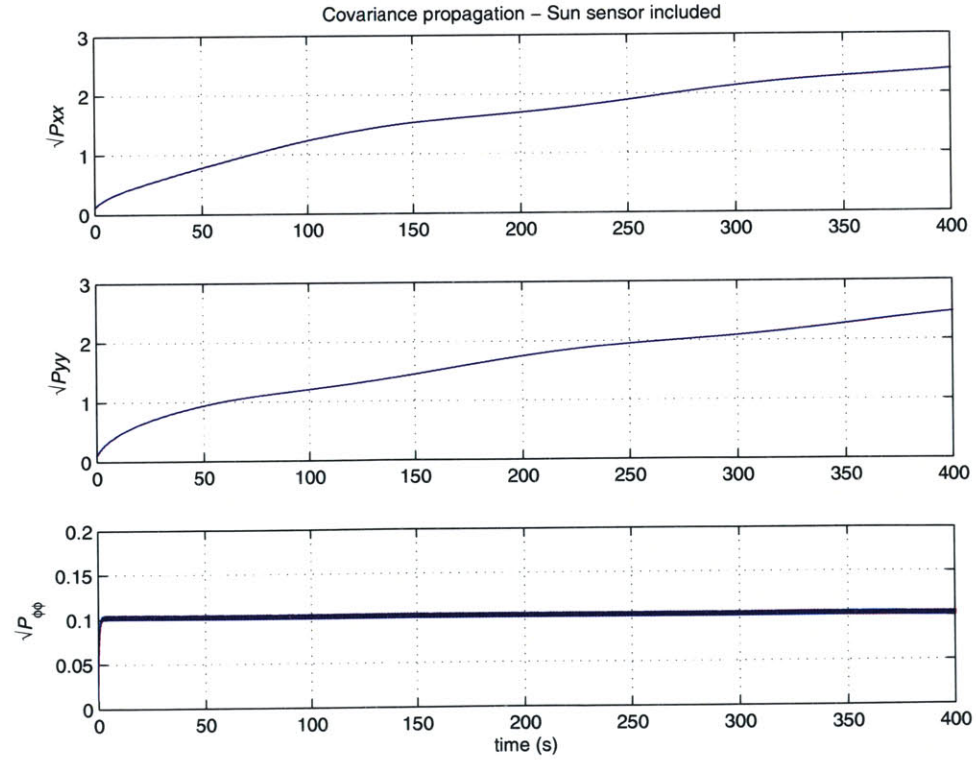

Figure 4-6: Covariance propagation, with Sun Sensor

4.2 Results and Recommendations

Most of the results presented in this section are also available in [6], which is a report written during the course of the study presented in this thesis.

4.2.1 Metrics levels definitions

The evaluation of the three architectures developed on Chapter 3 leads to the definition of the following metric levels. These levels apply to the metrics presented in Chapter 2 and will be called *Poor*, *Fair*, and *Good*, depending on the evaluation of the metric. From these three levels, only *Fair* and *Good* do correspond to satisfied requirements. The detailed choice of these levels is discussed below.

Navigation Coverage: The coverage levels can be defined in terms of surface area. From the navigation elements considered and the architectures developed, the minimal coverage is the one obtained using a ranging/heading beacon that provides line-of-sight coverage around the base station. The maximum coverage that can be provided using navigation satellites is global, or quasi-global, (i.e., the whole or most of the surface of the planet). One intermediate level is related to the capability of vision-based navigation systems as it is limited to areas where accurate elevation maps of the area explored are available. So the three coverage levels defined are

- *Poor*: Limited to Line-Of-Sight distance
- *Fair*: Limited to existing maps
- *Good*: Continental (as defined by covering at least 10% of the planet's surface)

Navigation Accuracy: The accuracy levels are defined in terms of the accuracy obtained from the whole navigation architecture. The levels are as follows

- *Poor*: $\approx$ 1km
- *Fair*: $\approx$ 100m
- *Good*: $\approx$ 10m

Navigation Operability: The definition of the operability levels is driven by two considerations. First, the navigation fix provided by a navigation constellation is available only after a certain waiting time given by the *MRT* metric. A high value lowers the operability of the navigation architecture. In addition, the use of a beacon network requires significant effort from the astronauts during setup tasks.

- *Poor*: Low operability, navigation requires intensive training and/or long navigation fixes ($MRT >$ 1hour)
- *Fair*: Medium operability, navigation requires a significant setup and/or timely navigation fixes ($MRT >$ 15min)
- *Good*: High operability, navigation is automatic and the navigation fixes are continuous or quasi-continuous ($MRT <$ 15min)

4.2.2 Minimalist architecture

The composition of the Minimalist architecture is fully described in Chapter 3. Except for the Communication Availability metric, all evaluations are identical for the Moon and Mars cases.

- **Navigation Coverage**: the Minimalist architecture offers Line-Of-Sight beacon navigation. For beyond Line-Of-Sight exploration, the only absolute navigation device is vision. So the navigation coverage is limited to the surface area where "good enough" elevation maps are available, which corresponds to the *Fair* level.
- **Navigation Accuracy**: Most of the exploration is likely to take place in areas where direct link with the base station will not be possible (beyond Line-Of-Sight), so that the navigation tasks will rely on the onboard devices. The accuracy is therefore the one achieved by the vision system (as it is used to reset the error drift caused by the other onboard devices, such as inertial sensors and odometers), and is of $\approx$ 100m, which corresponds to the *Fair* level (see section 3.3.3 for details on the vision system accuracy).

- **Navigation Operability**: The navigation operability of the Minimum architecture is once again determined by the operability of the vision system. Is is chosen to be *Medium* as the task of determining the position should be fully automated but should require the used to be in view of distinctive landmarks, which could be a constraint on the exploration paths.

- **Communication Coverage**: The communication links are possible in a disk with radius the line-of-sight distance around the base station only. So the communication coverage is *Poor*.

- **Communication Availability**: the communication availability is of $\approx 40\%$ for Mars, which is *Fair*. But for the lunar South Pole, it is 0%, which is *Poor*.

- **Maximum Gap Time**: it is of 15 hours, which is *Poor*.

- **Mass (IMLEO)**: the only offboard device is the navigation beacon at the base station, which gives a total mass of $\approx$ 16kg.

The evaluation of these top-level metrics is summarized in Table 4.2.

Table 4.2: Minimalist Architecture Evaluation

Metric	Evaluation (Mars/Moon)	Level (Mars/Moon)
Nav. Coverage	Map-limited	*Fair*
Nav. Accuracy	$\approx$ 100m	*Fair*
Nav. Operability	*Medium*	*Fair*
Comm. Coverage	LOS	*Poor*
Comm. Availability	$\approx 40\%/ \approx 0\%$	*Fair/Poor*
Max. Gap Time	15h	*Poor*
Mass	$\approx$ 16kg	*Good*

4.2.3 Simple architecture

The composition of the Simple architecture is fully described in Chapter 3. The constellation geometry is shown on Figures 4-7 (Mars) and 4-8 (Moon), in both inertial and planet-fixed reference frames. The results for the constellation analysis part are as follows:

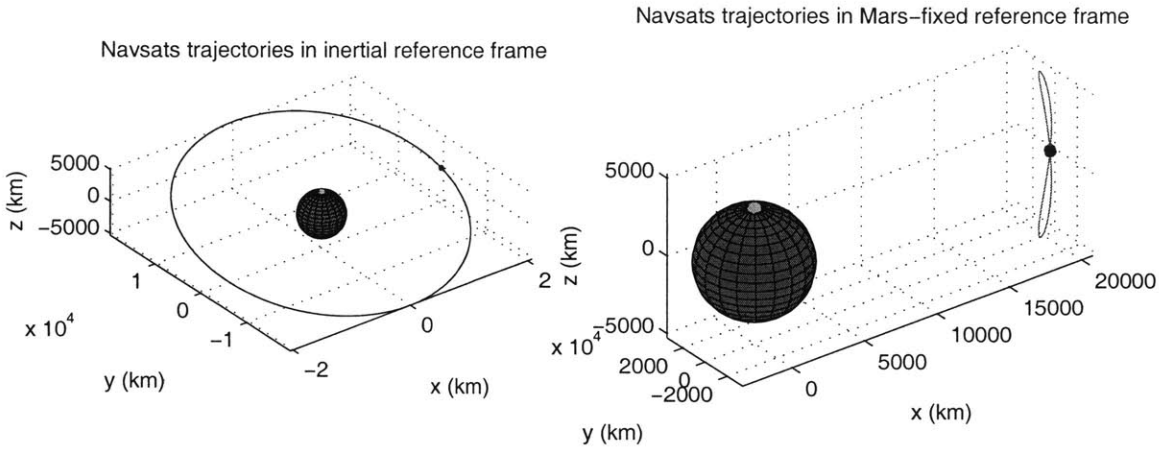

Figure 4-7: Simple architecture: Mars constellation geometry

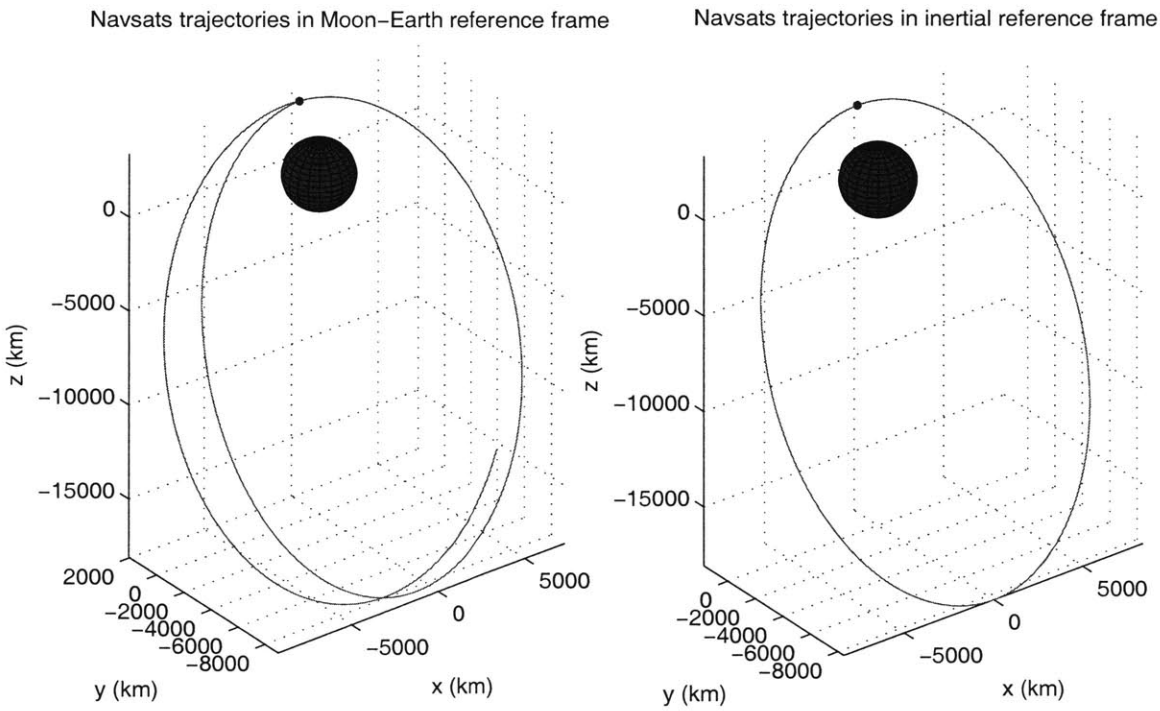

Figure 4-8: Simple architecture: Moon constellation geometry

- Mean Response Time (MRT): this metric is evaluated to $\approx$ 11h for both the Moon (South Pole) and the Mars (equator) cases.

- Navigation Coverage: both coverage metrics $Coverage_1$ and $Coverage_2$ are equal to 0% for the Simple architectures (both Moon and Mars). Indeed, the MRT values are above 1h on the whole surface of the planet. The corresponding coverage map are shown on Figures 4-9 and 4-10. The thick black curve represents the ground track of the navigation satellite, whereas the other lines are contour plots of the Mean Response Time.

In terms of top-level metrics, these results lead to the following conclusions:

- **Navigation Coverage**: As the navigation satellite does not provide with quick enough navigation fixes, the coverage is determined by the availability of elevation maps as for the Minimalist architecture. It corresponds to a *Fair* level.

- **Navigation Accuracy**: When using the vision-based navigation system, the accuracy reached is as for the Minimalist architecture of $\approx$ 100m (see section 3.3.3 for details). . The accuracy obtained with the satellite navigation fixes is of $\approx$ 20m. Nevertheless, the frequency of these fixes being very low (MRT$\approx$ 11h for both the Moon and Mars), the accuracy achieved most of the time is the one provided by the vision system. So the overall accuracy is of $\approx$ 100m, which corresponds to the *Fair* level.

- **Navigation Operability**: The operability of the vision system is evaluated to *Medium* as for the Minimalist architecture. The Mean Response Time of the satellite navigation being very low, the overall operability level is *Fair* as for the Minimalist architecture.

- **Communication Coverage**: The addition of a Nav/Comm satellite provides with continental communication coverage for both the Moon and Mars, and the corresponding level is *Good*.

- **Communication Availability**: The communication availability is $\approx$ 95% for Mars (*Good*), and $\approx$ 80% for the Moon (*Fair*).

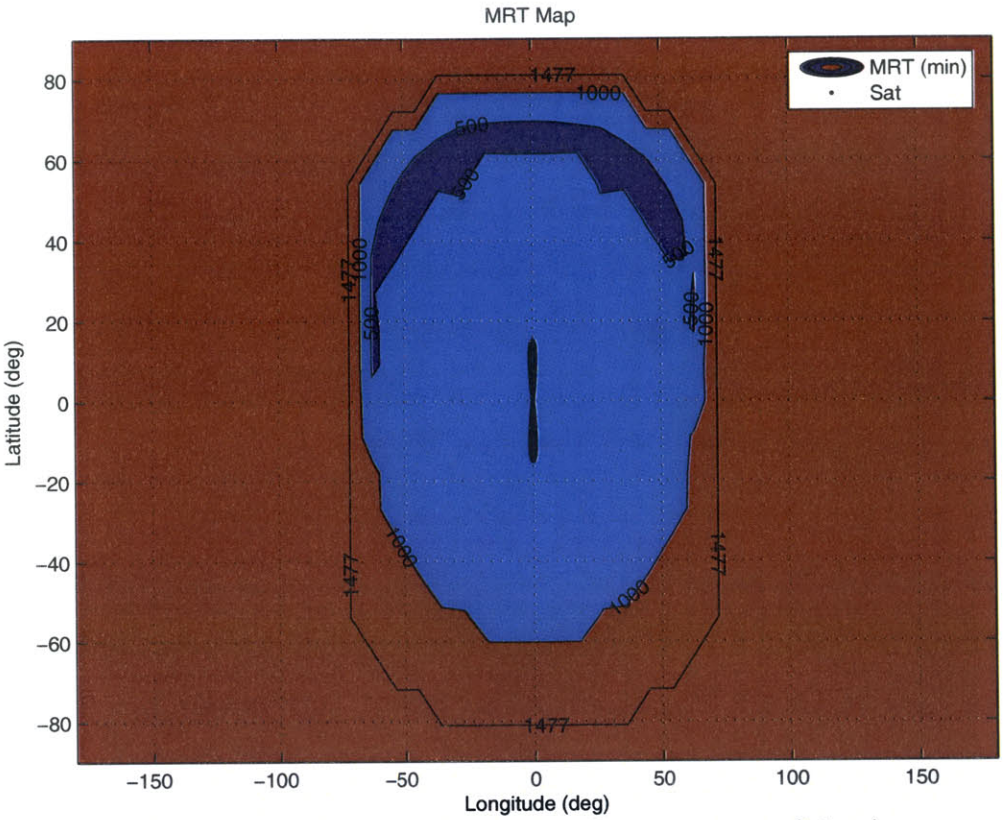

Figure 4-9: Simple architecture: Coverage map (Mars)

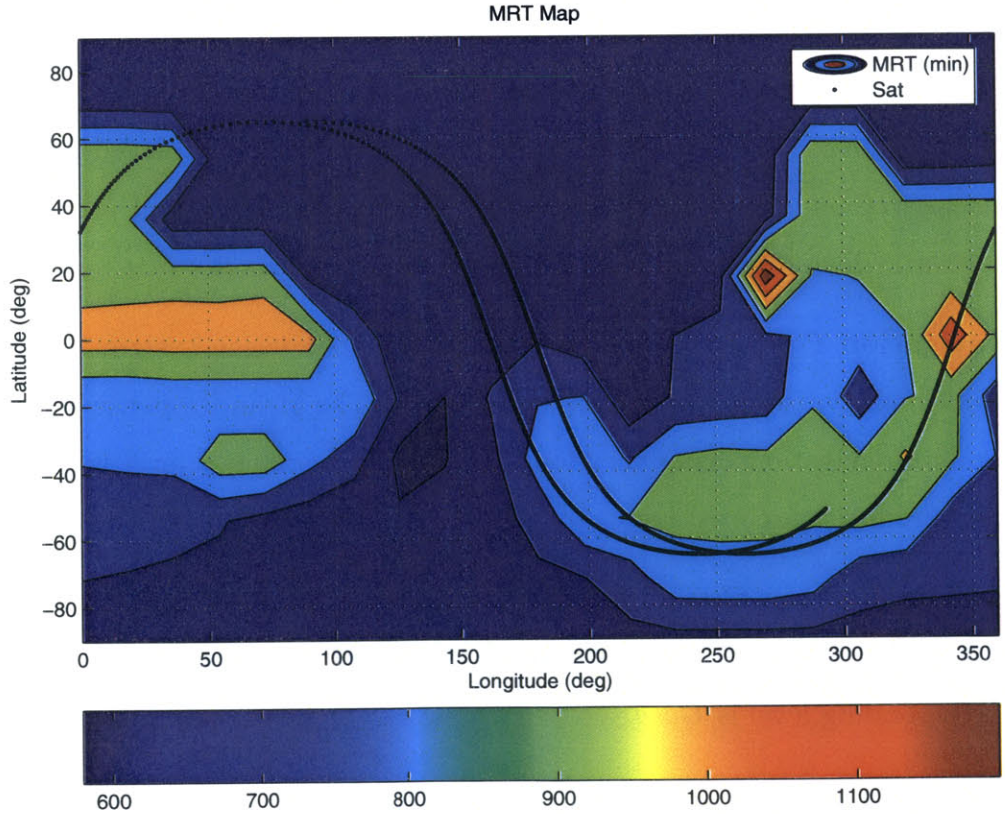

Figure 4-10: Simple architecture: Coverage map (the Moon)

Table 4.3: Simple Architecture Evaluation

Metric	Evaluation (Mars/Moon)	Level (Mars/Moon)
Nav. Coverage	Map-limited	*Fair/Fair*
Nav. Accuracy	$\approx$ 100m	*Fair*
Nav. Operability	*Medium*	*Fair*
Comm. Coverage	continental	*Good*
Comm. Availability	$\approx$ 95%/$\approx$ 80%	*Good/Fair*
Max. Gap Time	$<$ 1.5h/$\approx$ 6h	*Good/Fair*
Mass	1900kg/250kg	*Fair/Good*

- **Maximum Gap Time**: The Maximum Gap Time is $<$ 1.5h for Mars (*Good*), and $\approx$ 6 h for the Moon (*Fair*).

- **Mass (IMLEO)**: Contrary to some of the previous metrics (Communication Coverage, Communication availability, Maximum Gap Time), and as expected, the Simple architecture performs better in terms of LEO mass in the Moon case: 250kg (*Good*) than in the Mars case: 1900kg (*Fair*).

The evaluation of these top-level metrics is summarized in Table 4.3.

4.2.4 Performance architecture

The composition of the Performance architecture is fully described in Chapter 3. The constellation geometry is shown on Figures 4-11 (Mars) and 4-12 (Moon), in both inertial and planet-fixed reference frames. About the constellation analysis, the results for the intermediate metrics defined in Chapter 2 and 3 are as follows:

- Mean Response Time (MRT): this metric is evaluated to be $<$ 1min for both the Moon (user at the South Pole) and the Mars (user on the equator) cases.

- Navigation Coverage: for Mars case, $Coverage_1 = 24.2\%$ and $Coverage_2 = 20.0\%$, and for the Moon case, $Coverage_1 = 38.5\%$ and $Coverage_2 = 100\%$, so the coverage is continental for both cases which corresponds to a *Good* level. The corresponding coverage maps are shown on Figures 4-13 and 4-14. The thick black curve represents the ground track of the navigation satellite, whereas the other lines are contour plots of the Mean Response Time.

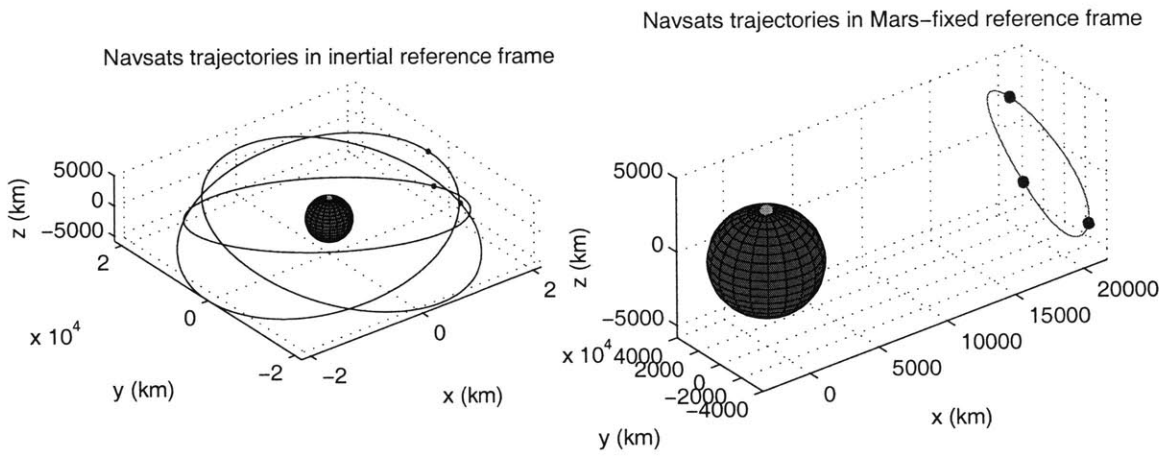

Figure 4-11: Performance architecture: Mars constellation geometry

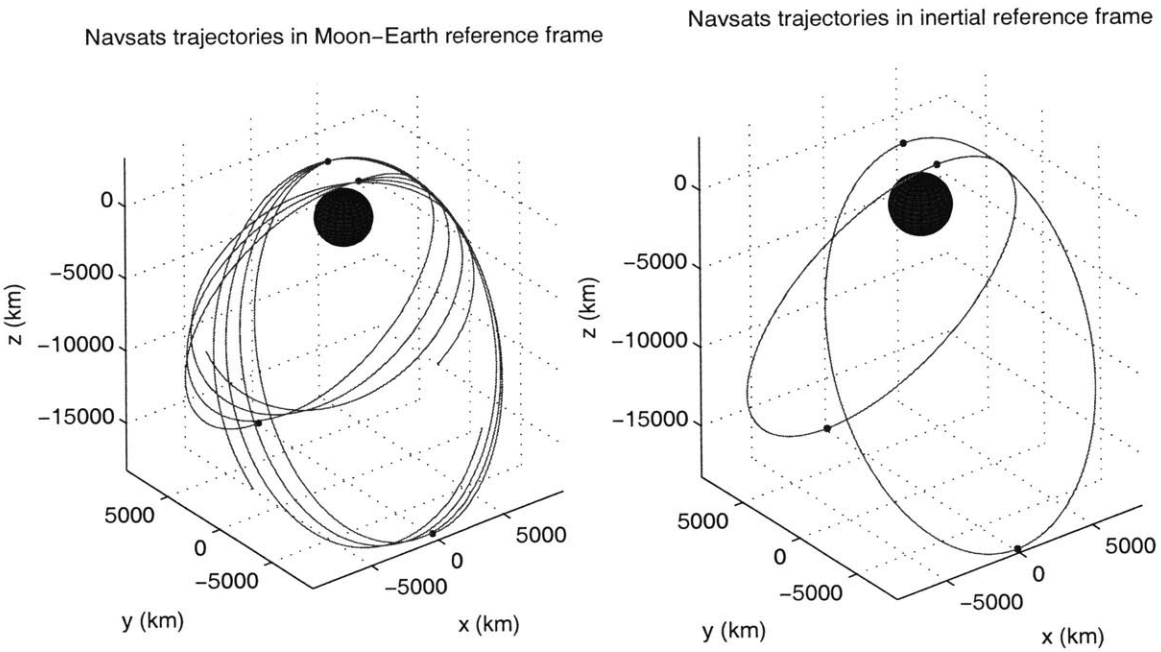

Figure 4-12: Performance architecture: Moon constellation geometry

In terms of top-level metrics, these results lead to the following conclusions:

- **Navigation Coverage**: The navigation coverage provided by the Nav/Comm constellation is continental for both the Moon and Mars, which corresponds to a *Good* level. The vision system serves here as a backup in case of constellation outages.

- **Navigation Accuracy**: The accuracy obtained with the satellite navigation fixes is of $\approx$ 20m.

- **Navigation Operability**: Due to the low Mean Response Time and the large coverage, a real-time or quasi-real-time navigation fix from the Nav/Comm constellation will be available for most of exploration activities, without requiring any effort from the astronauts. Therefore the navigation operability is *High*.

- **Communication Coverage**: As for the Simple architecture, the communication coverage is continental (*Good*).

- **Communication Availability**: The communication availability is 100% for both Mars and the Moon (*Good*).

- **Maximum Gap Time**: The Maximum Gap Time is 0h for both Mars and the Moon (*Good*).

- **Mass (IMLEO)**: Because of the heavy infrastructure due to the Nav/Comm constellation, the LEO mass is much larger than for the previous two architectures: $\approx$ 5500kg for Mars (*Poor*) and $\approx$ 1000kg (*Fair*) for the Moon.

The evaluation of these top-level metrics is summarized in Table 4.4.

4.2.5 Non-dedicated orbital asset option

The use of an existing orbital asset (e.g. the orbiting Crew Exploration Vehicle) is considered as a way to augment navigation and communications capabilities. The orbital asset parameters, as recommended by the Transportation team are as follows

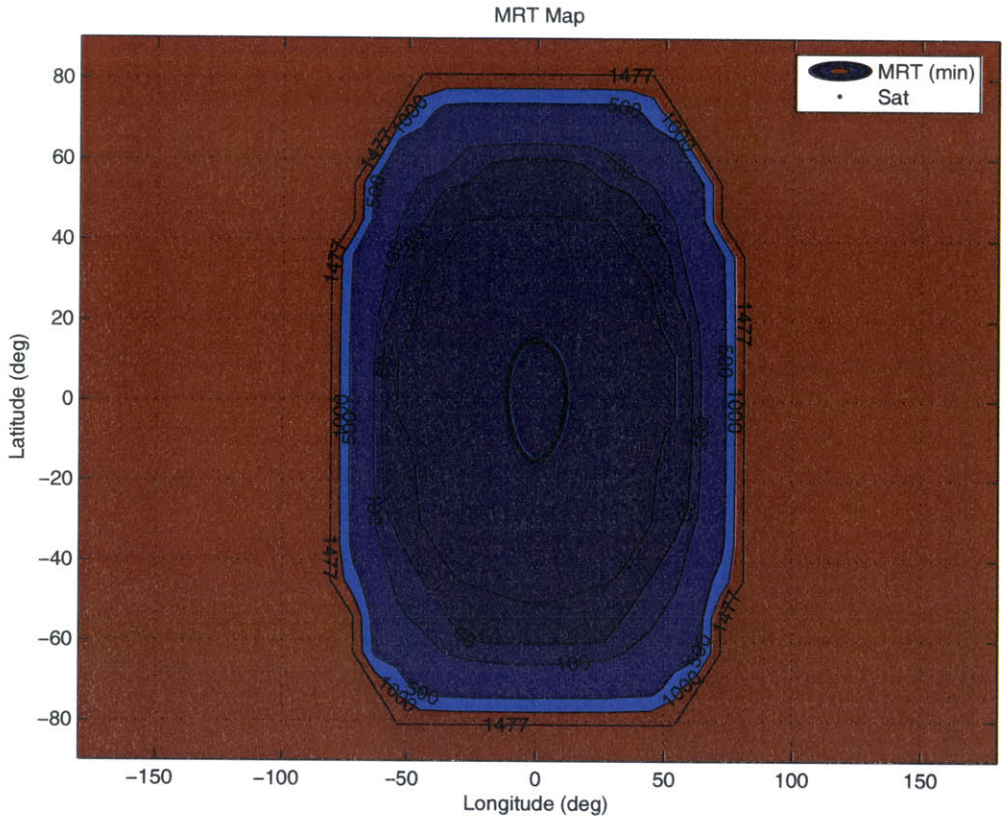

Figure 4-13: Performance architecture: Coverage map (Mars)

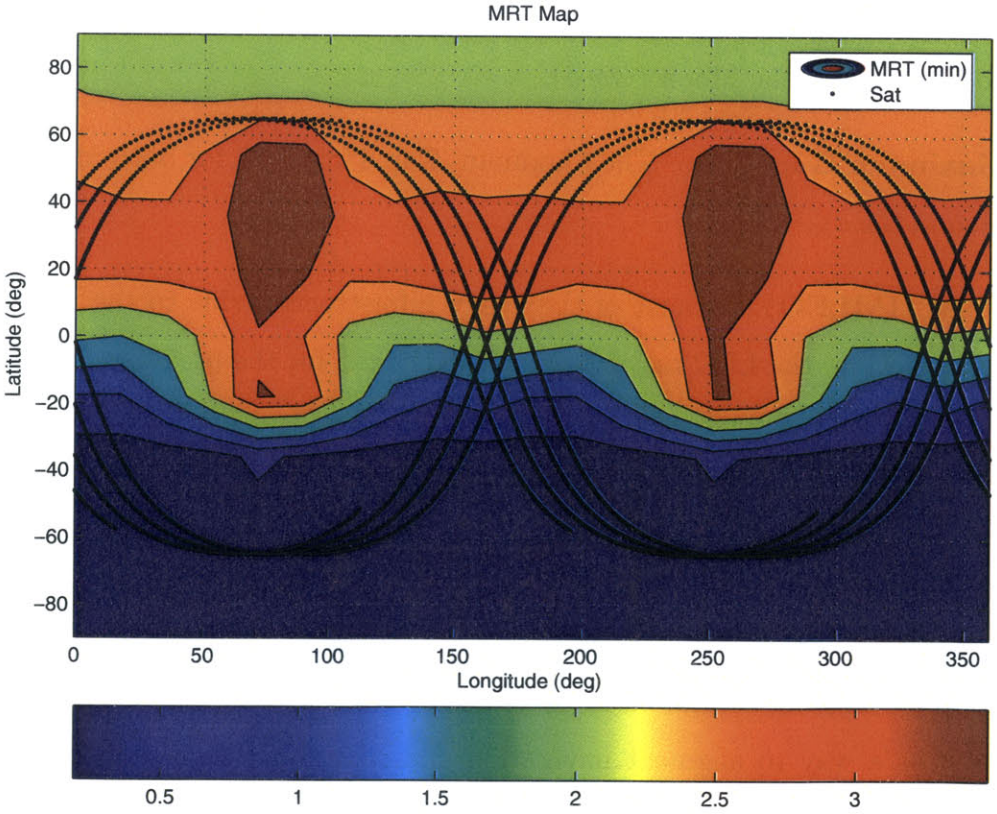

Figure 4-14: Performance architecture: Coverage map (the Moon)

Table 4.4: Performance Architecture Evaluation

Metric	Evaluation (Mars/Moon)	Level (Mars/Moon)
Nav. Coverage	continental	*Good*
Nav. Accuracy	$\approx$ 20m	*Good*
Nav. Operability	*High*	*Good*
Comm. Coverage	continental	*Good*
Comm. Availability	100%	*Good*
Max. Gap Time	0	*Good*
Mass	$\approx$ 5500kg/1000kg	*Poor/Fair*

- Moon: 100km altitude in a polar orbit
- Mars: 500km altitude in a slightly inclined equatorial orbit

This non-dedicated orbital asset is treated simply a an additional asset augmenting the Nav/Comm constellation. Therefore the analysis required to include the benefits in terms of navigation metrics obtained with this additional asset is done in the same fashion as the navigation analysis detailed in section 3.1.

The main impacts on the navigation metrics concern the MRT metric and therefore the coverage metrics $Coverage_1$ and $Coverage_2$. These changes are summarized in Tables 4.5, 4.6, and 4.7.

Table 4.5: Non-dedicated orbital asset option, Minimalist architecture

Metric	Mars	Moon South Pole
MRT	$\simeq$ 3h	$\simeq$ 12h
$Coverage_1$	0%	0%
$Coverage_2$	0%	0%

Table 4.6: Non-dedicated orbital asset option, Simple architecture

Metric	Mars	Moon South Pole
MRT	49.8min	66.8min
$Coverage_1$	7.2%	0%
$Coverage_2$	0%	0%

The most important improvements concern the simple architecture, for both the Moon and Mars. Indeed, the MRT metric is $\simeq$ 1h, instead of $\simeq$ 11h. In addition to that, the navigation coverage is now regional ($Coverage_1 = 7.2\%$) for Mars. The navigation metrics are also improved for the performance architecture, but very slightly

Table 4.7: Non-dedicated orbital asset option, Performance architecture

Metric	Mars	Moon South Pole
MRT	0min	1.11min
$Coverage_1$	26.3%	100%
$Coverage_2$	20.0%	39.4%

only, as the extra navigation satellite does not add much to the already large on-orbit infrastructure.

The resulting coverage maps are shown in Figures 4-15 and 4-16 for the Simple and Performance architectures, in the Mars case.

4.2.6 Beacon network option

As stated in Chapter 3, section 3.2, the use of any beacon network should be focused on local exploration of a small area (with dimensions similar to the Line-Of-Sight distance). The high accuracy achieved would suit most of the high precision scientific requirements.

4.3 Recommendations

One of the main deliverables of the MIT/Draper Lab team to NASA is a set of recommendations aimed at supporting the objectives of exploration. As far as navigation and communication are concerned, this set of recommendations is divided into three parts: architectures, performance and technologies. The list of these recommendations is also available in [6].

Architectures: At least one dedicated communication satellite will be needed to satisfy the communication availability requirement. For Mars, the simple architecture is recommended for the initial mission. If the traverses are kept to line-of-sight, the Minimalist architecture is recommended and gradual accretion of assets and transition to performance architecture can be achieved in two missions. For the Moon, the simple architecture provides the necessary communication availability. The minimal-

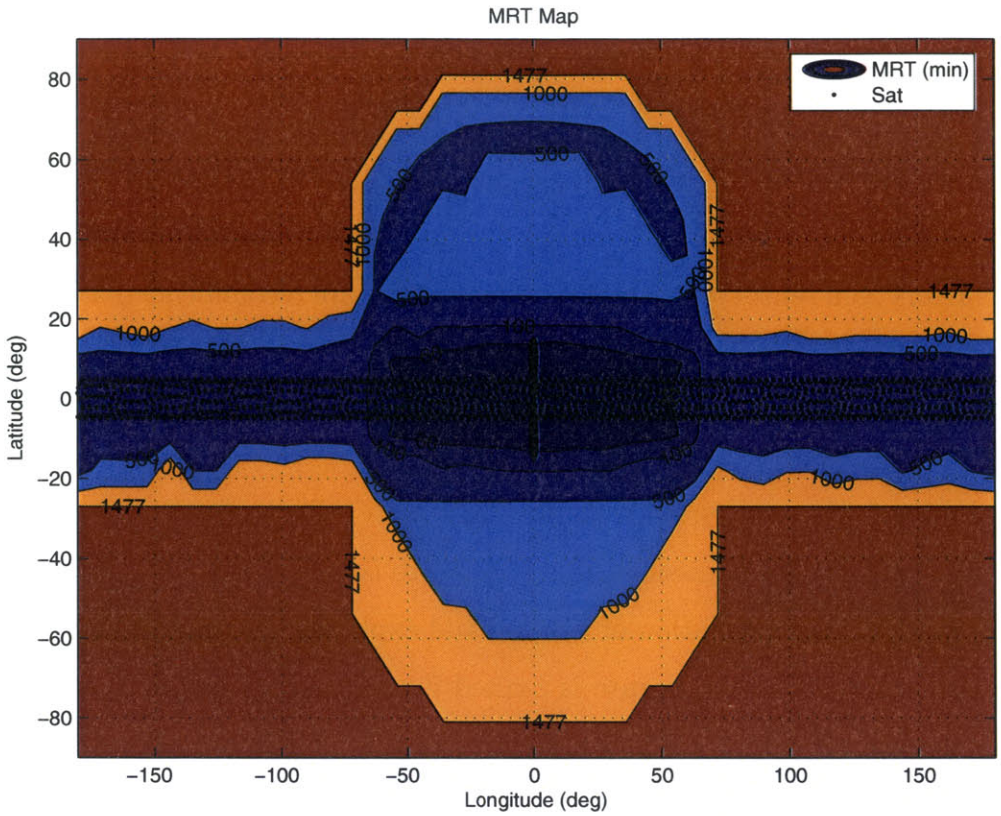

Figure 4-15: Simple architecture and additional asset: Coverage map (Mars)

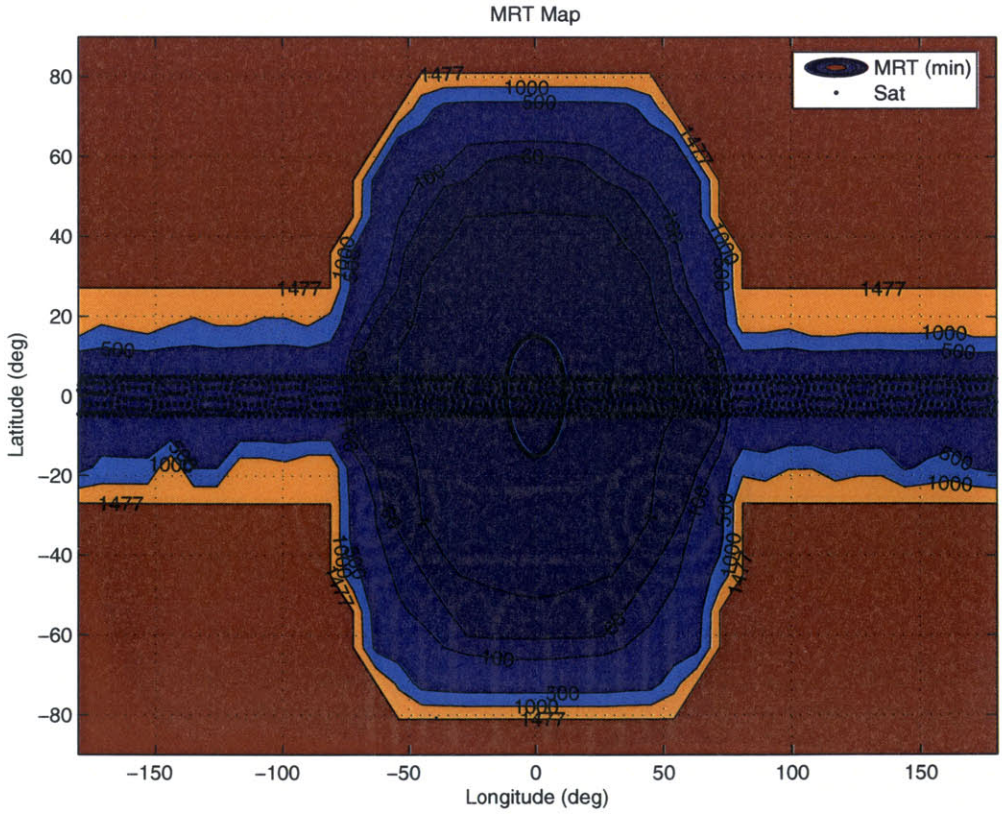

Figure 4-16: Performance architecture and additional asset: Coverage map (Mars)

ist architecture will only provide 50% availability which can be good enough for 10 day missions.

Performance: Surface beacons are recommended for cm-level navigation accuracy for local surface operations (e.g. drilling or excavation). Usual onboard (inertial sensor, odometers, sun sensor) sensors and vision system are recommended as the fundamental navigation equipment. Satellite constellations are recommended for "Earth-like" navigation and communication capabilities over continental distances.

Technologies: No existing or planned satellites are still expected to be operational by the time manned Mars missions are expected to launch. Prior imaging missions is key for precision map generation of landing and exploration sites. As far as communication is concerned, the data rate is limited by the rover power and antenna size. Moon exploration is a real validation step for testing new information technologies, devices and designs.

Chapter 5

Analysis of Formation Flying Dynamic Models Around L_2

5.1 Introduction

5.1.1 Libration points

The three-body problem is the problem of describing the motion of three particles, each of these being under the gravitational attraction of the other two. The first solutions of this problem were described by Joseph-Louis Lagrange in his memoir *Essai sur le Problème des Trois Corps*, which won the prize from the Académie des Sciences of Paris in 1772. In the so-called *restricted three-body problem*, one of the three masses is considered infinitesimal, so that it does not perturb the motion of the other two, called *the primaries*. These two are considered to rotate about their common center of gravity. When this motion is assumed to be circular, the problem is called *the circular restricted three-body problem*. This model is well suited to the study of the motion of a spacecraft in the Earth-Moon or Sun-Earth systems, for instance.

This dynamical problem has five equilibrium points in the reference frame that rotates with the two primaries (*the synodic coordinates*), called *libration points* or *Lagrange points*. Their location is illustrated in Fig. 5-1. At these points the gravi-

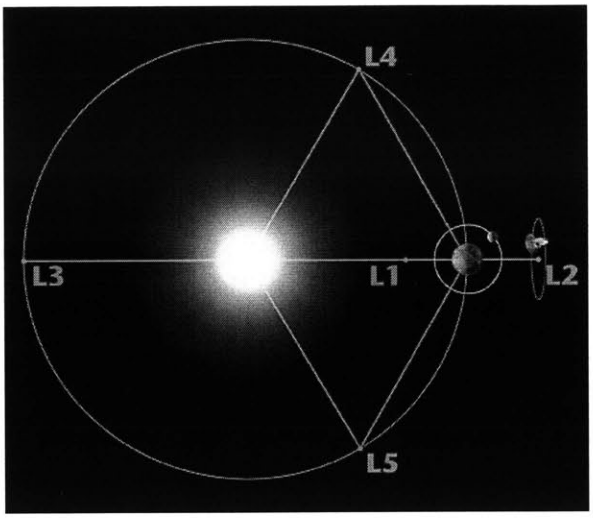

Figure 5-1: Lagrangian points in the Sun-Earth system [34]

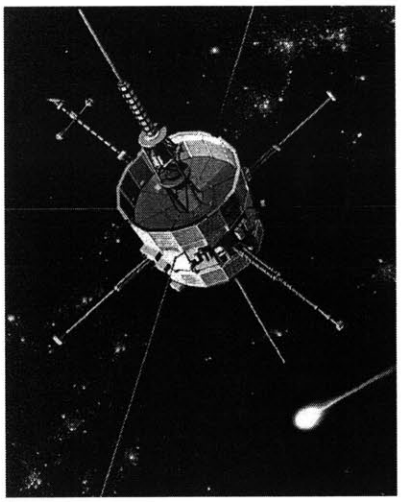

Figure 5-2: ISEE-3 Spacecraft [36]

tational forces from the two primaries equilibrate the centripetal acceleration due to the rotation of the system with respect to inertial space.

Of the five Libration points, three are on the line joining both primaries. They are L_1 (between the primaries), L_2 (closer to the smaller primary), and L_3 (closer to the bigger primary), and they are called the *collinear points*. The other two (L_4 and L_5) are at the vertices of two equilateral triangles formed with the primaries, symmetric with respect to the line joining the primaries. These are called the *triangular points*. The collinear points are unstable, while L_4 and L_5 are stable for the Sun-Earth system (their stability relies on a condition on the ratio of the two primaries' masses which is satisfied in the Sun-Earth case [33, 34]).

Despite their natural instability, the collinear points of the Sun-Earth system are places of great interest for space missions (some examples being given below). Firstly they are fixed with respect to the two primaries, among them the Earth. In addition to that, in the restricted problem one can find near these points periodic orbits called *halo orbits* and quasi-periodic orbits called *Lissajous orbits*, which make them suitable for space missions. ISEE-3 was the first libration point mission in 1978. It stayed in a halo orbit for 3.5 years. Seventeen years later, the Solar and Heliospheric Observatory Satellite SOHO [35] traveled to the L_1 point of the Sun-Earth system,

which is particularly well-suited for solar observatories.

The L_2 libration point is a very good location for science such as cosmic background observation. The observing efficiency is excellent because the Sun, Earth, and Moon are always behind the instrument's field of view. It also allows great protection from the Earth's disturbances (such as microwave emission and magnetic field) because of its distance (1.5 million km from Earth). L_2 is the location of the Wilkinson Microwave Anisotropy Probe, who was the first mission to the Earth-Sun L_2 point [34]. It also provides for a very stable thermal environment.

In addition to these interesting properties, the very low differential gravity effects around libration points makes them a good location for formation flight missions. Many interferometry mission concepts have been proposed that form a large aperture using a formation of several spacecraft with precisely controlled relative positions. The following focuses on the L_2 point of the Sun-Earth system, which is the location chosen for several proposed formation flying missions, including the MicroArcsecond X-ray Imaging Mission (MAXIM) (see [38] and [37] for instance).

5.1.2 Problem statement and methodology

The Circular Restricted Three Body Problem (CRTBP), see Section 5.2.1 is a highly nonlinear dynamics problem. And although some results are available from linear analysis, in particular to assess the stability of the points themselves or study quasi-periodic Lissajous orbits [39, 40], one has to tackle the fully nonlinear problem to study other phenomena, such as halo orbits. Accordingly the relative dynamics of formation flight around libration points as derived from the CRTBP are highly nonlinear too. Though this nonlinear aspect, lots of publications on libration points dynamics [43, 44] are focused on the development of simpler, linear models for specific applications such as formation flight control around collinear points. These simpler models do not predict the relative motion as well, which can lead to poor navigation estimates and control performance, but they take much less computational effort and are easier to implement. So there is clearly a trade-off between model fidelity and complexity. The objective of this research was to assess the quality of these different dynamical

models of the relative motion of two spacecraft in orbit around Sun-Earth L_2.

To do this analysis, one possibility is to perform open-loop simulation and capture the difference between each model and the reference model and it is a way to capture intrinsic fidelity of each model. But a important consequence of model choice is its impact on fuel cost when implemented in a controller. Therefore we also performed closed-loop simulations with different controllers, which gives an evaluation of modeling errors on fuel costs. More precisely, each of these model has been implemented in an optimal controller and they have been compared to each other in the performance (as given by the mean error between the desired and actual states) vs. fuel plane.

5.2 Libration Point Dynamics

5.2.1 The Circular Restricted Three Body Problem

Here are the main assumptions of the Circular Restricted Three Body Problem, or CRTBP, on which our analysis is based:

- the gravitational forces of the two primaries are the only forces taken into account;
- the third body's mass is neglected;
- the eccentricity of the orbit of the Earth around the Sun is neglected, so that the motion of the primaries is considered to be circular about their common center of mass.

To study this problem, it is far more convenient to use a coordinate system fixed with the two primaries, i.e. that rotates with them with respect to inertial space (these are the *synodic coordinates*). Let M_1 and M_2 be the masses of the two primaries, with $M_1 > M_2$. In our case M_1 will be the mass of the Sun, and M_2 will be the mass of the Earth-Moon barycenter. Let now $\mu = \frac{M_2}{M_1+M_2}$ be the ratio of the smaller mass with the sum of the two masses. Let the origin of the rotating reference frame be L_2 for convenience. Now the x-axis will be aligned with the L_2-Earth-Sun line, pointing this way, the y-axis is perpendicular to the x-axis and in the plane of rotation of the

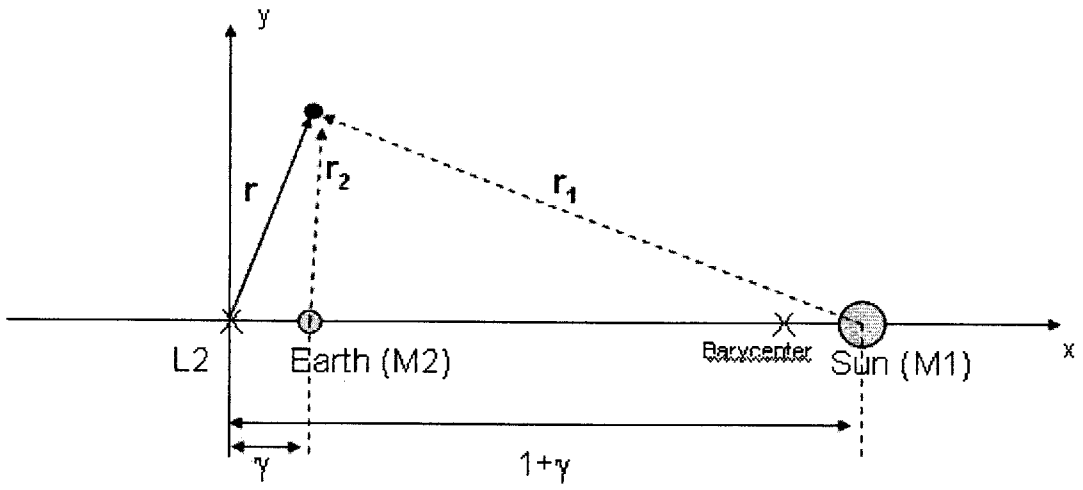

Figure 5-3: Coordinate axis definition

primaries, and the z-axis is such that $(L_2;\overrightarrow{e_x}, \overrightarrow{e_y}, \overrightarrow{e_z})$ is a right-handed reference frame. A picture of the above description can be seen in Fig. 5-3.

For simplicity, the following uses dimensionless values. Let d be the distance between the two primaries, then

$$\bar{x} = \frac{x}{d},\ \bar{y} = \frac{y}{d},\ \bar{z} = \frac{z}{d} \tag{5.1}$$

are the dimensionless coordinates, which will be simply denoted as x, y and z. γ is the dimensionless distance from L_2 to the Earth. Similarly, the mean motion of the Earth-Moon barycenter around the Sun is

$$n = \sqrt{\frac{G(M_1 + M_2)}{d^3}} \tag{5.2}$$

Define $\tau = nt$ as the dimensionless time, and convert all derivatives so that they are done with respect to τ, where

$$\frac{d}{d\tau} = \frac{1}{n}\frac{d}{dt} \tag{5.3}$$

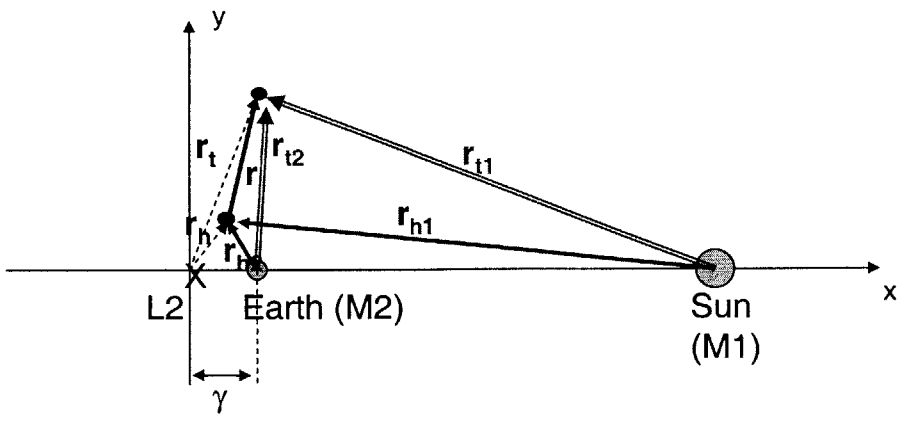

Figure 5-4: Coordinate axis definition

Using the above conventions and notation, the derivation of the equations of motion leads to the following set of dimensionless equations (see [42] for more details)

$$\begin{aligned}
\ddot{x} - 2\dot{y} - x &= -(1+\gamma-\mu) - \frac{1-\mu}{r_1^3}(x-\gamma-1) - \frac{\mu}{r_2^3}(x-\gamma) \\
\ddot{y} + 2\dot{x} - y &= -(\frac{1-\mu}{r_1^3} + \frac{\mu}{r_2^3})y \\
\ddot{z} &= -(\frac{1-\mu}{r_1^3} + \frac{\mu}{r_2^3})z
\end{aligned} \tag{5.4}$$

where r_1 and r_2 are the distances from the primaries to the spacecraft

$$\begin{aligned}
r_1 &= \sqrt{(x-\gamma-1)^2 + y^2 + z^2} \\
r_2 &= \sqrt{(x-\gamma)^2 + y^2 + z^2}
\end{aligned} \tag{5.5}$$

5.2.2 Relative flight dynamics

In the formation considered, one *telescope* spacecraft (subscript t) is in motion with respect to one *hub* spacecraft (subscript h), called the *relative motion.* Fig. 5-3 shows the notation chosen for the analysis of the relative motion. Note that all letters without subscripts denote relative variables (x, y, z, and r).

The equations for the relative motion are derived from the equations 5.4 for the absolute motion described above. These equations are simply the difference between

the equations for the telescope spacecraft and the equations for the hub spacecraft, which leads to the following set of equations

$$\begin{aligned}
\ddot{x} - 2\dot{y} - x = & -(1-\mu)(\tfrac{1}{r_{t1}^3} - \tfrac{1}{r_{h1}^3})(x_h - \gamma - 1) - \mu(\tfrac{1}{r_{t2}^3} - \tfrac{1}{r_{h2}^3})(x_h - \gamma) - (\tfrac{1-\mu}{r_{t1}^3} + \tfrac{\mu}{r_{t2}^3})x \\
\ddot{y} + 2\dot{x} - y = & -(1-\mu)(\tfrac{1}{r_{t1}^3} - \tfrac{1}{r_{h1}^3})y_h - \mu(\tfrac{1}{r_{t2}^3} - \tfrac{1}{r_{h2}^3})y_h - (\tfrac{1-\mu}{r_{t1}^3} + \tfrac{\mu}{r_{t2}^3})y \\
\ddot{z} = & -(1-\mu)(\tfrac{1}{r_{t1}^3} - \tfrac{1}{r_{h1}^3})z_h - \mu(\tfrac{1}{r_{t2}^3} - \tfrac{1}{r_{h2}^3})z_h - (\tfrac{1-\mu}{r_{t1}^3} + \tfrac{\mu}{r_{t2}^3})z
\end{aligned} \tag{5.6}$$

5.3 Hub Motion Description

This section discusses the orbit of the hub spacecraft around L_2 (the *absolute orbit*) in more detail.

5.3.1 Linearized motion and existence of periodic and quasi-periodic orbits

Despite the instability of L_2, it is possible to find quasi-periodic (*Lissajous*) orbits and periodic (*halo*, as called by R. Farquhar in 1968) orbits around L_2, under the assumptions of the CRTBP. These orbits can be found analytically, using a form of the Lindstedt-Poincaré method to constrain solutions to be periodic or quasi-periodic, from the equations of motion 5.4. Refs. [42, 39, 40] give a complete explanation of this analytical method. To provide some insights into the existence of these orbits the simpler case of linearized equations is treated below. The linearized form of Eq. 5.4 are

$$\begin{aligned}
\ddot{x} - 2\dot{y} - (1 + 2c_2)x &= 0 \\
\ddot{y} + 2\dot{x} - (1 - c_2)y &= 0 \\
\ddot{z} + c_2 z &= 0
\end{aligned} \tag{5.7}$$

with $c_n = \frac{1}{\gamma^{n+1}}[\mu + (1-\mu)(\frac{\gamma}{1+\gamma})^{n+1}]$. Eq. 5.7 shows that the motion in the z-direction is harmonic and decoupled from the motion in the x–y plane. The motion in the x–y

plane is described by the following set of equations

$$\dot{\mathbf{x}} = \begin{bmatrix} 0 & 0 & 1 & 0 \\ 0 & 0 & 0 & 1 \\ 1+2c_2 & 0 & 0 & 2 \\ 0 & 1-c_2 & -2 & 0 \end{bmatrix} \mathbf{x} \tag{5.8}$$

with

$$\mathbf{x} = \begin{bmatrix} x \\ y \\ \dot{x} \\ \dot{y} \end{bmatrix} \tag{5.9}$$

With $c_2 \simeq 4$, this system has two imaginary eigenvalues and two real eigenvalues of opposite signs. Therefore arbitrarily chosen initial conditions will lead to unbounded trajectories because of the real positive eigenvalue. However, as shown in [39], it is possible to chose initial conditions so that only the oscillatory modes (corresponding to the imaginary eigenvalues) are excited, and in this case the solution of the linearized equations is

$$\begin{aligned} x(t) &= -A_x \cos(\lambda t + \phi) \\ y(t) &= kA_x \sin(\lambda t + \phi) \\ z(t) &= A_z \sin(\nu t + \psi) \end{aligned} \tag{5.10}$$

where $k = \frac{1}{2\lambda}(1 + 2c_2 + \lambda^2)$. These are the equations of a quasi-periodic motion as the ratio of the in-plane and out-of-plane frequencies $\frac{\lambda}{\nu}$ is generally irrational (this motion is usually called *Lissajous orbit*)

Periodic motion will occur when the two frequencies λ and ν are equal, and it can be shown that this will happen with large enough amplitudes A_x and A_z (see [42, 39] for instance). In this case, the linearized solution is

$$\begin{aligned} x(t) &= -A_x \cos(\lambda t + \phi) \\ y(t) &= kA_x \sin(\lambda t + \phi) \\ z(t) &= A_z \sin(\lambda t + \psi) \end{aligned} \tag{5.11}$$

and the use of the Lindstedt-Poincaré method [42, 39, 40] leads to the following constraints on the amplitude and phase-angles

$$l_1 A_x^2 + l_2 A_z^2 + \lambda^2 - c_2 = 0 \tag{5.12}$$

$$\psi - \phi = m\frac{\pi}{2} \ (m = 1, 3) \tag{5.13}$$

with l_1 and l_2 being constants that can be found in [39]. The amplitude constraint gives the minimum permissible value for the amplitude A_x (obtained for a planar orbit where $A_z = 0$), which is about 200,000km.

5.3.2 Numerical method to find halo orbits

Halo orbits can be generated with an iterative numerical refinement of the initial conditions according to a method described in [41].

The set of equations 5.4 can be written in the more compact form $\dot{\mathbf{x}} = \mathbf{f}(\mathbf{x})$, with $\mathbf{x} = [x, y, z, \dot{x}, \dot{y}, \dot{z}]^T$. The linearization of this set of equations about any trajectory $\mathbf{x}_{ref}$ gives

$$\delta\dot{\mathbf{x}} = \left(\frac{\partial \mathbf{f}}{\partial \mathbf{x}}\right)_{\mathbf{x}_{ref}} \delta\mathbf{x} \Rightarrow \delta\dot{\mathbf{x}} = \mathbf{A}(t)\delta\mathbf{x} \tag{5.14}$$

The state transition matrix $\mathbf{\Phi}(t, 0)$ is subject to the following differential equation, called the *variational equations*

$$\frac{d}{dt}\mathbf{\Phi}(t, 0) = \mathbf{A}(t)\mathbf{\Phi}(t, 0) \tag{5.15}$$

with the initial condition

$$\mathbf{\Phi}(0, 0) = \mathbf{I}_{6\times 6} \tag{5.16}$$

Eq. 5.15 will be integrated along the trajectory as the method presented in this section requires values of the state transition matrix $\mathbf{\Phi}$ at some given times.

A closed, periodic trajectory such as a halo orbit is a natural choice for placing a formation of satellites in the vicinity of L_2, but this is a complicated design process because any motion about L_2 is generally unstable, and only certain non-trivial initial

conditions will lead to the desired halo orbit about L_2.

There are different techniques that can be used to find these initial conditions. For instance, it is possible to compute analytical approximations of periodic solutions of the CRTBP, using the Lindstedt-Poincaré method. Then both the initial conditions and the whole trajectory are obtained. The problem with this technique is that it only provides approximate values for the initial conditions, which do not provide perfectly closed orbit when the trajectory is numerically integrated. So this method is rather used as a way to get a first guess for a possible numerical iterative refinement of these initial conditions. Such a numerical method is described below, using the state transition matrix introduced in the previous paragraph. This approach has been presented in [40] and [41] but it rarely mentioned in more recent literature on the topic.

As shown in the literature, halo orbits are periodic orbits that are symmetric with respect to the $y = 0$ plane in the coordinate system shown in Fig. 5-3 [42]. Starting from the $y = 0$ plane, the initial state vector should therefore be of the form $\mathbf{x_0} = [x_0, 0, z_0, 0, \dot{y}_0, 0]^T$. After a half-period (or half-cycle) the trajectory will again cross the $y = 0$ plane, with a velocity vector that should be perpendicular to this plane, so that $\mathbf{x_1} = [x_1, 0, z_1, 0, \dot{y}_1, 0]^T$ at $t = T/2 = t_1$. This condition is typically not satisfied after the first iteration using the approximate initial conditions. However, any component of the velocity vector at $t = t_1$ not perpendicular to the $y = 0$ plane can be used to correct the initial conditions via the state transition matrix $\mathbf{\Phi}(t_1, 0)$ at the end of a half-cycle.

From the definition of the state transition matrix

$$\mathbf{x}(t) = \mathbf{\Phi}(t, 0)\mathbf{x_0} \tag{5.17}$$

Differentiating with respect to both the initial state vector $\mathbf{x_0}$ and the half-cycle time t_1 (since the half-cycle time must also be corrected during the iteration), and taking

the derivative at the half-cycle time

$$\delta \mathbf{x_1} = \mathbf{\Phi}(t_1, 0)\delta \mathbf{x_0} + \dot{\mathbf{x}}_\mathbf{1}\delta t_1 \tag{5.18}$$

It is straightforward to compute deviations from the desired values of $\dot{x}_1$ and $\dot{z}_1$ at the half-cycle, as both are equal to 0 for a halo orbit, as explained above. So only the following subset of equations must be considered

$$\begin{bmatrix} \delta\dot{x}_1 \\ \delta\dot{z}_1 \end{bmatrix} = \begin{bmatrix} \Phi_{41} & \Phi_{43} & \Phi_{45} \\ \Phi_{61} & \Phi_{63} & \Phi_{65} \end{bmatrix} \begin{bmatrix} \delta x_0 \\ \delta z_0 \\ \delta\dot{y}_0 \end{bmatrix} + \begin{bmatrix} \delta\ddot{x}_1 \\ \delta\ddot{z}_1 \end{bmatrix} \delta t \tag{5.19}$$

By fixing δx_0, Eq. 5.19 reduces to

$$\begin{bmatrix} \delta\dot{x}_1 \\ \delta\dot{z}_1 \end{bmatrix} = \begin{bmatrix} \Phi_{43} & \Phi_{45} \\ \Phi_{63} & \Phi_{65} \end{bmatrix} \begin{bmatrix} \delta z_0 \\ \delta\dot{y}_0 \end{bmatrix} + \begin{bmatrix} \delta\ddot{x}_1 \\ \delta\ddot{z}_1 \end{bmatrix} \delta t \tag{5.20}$$

which, combined with Eq. 5.18 gives

$$\delta y_1 = \begin{bmatrix} \Phi_{23} & \Phi_{25} \end{bmatrix} \begin{bmatrix} \delta z_0 \\ \delta\dot{y}_0 \end{bmatrix} + \dot{y}_1\delta t \tag{5.21}$$

At the crossing of the $y = 0$ plane, $\delta y_1 = 0$, so it is possible to eliminate δt in Eq. 5.20 using Eq. 5.21, which yields a relationship between the velocity components at the half-cycle time to small changes to the initial conditions

$$\begin{bmatrix} \delta\dot{x}_1 \\ \delta\dot{z}_1 \end{bmatrix} = \left\{ \begin{bmatrix} \Phi_{43} & \Phi_{45} \\ \Phi_{63} & \Phi_{65} \end{bmatrix} - \frac{1}{\dot{y}_1} \begin{bmatrix} \delta\ddot{x}_1 \\ \delta\ddot{z}_1 \end{bmatrix} \begin{bmatrix} \Phi_{23} & \Phi_{25} \end{bmatrix} \right\} \begin{bmatrix} \delta z_0 \\ \delta\dot{y}_0 \end{bmatrix} \tag{5.22}$$

For a periodic orbit

$$\begin{bmatrix} \delta\dot{x}_1 \\ \delta\dot{z}_1 \end{bmatrix} = 0 \tag{5.23}$$

and x_0 is given and fixed. Starting with a first guess for the other initial conditions

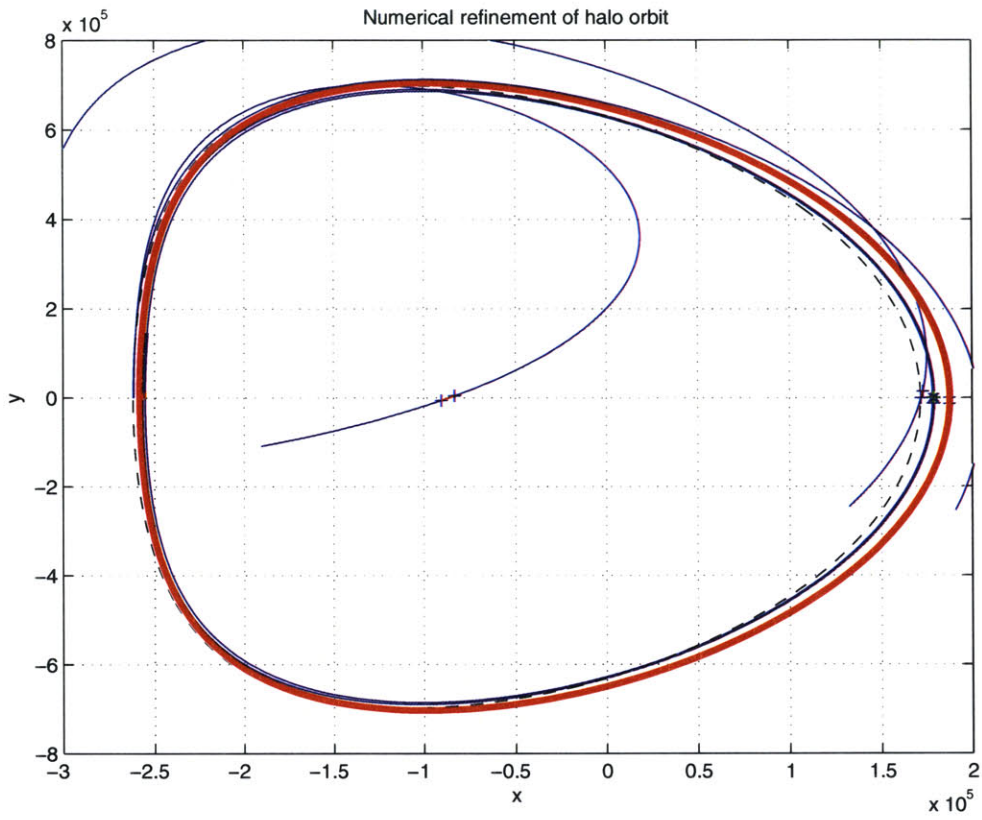

Figure 5-5: Numerical refinement of the initial conditions

z_0 and $\dot{y}_0$ (e.g., from an approximate analytical solution such as the one in [39]) the trajectory is numerically integrated until the crossing of the $y = 0$ plane. At this point, the correction to be applied to the initial conditions δz_0 and $\delta \dot{y}_0$ is computed from the velocity vector components and Eq. 5.22, and then the integration is repeated. Typically 5–6 iterations leads to a very good result ($\delta \dot{x}_1$ and $\delta \dot{z}_1$ less than 10^{-11}, dimensionless values). Fig. 5-5 shows the $x - y$ projection of a halo orbit obtained through this method.

The halo orbit in this example has an x amplitude of $A_x = 220,000km$. L_2 is at the origin, the Earth and the Sun are on the positive x-axis, in this order. The dashed line shows the orbit as given by the analytical formulation. The 5 thin trajectories correspond to the 5 iterations that had to be done before reaching a closed orbit. The thick line is the result of the 6th iteration and corresponds to a closed halo orbit.

The "deviation" from the halo orbit at each iteration can be defined as being the square root of the sum of the velocity vector components $\delta \dot{x}_1$ and $\delta \dot{z}_1$, as these are

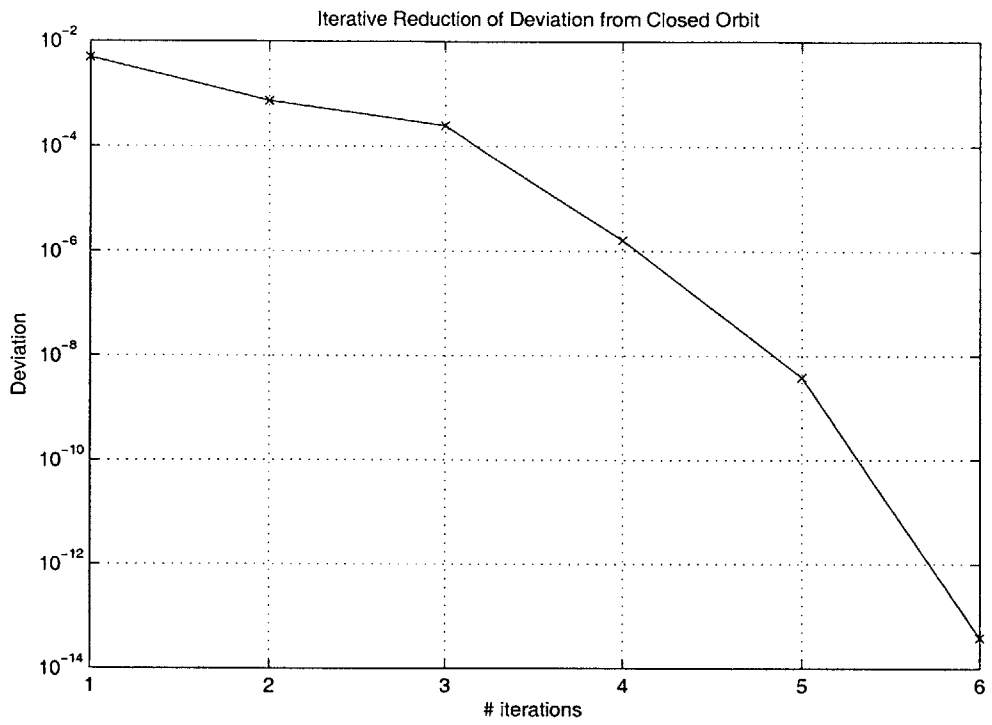

Figure 5-6: Iterative reduction of the deviation from a closed orbit

the variables that are brought to 0 through the iterative process

$$Deviation = \sqrt{\delta\dot{x}_1^2 + \delta\dot{z}_1^2} \tag{5.24}$$

The reduction of the deviation is shown in Figure 5-6.

5.4 Relative Flight Dynamics Models

5.4.1 Series expansion

Several approximations of the full nonlinear reference model 5.6 have been developed in recent literature. To obtain them, the procedure chosen here is to expand the nonlinear terms of the form $\frac{1}{r^3}$ in Eq. 5.6. The algebraic development presented below is mostly based on [43]. The series expansion that follows consists of terms that will be ordered according to their magnitude. Truncations of the series expansion at different levels of magnitude will give models showing different levels of fidelity.

As stated above, terms of the form $\frac{1}{r^3}$ for both the hub and the telescope vehicles are now expanded. Using basic geometric arguments, it is easy to show that

$$\frac{1}{r_{h1}^3} = \frac{1}{(1+\gamma)^3}(1+\varepsilon_{h1})^{-\frac{3}{2}} \tag{5.25}$$

with

$$\varepsilon_{h1} \equiv \left(\frac{r_h}{1+\gamma}\right)^2 - \frac{2x_h}{1+\gamma} \tag{5.26}$$

which can be transformed using the binomial expansion

$$\frac{1}{r_{h1}^3} = \frac{1}{(1+\gamma)^3}\sum_{k=0}^{\infty}\begin{pmatrix} -3/2 \\ k \end{pmatrix}\varepsilon_{h1}^k \tag{5.27}$$

and for the telescope spacecraft

$$\frac{1}{r_{t1}^3} = \frac{1}{(1+\gamma)^3}\sum_{k=0}^{\infty}\begin{pmatrix} -3/2 \\ k \end{pmatrix}\varepsilon_{t1}^k \tag{5.28}$$

with

$$\varepsilon_{t1} \equiv \left(\frac{r_t}{1+\gamma}\right)^2 - \frac{2x_t}{1+\gamma} \tag{5.29}$$

The telescope variables are now being replaced by combinations of the hub variables and relative variables. This is done introducing δ_1 as follows

$$\varepsilon_{t1} = \varepsilon_{h1} + \delta_1 \tag{5.30}$$

with

$$\delta_1 \equiv \left(\frac{r^2 + 2\mathbf{r_h}\cdot\mathbf{r}}{1+\gamma}\right)^2 - \frac{2x}{1+\gamma} \tag{5.31}$$

Combining 5.28 and 5.30 and using another binomial expansion leads to

$$\frac{1}{r_{t1}^3} = \frac{1}{r_{h1}^3} + \frac{1}{(1+\gamma)^3}\sum_{k=1}^{\infty}\begin{pmatrix} -3/2 \\ k \end{pmatrix}\sum_{l=1}^{k}\begin{pmatrix} k \\ l \end{pmatrix}\delta_1^l\varepsilon_{h1}^{k-l} \tag{5.32}$$

Table 5.1: Terms magnitudes

Term	Value
$\frac{r_h}{1+\gamma}$	1.46×10^{-3}
$\frac{r_h}{\gamma}$	1.47×10^{-1}
$\frac{r}{1+\gamma}$	6.62×10^{-9}
$\frac{r}{\gamma}$	6.67×10^{-7}

The same process is applied to terms of the form $\frac{1}{r^3}$ involving the second primary, which gives

$$\frac{1}{r_{t2}^3} = \frac{1}{r_{h2}^3} + \frac{1}{\gamma^3} \sum_{k=1}^{\infty} \begin{pmatrix} -3/2 \\ k \end{pmatrix} \sum_{l=1}^{k} \begin{pmatrix} k \\ l \end{pmatrix} \delta_2^l \varepsilon_{h2}^{k-l} \tag{5.33}$$

Eq. 5.6 can be transformed using Eqs. 5.27, 5.32 and 5.33. These equations including only powers of ε_{h1}, ε_{h2}, δ_1 and δ_2, it is now possible to proceed to a magnitude ordering to keep only the most significant terms.

5.4.2 Magnitude ordering

ε_{h1}, ε_{h2}, δ_1 and δ_2 are composed of terms of the form $\frac{r_h}{1+\gamma}, \frac{r_h}{\gamma}, \frac{r}{1+\gamma}$, and $\frac{r}{\gamma}$. With a hub orbit amplitude of $\sim 220,000$km and a relative amplitude of $\sim$ 1km, the numerical values for these ratios are presented in Table 5.1.

According the numerical values presented above, and following the terminology used in [43], the terms scaled by $\frac{r_h}{1+\gamma}$ and $\frac{r_h}{\gamma}$ are said to be of order 1, and the terms scaled by $\frac{r}{1+\gamma}$ and $\frac{r}{\gamma}$ are said to be of order 3. Then a truncation of Eq. 5.6 at order

5 gives the following set of equations [43]

$$\begin{aligned}
\ddot{x} - 2\dot{y} - x &= 2c_2 x - c_3[6xx_h + (3\mathbf{r_h}\cdot\mathbf{r} - 15xx_h)] \\
&\quad + c_4[(3\mathbf{r_h}\cdot\mathbf{r} - 15xx_h)x_h + \frac{3}{2}(r_h^2 - 5x_h^2)x - \frac{15}{2}(2x_h\mathbf{r_h}\cdot\mathbf{r} - 7xx_h^2 + xr_h^2)] \\
\ddot{y} + 2\dot{x} - y &= -c_2 y - c_3(3xy_h + 3x_h y) \\
&\quad + c_4[(3\mathbf{r_h}\cdot\mathbf{r} - 15xx_h)y_h + \frac{3}{2}(r_h^2 - 5x_h^2)y] \\
\ddot{z} &= -c_2 z - c_3(3xz_h + 3x_h z) \\
&\quad + c_4[(3\mathbf{r_h}\cdot\mathbf{r} - 15xx_h)z_h + \frac{3}{2}(r_h^2 - 5x_h^2)z]
\end{aligned} \tag{5.34}$$

with $c_n = \frac{1}{\gamma^{n+1}}[\mu + (1-\mu)(\frac{\gamma}{1+\gamma})^{n+1}]$ as before. Note that in this truncated model, the right-hand-side terms are linear functions of the coordinates of $\mathbf{r}$ and quadratic in the coordinates of $\mathbf{r_h}$. Now a set a models corresponding to different levels of approximations will be developed, mostly based on the one just presented in 5.35.

5.4.3 Linear models

Free-flyer In this model all the gravitational forces are canceled, leaving only the acceleration terms. This leads to the following system of equations

$$\begin{aligned}
\ddot{x} - 2\dot{y} - x &= 0 \\
\ddot{y} + 2\dot{x} - y &= 0 \\
\ddot{z} &= 0
\end{aligned} \tag{5.35}$$

LTI Model Here in addition to the acceleration terms, the other linear and time invariant terms are taken into account:

$$\begin{aligned}
\ddot{x} - 2\dot{y} - (1 + 2c_2)x &= 0 \\
\ddot{y} + 2\dot{x} - (1 - c_2)y &= 0 \\
\ddot{z} + c_2 z &= 0
\end{aligned} \tag{5.36}$$

LPV1 Two higher Order Models are derived from [43], including the 4th order model (LPV1)

$$\begin{aligned} \ddot{x} - 2\dot{y} - x &= 2c_2x - c_3[6xx_h + (3\mathbf{r_h} \cdot \mathbf{r} - 15xx_h)] \\ \ddot{y} + 2\dot{x} - y &= -c_2y - c_3(3xy_h + 3x_hy) \\ \ddot{z} &= -c_2z - c_3(3xz_h + 3x_hz) \end{aligned} \tag{5.37}$$

In this model, the right-hand-side terms are linear functions of both the coordinates of $\mathbf{r}$ and the coordinates of $\mathbf{r_h}$.

LPV2 The 5th order Model (LPV2) is simply the set of equations 5.35 presented above.

LPV3 A final model is the linearization of the reference model about the trajectory of the hub spacecraft (LPV3), which leads to

$$\begin{aligned} \ddot{x} - 2\dot{y} - (1 + 2c_2)x &= \mathbf{h_1}(\mathbf{r_h}) \cdot \mathbf{r} \\ \ddot{y} + 2\dot{x} - (1 - c_2)y &= \mathbf{h_2}(\mathbf{r_h}) \cdot \mathbf{r} \\ \ddot{z} + c_2z &= \mathbf{h_3}(\mathbf{r_h}) \cdot \mathbf{r} \end{aligned} \tag{5.38}$$

where the coordinates of $\mathbf{h_1}$, $\mathbf{h_2}$ and $\mathbf{h_3}$ are nonlinear functions of the coordinates of $\mathbf{r_h}$.

Note that the first two models are Linear Time Invariant, therefore easy to implement and computationally simple, whereas the last three are Linear Parameter Varying (the parameter being the position of the hub spacecraft around the reference orbit as a function of time). These LPV models are a more precise representation of the reference model, but they are more complicated and more computationally intensive. So there is a trade-off between model fidelity and complexity.

5.5 Numerical Integration

5.5.1 Extrapolation method algorithm

The simulations shown in this chapter were done using the reference model described in Eq. 5.6 in the orbit propagator. The numerical integration of this nonlinear model has been done using the extrapolation method (also called the Bulirsch-Stoer method) [45]. This choice achieved the very high accuracy required for this problem. Indeed, the relative motion of the two spacecraft is very small ($\sim$ 1km) compared with their absolute motions with respect to L_2 ($\sim 10^5$km). This integration scheme has been validated on well-known test cases such as the two-body problem.

Here the equation to integrate is of the form $\dot{\mathbf{y}} = \mathbf{f}(t, \mathbf{y})$. The extrapolation method is a single-step method in the sense that the value at step $n+1$ is computed as a function of the value at step n only. There is no storage needed of the other previous values.

The objective is to compute $\mathbf{y}(t_0 + H)$ with the initial condition $(t_0, \mathbf{y_0})$. As described in [45], the first step of this method is to subdivide each integration step H into n microsteps of size $h = H/n$. The integration from $t = t_0$ to $t = t_0 + H$ is done along the n microsteps, which gives a certain value for $\mathbf{y}(t_0 + H)$. The approximated values of $\mathbf{y}$, noted $\mathbf{u_i}$, are found using a Euler step first and then the mid-point rule

$$\begin{aligned} \mathbf{u}_1 &= \mathbf{y}_0 + h\mathbf{f}(t_0, \mathbf{y}_0) \\ \mathbf{u}_{i+1} &= \mathbf{u}_{i-1} + 2h\mathbf{f}(t_0 + ih, \mathbf{y}_i) \quad (i = 1, \ldots, n-1) \end{aligned} \tag{5.39}$$

The approximated value for $\mathbf{y}(t_0 + H)$ is then

$$\boldsymbol{\eta}(h) = \frac{1}{4}\mathbf{u}_{n-2} + \frac{1}{2}\mathbf{u}_{n-1} + \frac{1}{4}\mathbf{u}_n \tag{5.40}$$

This operation is repeated several times (usually 5 in our case), with different microstep sizes of the form $h_i = H/n_i$. The different n_i have been taken from the so-called *Bulirsch sequence* $n = 2, 4, 6, 8, 12, 16, \ldots$. Then, for convenience, each $\boldsymbol{\eta}(h_i)$ is denoted as $\boldsymbol{\eta}(h_i) = \boldsymbol{\eta}_{i,1}$. And finally these are combined in the following polynomial

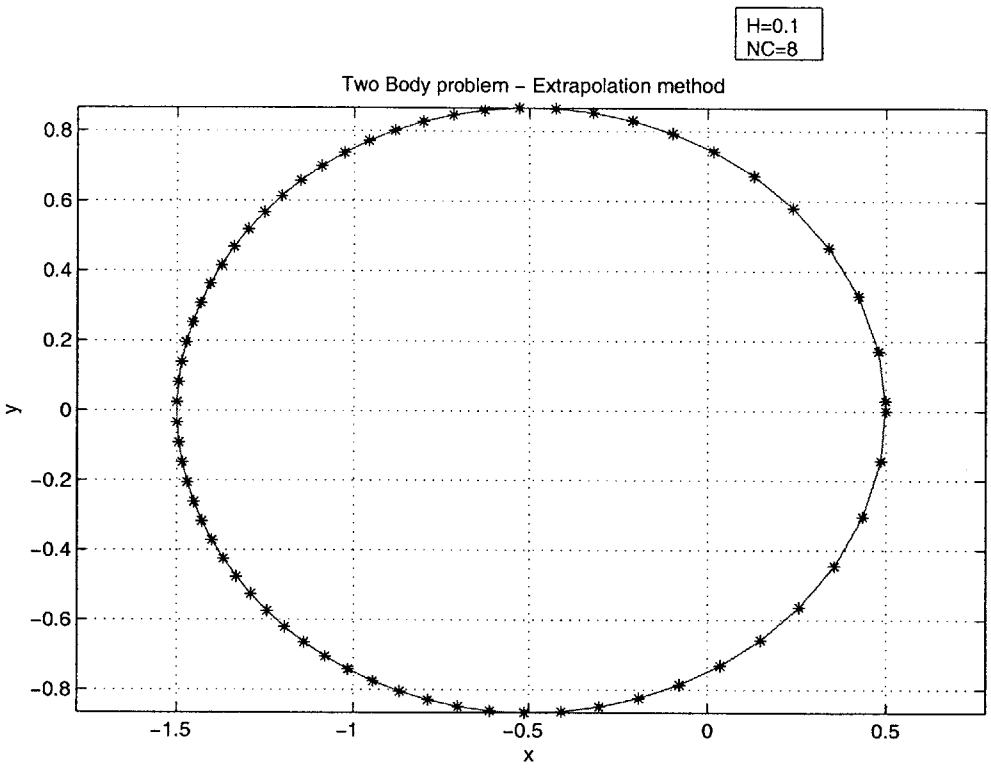

Figure 5-7: 2-Body problem, analytical and numerical trajectories

extrapolation formula to get a final value for $\mathbf{y}(t_0 + H)$

$$\eta_{i,j+1} = \eta_{i,j} + \frac{1}{(n_i/n_{i-j})^2 - 1}(\eta_{i,j+1} - \eta_{i-1,j}) \tag{5.41}$$

With 5 consecutive subdivision as used in our study, $\eta_{5,5}$ gives theoretically an approximation comparable to that of a Runge-Kutta method of order 10.

5.5.2 Comparison with Runge-Kutta methods and validation

As a way to validate this integration algorithm, a numerical integration of the classical two-body problem has been done and errors with the analytical solution has been compared for both the extrapolation method and a Runge-Kutta algorithm as implemented in Matlab©.

Fig. 5-7 is a plot of the analytical 2-body trajectory used to validate the integration algorithms. The trajectory is an ellipse with a semimajor axis $a = 1$ and an

eccentricity $e = 0.5$. Blue asterisks correspond to the numerical integration of the 2-body dynamics equations. The Runge-Kutta used to do the comparison is the algorithm implemented in the `ode45` function in Matlab ©, which is the implementation of an explicit Runge-Kutta (4,5) formula, the Dormand-Prince pair.

The $x-$axis in Figs. 5-8 and 5-9 is the number of steps along the orbit path. The $y-$axis corresponds to the absolute error, i.e. the difference between the value numerically computed and the analytical solution. Fig. 5-8 shows that the error for the Runge-Kutta method is around 10^{-3}, whereas the error for the extrapolation method is on the order of 10^{-10}, a difference of 7 orders of magnitude. As discussed previously, in our three-body formation flight problem the relative motion of the two spacecraft is very small ($\sim$ 1km) compared with their absolute motions with respect to L_2 ($\sim 10^5$km). As a consequence, a relative required accuracy of at least 10^{-5} is required to be able to distinguish the motion of two spacecraft in our formation. As shown in Fig. 5-9, the extrapolation method is suitable to such accuracy requirements and has been used throughout this study.

5.6 Control Algorithms

Open-loop simulation can be done to capture the difference between each model and the reference model. But all the models pale in comparison with the nonlinear reference model they are derived from, as can be seen on Fig. 5-10. This is a 6-month long simulation ($\sim$ the period of a halo orbit). The thick line correspond to a closed relative trajectory for two spacecraft with a relative orbit amplitude of 50m. All models diverge pretty quickly. In addition to that, in an open-loop simulation it is typically difficult to determine the impact of modeling errors on the control effort. So each of these model has been implemented in an optimal controller and they are compared with each other in the performance vs. fuel plane. This method gives us both a measure of the intrinsic fidelity of each model and a measure of the performance of a controller using it. The resulting controllers are simple and not necessarily what you would want to implement on-orbit, but they are easy to develop

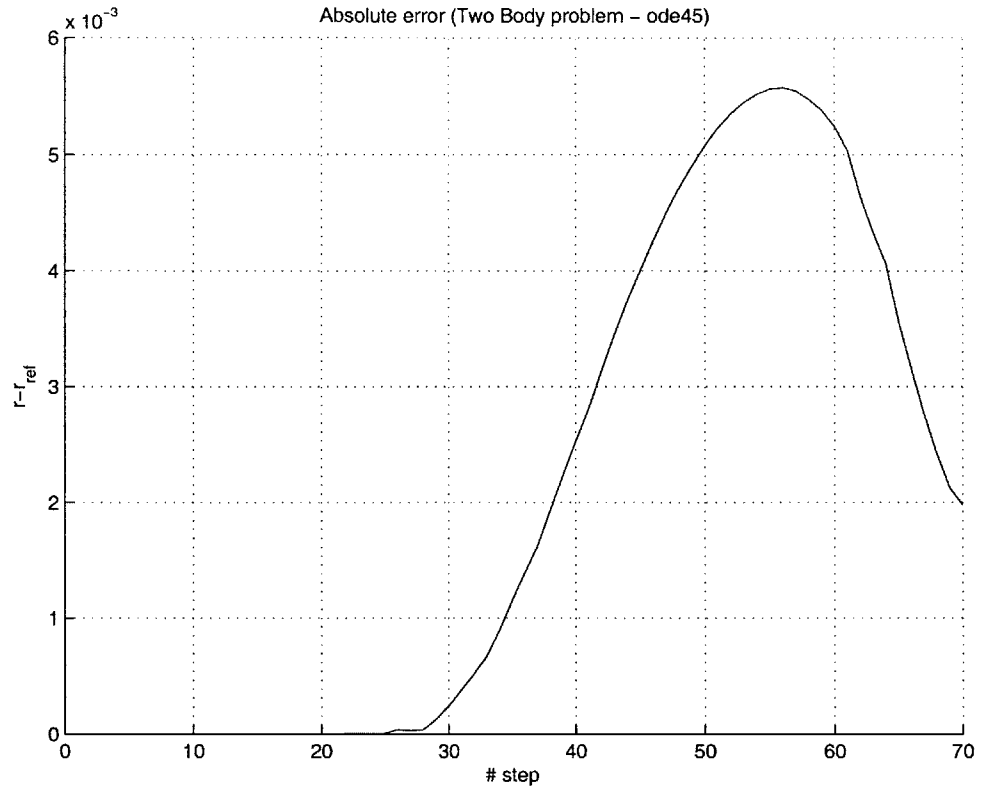

Figure 5-8: 2-Body problem, Runge-Kutta integrator

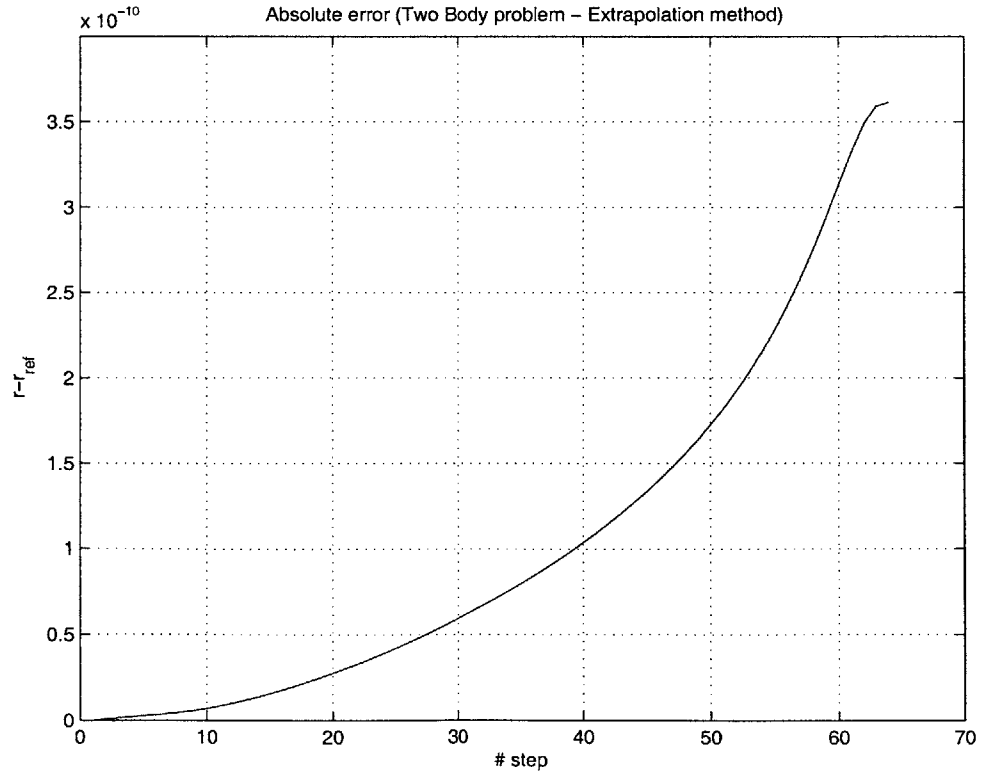

Figure 5-9: 2-Body problem, Extrapolation integrator

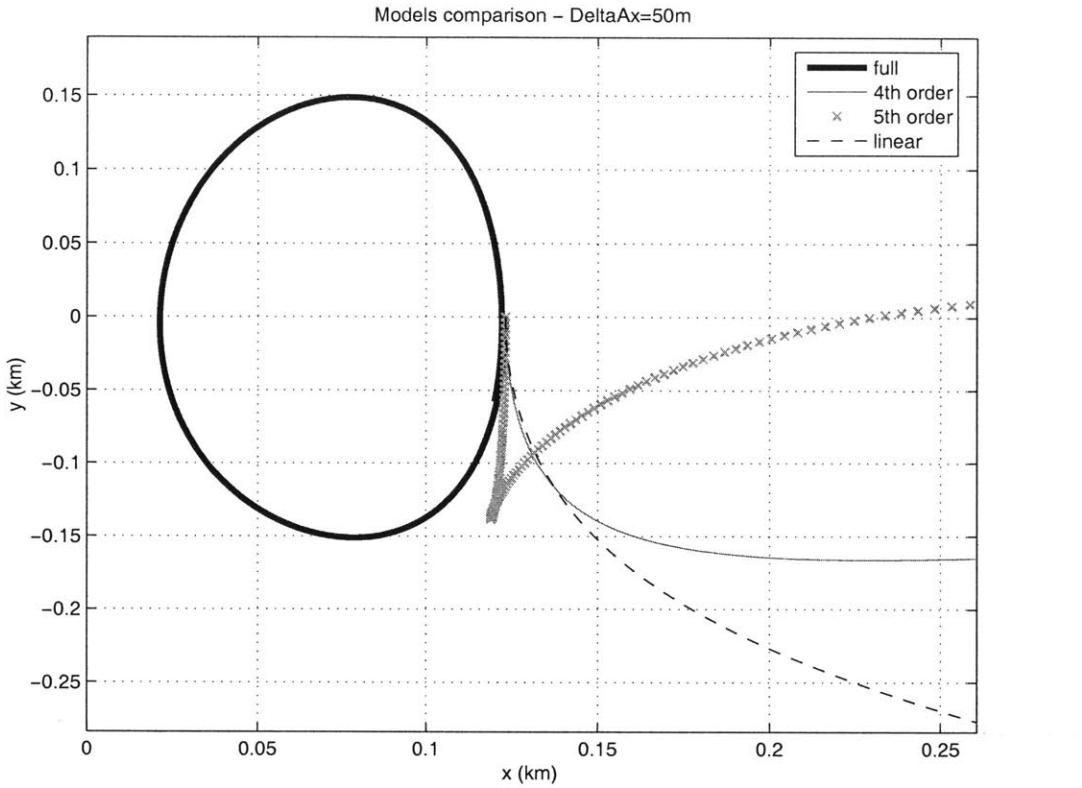

Figure 5-10: Open-loop models comparison

and which simplifies the evaluation of the different dynamics models. The different kinds of control algorithms that have been considered are described in the following paragraphs. For all controllers a reference relative trajectory (typically either a fixed or a circular relative configuration) is already given in the form of $\mathbf{r_{ref}}$.

5.6.1 Proportional controller

Being given a reference relative trajectory by r_{ref}, the control is described by

$$\mathbf{u} = -k(\mathbf{r} - \mathbf{r_{ref}}) \tag{5.42}$$

Different values for the gain k have been used.

5.6.2 Proportional-Derivative controller

this time the control is

$$\mathbf{u} = -k_1(\mathbf{r} - \mathbf{r_{ref}}) - k_2(\dot{\mathbf{r}} - \dot{\mathbf{r}}_{\mathbf{ref}}) \tag{5.43}$$

As for the proportional controller, different values for the gains k_1 and k_2 have been used.

Note that the simple Proportional and Proportional-Derivative controllers are used to provide a reference mostly. The comparison of the different models is done using the Linear-Quadratic-Regulator controller described below.

5.6.3 Optimal control

develops a controller that minimizes the cost

$$J = \frac{1}{2}\int_0^\infty [(\mathbf{r} - \mathbf{r_{ref}})^T \mathbf{Q}(\mathbf{r} - \mathbf{r_{ref}}) + \mathbf{u}^T \mathbf{R}\mathbf{u}]dt \tag{5.44}$$

$\mathbf{Q}$ and $\mathbf{R}$ being the weighting matrices. The resulting control is

$$\mathbf{u} = -\mathbf{F}\mathbf{x} - \mathbf{G}\mathbf{s} \tag{5.45}$$

with $\mathbf{x}$ being the full state

$$\mathbf{x} = \begin{bmatrix} \mathbf{r} \\ \dot{\mathbf{r}} \end{bmatrix} \tag{5.46}$$

and $\mathbf{F}$, $\mathbf{G}$ and $\mathbf{s}$ coming from the resolution of the Riccati equation and the reference relative trajectory.

5.7 Results

The various dynamical models described in the first section have been implemented with the controllers described in the previous section for different scenarios

1. reach and follow a closed reference orbit;

2. keep a fixed relative configuration between the two spacecraft, aligned along the x-axis with $\Delta x = 1$km;

3. keep a fixed relative configuration between the two spacecraft, aligned along the x-axis with $\Delta x = 1$km, with an initial offset of 1%;

4. follow a circular reference trajectory, with a radius of 1km;

To compare these models, consider the fuel effort/performance plot for scenario #2 for different levels of control effort (Figure 5-11). The plot compares the controllers described above (P/PD/LQR) using our different models. In general one would expect the curves to have a negative slope - more control effort should lead to a reduced mean error. However, the performance and fuel costs were evaluated on the full nonlinear system, so the curves for the poorer models are quite different (actually have a positive slope). For a given level of performance, i.e. a given level of error, a way to compare the models is to look at the control effort required.

5.8 Observations

There are several interesting observations from Figure 5-11

1. As expected, from this plot a consistent scheme from one model to another is clear: the more sophisticated, the better the performance. More specifically, it is clear that the proportional controller is much worse than the others, with 2 or 3 times as much fuel usage for a given level of error (depending on the models and the level of error considered). The LQR controller is always better than the other proportional and proportional-derivative controllers.

2. Using the free-flyer model leads to very poor performance, and providing more control effort ends up with larger errors. Although there is a large difference

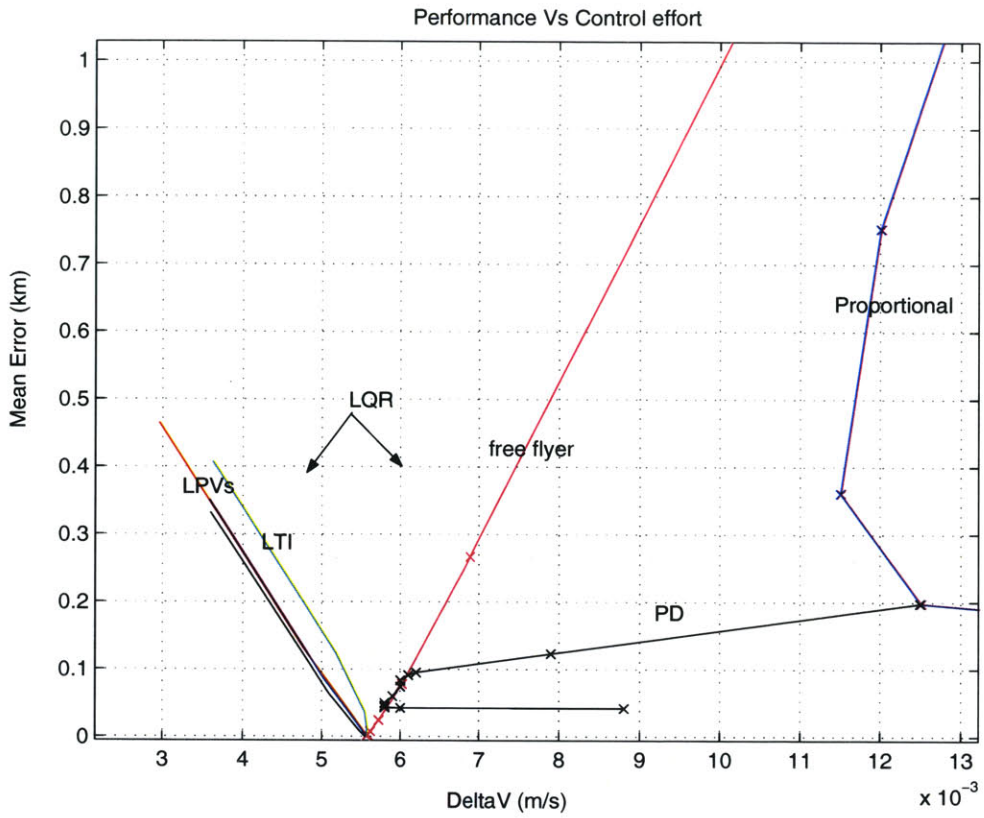

Figure 5-11: Controllers comparison

between the free-flyer model and the others, the LTI and the three LPV models have very similar performances

3. Figure 5-12 shows Figure 5-11 zoomed in to much smaller errors, and it shows that each of the models shows the same "non-intuitive behavior" of the free-flyer model for small errors, the more fuel you spend to control this error, the larger it grows. But the transition points occur at different levels of authority. A possible conjecture would be that this transition and the subsequent non-intuitive plot (lower error for less fuel) is a result of the differences between the model and the true nonlinear system, which are accentuated for higher control authority. Because different models capture the nonlinearity to different extents, the transitions occur at different levels of authority.

The conclusion from this analysis is that the more sophisticated models do give better closed-loop performance, and that the difference appears to be sufficient to justify the

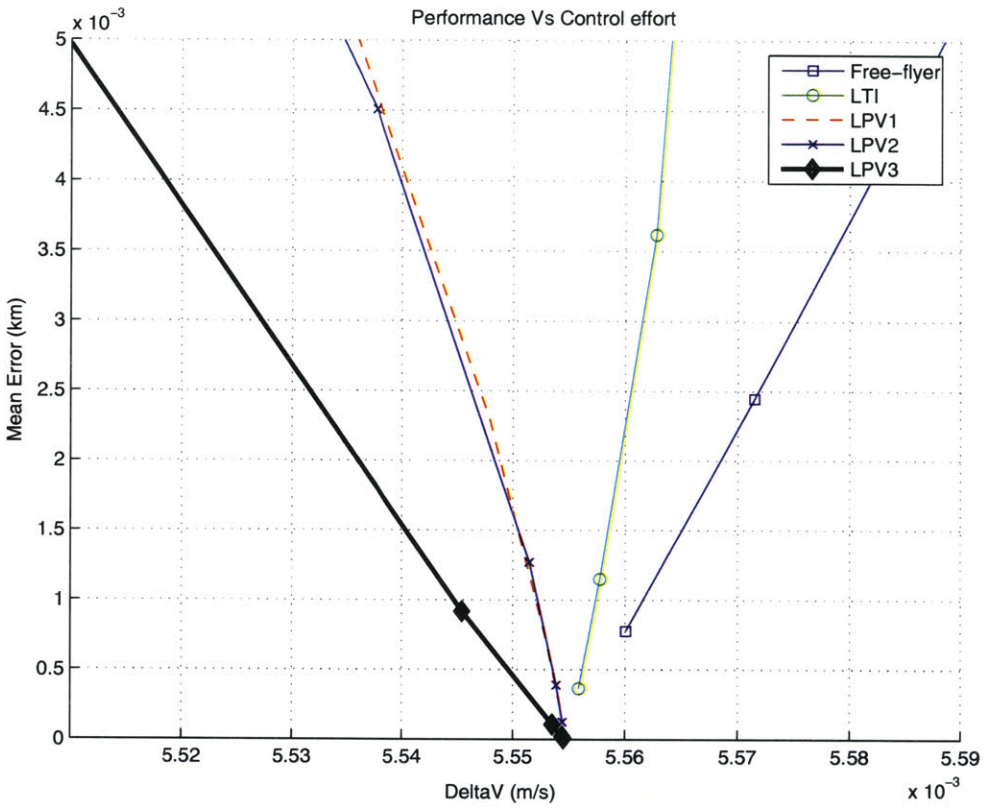

Figure 5-12: Controllers comparison (zoomed)

additional effort required to implement and use them.

Chapter 6

Conclusions

In order to support the surface exploration objectives on the Moon and Mars, navigation and communication capabilities are required, and a set of Nav/Comm requirements have been expressed by the Surface Operation team of the CE&R project at MIT. In response to this need, a set of Nav/Comm architectures have been designed and evaluated through the definition of navigation and communication metrics, the choice of a set of Nav/Comm elements constituting the architectures, and the development of analysis tools aimed at evaluating the architectures. Although the work presented in this thesis mostly concerns the navigation, similar analysis on communication issues has been done in parallel and the solutions (i.e. architectures) presented in this thesis integrate both communication and navigation considerations.

The main contribution of the work presented in this thesis is the integration of the different navigation assets presented in Chapter 2 in a set of complete Nav/Comm architectures:

- A *Minimalist* architecture, the simplest and cheapest adequate architecture, with minimum performance and minimum cost. The design chosen uses only onboard sensors.

- A *Simple* architecture, which consists of the Minimalist architecture augmented with a dedicated Nav/Comm satellite. It was designed to greatly improve the communication availability and provide some limited (i.e. with low response

time and poor coverage but the capability exists) absolute navigation capabilities.

- A *Performance* architecture based on a Nav/Comm satellite constellation. This allows for excellent communication capabilities and real-time or quasi-real-time navigation over continental areas with a limited number of satellites (three to four).

These three architectures span the design space, while meeting the navigation and communication requirements. In addition to reaching the extremes of the design space in terms of performance as well of cost, this set of three architectures also enables a gradual accretion of assets over time as better performance is required on the one hand, and funding becomes available on the other hand.

In addition to these architectures basic definitions, a complete preliminary design of the three architectures could be completed in this work. The onboard equipment should be composed of odometry sensors, a gyro and a sun sensor in addition to a vision-based navigation system. A VOR/DME beacon on the main base station provides with local coverage. The Nav/Comm constellations geometries for the Simple and Performance architectures have been defined. The evaluations of the three architectures along the top-level navigation and communication metrics, as well as mass, are summarized in Table 6.1, for both the Moon and Mars.

Table 6.1: Architectures evaluation summary (Mars/Moon)

Metric	Minimalist	Simple	Performance
Nav. Coverage	*Fair*	*Fair*	*Good*
Nav. Accuracy	*Fair*	*Fair*	*Good*
Nav. Operability	*Fair*	*Fair*	*Good*
Comm. Coverage	*Poor*	*Good*	*Good*
Comm. Availability	*Fair/Poor*	*Good/Fair*	*Good*
Max. Gap Time	*Poor*	*Good/Fair*	*Good*
Mass	*Good*	*Fair/Good*	*Poor/Fair*

In addition to these three architectures, two additional options have been proposed: surface beacons when precise (cm-level) navigation is required and the use

of a non-dedicated asset (such as a transportation asset left on-orbit) equipped with some Nav/Comm hardware to augment the existing Nav/Comm architecture. Its impact is the most beneficial when applied to the Simple architecture.

A number of tools have been developed through this study to evaluate the different architectures along the navigation and communication metrics, and give first estimates of the mass (therefore the cost) of these architectures. When applicable, the different types of measurements coming from different types of sensors have been integrated in a single tool. The evaluation and refinement of the architectures allowed us to express a set of recommendations to NASA detailed in the last chapter. In addition to these recommendations, some results about navigation can be highlighted:

- For specific coverage of a polar region, high-eccentric orbits similar to Molniya orbits give the best performance;
- For coverage of a continental region centered about the equator, synchronous orbits give the best performance;
- Onboard relative navigation equipment greatly benefits from the use of an absolute heading sensor such as a sun sensor.

Because of the system-level aspect of the CE&R project, many simplifying assumptions had to be made and some further work should concentrate on deepening some parts of the study. Items that would be of interest for further work include:

- An analysis of a beacon network deployment and initialization and its influence on the positioning accuracy (indeed, the beacon locations have been considered to be perfectly known in our study). However, the process for including beacon location uncertainties should be very similar to the one used to include the uncertainty on the spacecraft location in the constellation analysis presented in Chapter 3 (see section 3.1.2).
- A more detailed integration of vision-based navigation methods. So far, vision cameras have been assumed to provide with a position fix with $\simeq$ 100 m accuracy

based on Earth tests, without taking into account discrepancies due to the relief or maps. Alternate methods such as visual odometry should be considered too.

- An analysis of power issues for Nav/Comm satellites. The constellations designed in this study include high-altitude satellites, without taking into account the power issues arising with long distances. This could have an impact on the definitive design of the constellations.

- An analysis of the effects of orbital perturbations. The orbital perturbations (such as J_2) can have an important influence on the geometry of the constellation, and its performance could degrade over time, unless some station keeping capabilities are implemented. An analysis of the degradation of the orbit's geometry should provide with the corresponding station keeping fuel consumption and could also lead to modifications of the constellation design (as some particular choices of orbital elements can cancel the effects of some perturbations).

Bibliography

[1] National Aeronautics and Space Administration "The Vision for Space Exploration February," 2004

[2] H. N. Kleinwaks *A Mars-back Approach to Lunar Surface Operations,* Massachusetts Institute of Technology, S.M. thesis, June 2005

[3] P. Misra, P. Enge *Global Positioning System. Signals, Measurements, and Performance* Ganga-Jamuna Press, 2001

[4] R. G. Brown, P. Y. C. Hwang "Introduction to Random Signals and Applied Kalman Filtering," Third edition, John Wiley & Sons, 1997

[5] Lunar Roving Vehicle Operations Handbook, 1971

[6] Concept Exploration & Refinement Study, MIT-Draper Lab. Final Report, March 15, 2005

[7] Information IPT End of Spiral A Presentation CE&R Project, MIT-Draper

[8] F. Cozman, E. Krotkov "Robot Localization using a Computer Vision Sextant," Robotics Institute, Carnegie Mellon University International Conference on Robotics and Automation, pages 106-111, May 1995

[9] F. Cozman, E. Krotkov and C. Guestrin "Outdoor Position Estimation for Planetary Rovers," Autonomous Robots Journal 9 (2):135-150, September 2000

[10] F. Cozman, E. Krotkov "Automatic Mountain Detection and Pose Estimation for Teleoperation of Lunar Rovers," Robotics Institute, Carnegie Mellon Uni-

versity Proceedings of the 1997 IEEE International Conference on Robotics and Automation Albuquerque, New Mexico - April 1997

[11] R. Volpe "Mars Rover Navigation Results Using Sun Sensor Heading Determination," Proceedings of the 1999 IEEVRSJ International Conference on Intelligent Robots and Systems Jet Propulsion Laboratory

[12] S. I. Roumeliotis, G. A. Bekey "An Extended Kalman Filter for Frequent Local and Infrequent Global Sensor Data Fusion," in Proc. of the SPIE Sensor Fusion and Decentralized Control in Autonomous Robotic Systems, Pittsburgh, Pennsylvania, USA, Oct. 14-15, 1997, pp.11-22.

[13] S. I. Roumeliotis, A. E. Johnson and J. F. Montgomery "Augmenting Inertial Navigation with Image-Based Motion Estimation," in Proc. 2002 IEEE International Conference on Robotics and Automation, Washington D.C., May 11- 15, pp. 4326-4333

[14] A. Huster, S. M. Rock "Relative Position Sensing by Fusing Monocular Vision and Inertial Rate Sensors," ICAR 2003 The 11th International Conference on Advanced Robotics Coimbra, Portugal, June 30 - July 3, 2003

[15] D. Strelow, S. Singh "Motion Estimation from Image and Inertial Measurements," The International Journal of Robotics Research Vol. 23, No. 12, December 2004, pp. 1157-1195

[16] S. Se, H. -K. Ng, P. Jasiobedzki, T. -J. Moyung "Vision Based Modeling And Localization For Planetary Exploration Rovers," 55th International Astronautical Congress 2004

[17] C. F. Olson, L. H. Matthies, M. Schoppers, M. W. Maimone "Rover Navigation Using Stereo Ego-Motion," Computing and Software Systems Robotics and Autonomous Systems 43 (2003) 215.229 Received 30 January 2002; received in revised form 15 December 2002

[18] C. F. Olson, L. H. Matthies "Maximum Likelihood Rover Localization by Matching Range Maps," Proceedings of the IEEE International Conference on Robotics and Automation, pages 272-277, 1998.

[19] S. B. Goldberg, M. W. Maimone, L. Matthies "Stereo Vision and Rover Navigation Software for Planetary Exploration," Published in 2002 IEEE Aerospace Conference Proceedings, March 2002

[20] S. Hayati, R. Volpe, P. Backes, J. Balaram, R. Welch, R. Ivlev, G. Tharp, S. Peters, T. Ohm, R. Petras, and S. Laubach "The Rocky 7 Rover: A Mars Scientific Prototype," in Proceedings of the IEEE International Conference on Robotics and Automation, Albuquerque, NM, 1997

[21] B. Barshan, H . F. Durrant-Whyte "An Inertial Navigation System for a Mobile Robot," Proceedings the 1993 IEEE/RSJ International Conference on Intelligent Robots and Systems, Yokohama, Japan, July 26-30, 1993

[22] B. Barshan, H . F. Durrant-Whyte "Inertial Navigation Systems for Mobile Robots," IEEE Transactions on Robotics and Automation, Vol.11, No.3, June 1995

[23] J. Borenstein, H. R. Everett, L. Feng "Sensors and Methods for Mobile Robot Positioning," prepared by the University of Michigan for the Oak Ridge National Lab D&D Program and for the United States Department of Energy, 1996.

[24] E. M. Nebot "Sensors Used for Autonomous Navigation," Advances in Intelligent Autonomous Systems, Chapter 7, pp. 135-156, ISBN 0-7923-5580-6, March 1999, Kluwer Academic Publishers, Dordrecht

[25] Mechanical Engineering Design Project "Conceptual Development of a Ground-Based Radio-Beacon Navigation System for Use on the Surface of the Moon," The University of Texas at Austin, Spring 1988

[26] G. H. Baron, S. W. Shepperd, T. J. Brand "Proposed Lunar Autonomous Navigation System," AAS 93-713

[27] T. A. Ely, R. Anderson, Y. E. Bar-Sever, D. Bell, J. Guinn, M. Jah, P. Kallemeyn, E. Levene, L. Romans, S.-C. Wu "Mars Network Constellation Design Drivers and Strategies," AAS 99-301

[28] K. O'Keefe "Simulation and Evaluation of the Performance of the Proposed Mars Network Constellation for Positioning, Orbit Improvement, and Establishment of a Spatial Reference Frame for Mars," Department of Geomatics Engineering, University of Calgary, PhD Thesis, April 2004

[29] J. Guinn "Future Mars Navigation Architecture," Jet Propulsion Laboratory, Presentation, 1st September 2004

[30] J. H. MacNicol, Major, USAF "A Study of Satellite Navigation, Dilution of Precision, and Positioning Techniques for Use on and Around the Moon," Thesis AFIT/GE/ENG/02M-15 Department of the Air Force Air University, Air Force Institute of Technology

[31] E. A. LeMaster "Self-Calibrating Pseudolite Arrays: Theory and Experiment," Stanford University, PhD Thesis, May 2002

[32] G. R. Opshaug "A Leapfrog Navigation System," Stanford University, PhD Thesis, May 2003

[33] Battin, Richard H., *An Introduction to the Mathematics and Methods of Astrodynamics,* AIAA Education Series, New York, 1987.

[34] Cornish, Neil J., The WMAP Mission, WMAP's education and outreach program
http //map.gsfc.nasa.gov/m_mm/ob_techorbit1.html
http //map.gsfc.nasa.gov/ContentMedia/lagrange.pdf

[35] SOHO website http //sohowww.nascom.nasa.gov

[36] M. Beckman "Orbit Determination Issues for Libration Point Orbits," Libration Point Orbits and Applications, Parador d'Aiguablava, Girona, Spain 10 - 14 June, 2002

[37] D. Folta, K. Hartman, K. Howell, B. Marchand "Formation Control of the MAXIM L_2 Libration Orbit Mission," America Institute of Aeronautics and Astronautics

[38] MAXIM web site http://maxim.gsfc.nasa.gov

[39] D. L. Richardson "Analytic Construction of Periodic Orbits about the Collinear Points," Celestial Mechanics 22 (1980) 241-253

[40] D. L. Richardson "Halo Orbit Formulation for the ISEE-3 Mission," J. Guidance and Control, Vol. 3, No. 6, Nov.-Dec. 1980

[41] K. C. Howell "Three-Dimensional, Periodic, 'Halo' Orbits," Celestial Mechanics 32(1984) 53-71

[42] G. Gómez, J. Llibre, R. Martínez, C. Simó "Dynamics and Mission Design Near Libration Points Vol.1," World Scientific Monograph Series in Mathematics - Vol.2, 2001.

[43] A. Segerman, M. Zedd, "Investigations of Spacecraft Orbits Around the L_2 Sun-Earth Libration Point-Part 2," Naval Research Laboratory, Washington, D.C., Nov 2002.

[44] G. Collange, "Relative Motion of Two Spacecraft and Formation Design Near Sun-Earth L2 Point," Nov 2003.

[45] O. Montenbruck, E. Gill "Satellite Orbits Models, Methods, Applications," Springer, 2000.

Appendix A

Extended Kalman Filter Parameters

This Appendix presents the parameter values used in the Extended Kalman Filters in Chapter 4. There are two main sections corresponding to the two scenarios described in Chapter 4, section 4.1.3.

A.1 Scenario 1 – Complete Inertial Measurement Unit and Surface Beacons

A.1.1 Simulation parameters

Table A.1 gives the simulation parameters as well as the sensors update rates.

Table A.1: Simulation parameters

Simulation time	T	50 s
Time step	δt	0.1 s
Beacon update rate	f_b	1 Hz
IMU update rate	f_{IMU}	10 Hz

The beacon network is assumed to be an equilateral triangle. In a planet-fixed

reference frame, with unit of meters, the beacons are located at:

$$\begin{aligned}
\mathbf{r_1} &= 10^3 \times \begin{bmatrix} 1.2991 & 0 & 0.0020 \end{bmatrix} \\
\mathbf{r_2} &= 10^3 \times \begin{bmatrix} -0.6496 & 1.1251 & 0.0020 \end{bmatrix} \\
\mathbf{r_3} &= 10^3 \times \begin{bmatrix} -0.6496 & -1.1251 & 0.0020 \end{bmatrix}
\end{aligned} \tag{A.1}$$

A.1.2 Sensors parameters

The sensor parameters corresponding to the simulation presented in Chapter 4 are given in Chapter 3. More precisely, the measurement equations for the IMU is Eq. 3.56, and the bias error model and the corresponding parameters are given in Eq. 3.57 and Table 3.5.

The measurement noise matrix $\mathbf{R}$ for the IMU measurements is

$$\mathbf{R} = \begin{bmatrix} \sigma_g^2 & 0 & 0 & 0 & 0 & 0 \\ 0 & \sigma_g^2 & 0 & 0 & 0 & 0 \\ 0 & 0 & \sigma_g^2 & 0 & 0 & 0 \\ 0 & 0 & 0 & \sigma_a^2 & 0 & 0 \\ 0 & 0 & 0 & 0 & \sigma_a^2 & 0 \\ 0 & 0 & 0 & 0 & 0 & \sigma_a^2 \end{bmatrix} \tag{A.2}$$

where σ_g is the gyro noise standard deviation and σ_a is the accelerometer noise standard deviation (their values are given in Table 3.5). The measurement noise matrix for the ranging measurements is

$$\mathbf{R} = \sigma_b^2 \times \mathbf{I_{3\times 3}} \tag{A.3}$$

where σ_b is the ranging measurement noise standard deviation ($\sigma_b = 3$ cm).

A.1.3 Initial values

The state vector of the Inertial Measurement Unit located in the rover is

$$\mathbf{x} = \begin{bmatrix} \mathbf{x}_{Gx}^T & \mathbf{x}_{Gy}^T & \mathbf{x}_{Gz}^T & \mathbf{x}_{Ax}^T & \mathbf{x}_{Ay}^T & \mathbf{x}_{Az}^T \end{bmatrix}^T \tag{A.4}$$

where the elementary state vector for the x-axis gyro is

$$\mathbf{x}_{Gx} = \begin{bmatrix} \theta & \dot{\theta} & \ddot{\theta} & \dddot{\theta} & \epsilon_\theta \end{bmatrix}^T \tag{A.5}$$

and the elementary state vector for the x-axis accelerometer is

$$\mathbf{x}_{Ax} = \begin{bmatrix} x & v_x & a_x & \epsilon_{a_x} \end{bmatrix}^T \tag{A.6}$$

$\mathbf{x}_{Gy}$, $\mathbf{x}_{Gz}$, $\mathbf{x}_{Ay}$ and $\mathbf{x}_{Az}$ being defined in a similar fashion. Then the initial state estimate is

$$\hat{\mathbf{x}}_0^- = \begin{bmatrix} \hat{\mathbf{x}}_{Gx_0}^{-T} & \hat{\mathbf{x}}_{Gy_0}^{-T} & \hat{\mathbf{x}}_{Gz_0}^{-T} & \hat{\mathbf{x}}_{Ax_0}^{-T} & \hat{\mathbf{x}}_{Ay_0}^{-T} & \hat{\mathbf{x}}_{Az_0}^{-T} \end{bmatrix}^T \tag{A.7}$$

with

$$\hat{\mathbf{x}}_{Gx_0}^- = \begin{bmatrix} 0 & 0 & 0 & 0 & C_{2g} \end{bmatrix}^T \tag{A.8}$$

and

$$\hat{\mathbf{x}}_{Ax_0}^- = \begin{bmatrix} 0 & 0 & 0 & C_{2a_x} \end{bmatrix}^T \tag{A.9}$$

The initial covariance matrix is

$$\mathbf{P}_{0Gx}^- = \begin{bmatrix} \mathbf{P}_{0Gx}^- & \mathbf{0} & \mathbf{0} & \mathbf{0} & \mathbf{0} & \mathbf{0} \\ \mathbf{0} & \mathbf{P}_{0Gy}^- & \mathbf{0} & \mathbf{0} & \mathbf{0} & \mathbf{0} \\ \mathbf{0} & \mathbf{0} & \mathbf{P}_{0Gz}^- & \mathbf{0} & \mathbf{0} & \mathbf{0} \\ \mathbf{0} & \mathbf{0} & \mathbf{0} & \mathbf{P}_{0Ax}^- & \mathbf{0} & \mathbf{0} \\ \mathbf{0} & \mathbf{0} & \mathbf{0} & \mathbf{0} & \mathbf{P}_{0Ay}^- & \mathbf{0} \\ \mathbf{0} & \mathbf{0} & \mathbf{0} & \mathbf{0} & \mathbf{0} & \mathbf{P}_{0Az}^- \end{bmatrix} \tag{A.10}$$

with

$$\mathbf{P}_{0Gx}^{-} = \mathbf{P}_{0Gy}^{-} = \mathbf{P}_{0Gz}^{-} = \begin{bmatrix} 0.10^2 & 0 & 0 & 0 & 0 \\ 0 & 0.14^2 & 0 & 0 & 0 \\ 0 & 0 & 0.20^2 & 0 & 0 \\ 0 & 0 & 0 & 0.28^2 & 0 \\ 0 & 0 & 0 & 0 & 0.10^2 \end{bmatrix} \tag{A.11}$$

and

$$\mathbf{P}_{0Ax}^{-} = \mathbf{P}_{0Ay}^{-} = \mathbf{P}_{0Az}^{-} = \begin{bmatrix} 0.10^2 & 0 & 0 & 0 \\ 0 & 0.14^2 & 0 & 0 \\ 0 & 0 & 0.20^2 & 0 \\ 0 & 0 & 0 & 0.10^2 \end{bmatrix} \tag{A.12}$$

A.1.4 Process noise matrix

The power spectral density (PSD) of the process noise is chosen to be zero, except for the following diagonal elements

$$\begin{aligned} W_{5,5} &= A_g \\ W_{10,10} &= A_g \\ W_{15,15} &= A_g \\ W_{19,19} &= A_{ax} \\ W_{23,23} &= A_{ay} \\ W_{27,27} &= A_{az} \end{aligned} \tag{A.13}$$

with

$$\begin{aligned} A_g &= 0.01 \left(\frac{C_{1g} + C_{2g}}{T_g} \right)^2 \\ A_{ax} &= 0.01 \left(\frac{C_{1ax} + C_{2ax}}{T_{ax}} \right)^2 \\ A_{ay} &= 0.01 \left(\frac{C_{1ay} + C_{2ay}}{T_{ay}} \right)^2 \\ A_{az} &= 0.01 \left(\frac{C_{1az} + C_{2az}}{T_{az}} \right)^2 \end{aligned} \tag{A.14}$$

where C_{1g}, C_{2g}, T_g, C_{1ax}, C_{2ax}, T_{ax}, C_{1ax}, C_{2ax}, T_{ax}, C_{1ax}, C_{2ax}, T_{ax} are given in Table 3.5. Using this continuous noise power spectral density, the equivalent discrete process noise matrix is evaluated using the method described in [4] and briefly summarized here. Given the continuous state equation

$$\dot{\mathbf{x}} = \mathbf{F}\mathbf{x} + \mathbf{G}\mathbf{u} \tag{A.15}$$

where $\mathbf{u}$ is a white noise vector with PSD given by $\mathbf{W}$, the $\mathbf{A}$ matrix is formed as follows

$$\mathbf{A} = \begin{bmatrix} -\mathbf{F} & \mathbf{G}\mathbf{W}\mathbf{G}^{\mathbf{T}} \\ \mathbf{0} & \mathbf{F}^{T} \end{bmatrix} \delta t \tag{A.16}$$

where δt is the time step used for discretization. Forming the matrix exponential of $\mathbf{A}$ gives

$$\mathbf{B} = e^{\mathbf{A}} = \begin{bmatrix} \cdot & \mathbf{\Phi}_{\mathbf{k}}^{-1}\mathbf{Q}_{\mathbf{k}} \\ 0 & \mathbf{\Phi}_{\mathbf{k}}^{\mathbf{T}} \end{bmatrix} \equiv \begin{bmatrix} \mathbf{B}_{11} & \mathbf{B}_{12} \\ \mathbf{B}_{21} & \mathbf{B}_{22} \end{bmatrix} \tag{A.17}$$

$\mathbf{\Phi}_{\mathbf{k}}$ being the state transition matrix from step k to step $k+1$, and the discrete process noise matrix is obtained as follows

$$\mathbf{Q}_{\mathbf{k}} = \mathbf{\Phi}_{\mathbf{k}}\mathbf{B}_{12} = \mathbf{B}_{22}^{T}\mathbf{B}_{12} \tag{A.18}$$

A.2 Scenario 2 – Combination of Inertial Sensors, Odometers With a Sun Sensor

In this appendix are detailed all the constants and parameters used in the simulations presented in Chapter 4 of this thesis.

A.2.1 Simulation parameters

Table A.2 gives the simulation parameters as well as the sensors update rates for the second scenario.

Table A.2: Simulation parameters

Simulation time	T	400 s
Time step	δt	0.02 s
Sun sensor update rate	f_{SS}	10 Hz
Other sensors update rate	f_i	50 Hz

A.2.2 Rover parameters

Table A.3 gives the rover parameters as well as its reference trajectory corresponding to the simulation presented in Chapter 4, which is determined by the speed and steering angle.

Table A.3: Rover parameters

Rover length	L	1 m
Rover speed	V	1 m/s
Steering angle	α	1°

A.2.3 Sensors parameters

Table A.3 gives the sensors parameters corresponding to the simulation presented in Chapter 4, given in terms of sensors noises standard deviations.

Table A.4: Sensors parameters

Sensor	Standard deviation	Value
Encoders	σ_V	2 cm/s
Potentiometer	σ_α	0.31 rad
Gyro	$\sigma_{\dot{\phi}}$	0.0031 rad/s
Sun sensor	σ_ϕ	0.31 rad

When no sun sensor measurement is available, the corresponding measurement noise matrix $\mathbf{R}$ is

$$\mathbf{R} = \begin{bmatrix} \sigma_V^2 & 0 & 0 \\ 0 & \sigma_{\dot{\phi}}^2 & 0 \\ 0 & 0 & \sigma_\alpha^2 \end{bmatrix} \tag{A.19}$$

and when a sun sensor measurement is available, it is written as

$$\mathbf{R} = \begin{bmatrix} \sigma_V^2 & 0 & 0 & 0 \\ 0 & \sigma_{\dot{\phi}}^2 & 0 & 0 \\ 0 & 0 & \sigma_\alpha^2 & 0 \\ 0 & 0 & 0 & \sigma_\phi^2 \end{bmatrix} \tag{A.20}$$

A.2.4 Initial values

The state vector for this scenario is

$$\mathbf{x} = \begin{bmatrix} x \\ y \\ \phi \\ \dot{\phi} \\ V \\ \alpha \end{bmatrix} \tag{A.21}$$

with ϕ being the orientation of the rover and α the steering angle, as defined in Chapter 4. Then the initial state estimate is

$$\hat{\mathbf{x}}_0^- = \begin{bmatrix} 0 \\ 0 \\ 0 \\ 0 \\ V \\ 0 \end{bmatrix} \tag{A.22}$$

And accounting for $\sim$ 10cm of position error and $\sim 0.5^\circ$ of angular error, the initial covariance matrix is

$$\mathbf{P}_0^- = \begin{bmatrix} 0.1^2 & 0 & 0 & 0 & 0 & 0 \\ 0 & 0.1^2 & 0 & 0 & 0 & 0 \\ 0 & 0 & 0.010^2 & 0 & 0 & 0 \\ 0 & 0 & 0 & 0.014^2 & 0 & 0 \\ 0 & 0 & 0 & 0 & 0.1^2 & 0 \\ 0 & 0 & 0 & 0 & 0 & 0.01^2 \end{bmatrix} \tag{A.23}$$

where the first two diagonal elements are in m^2, the third and sixth in rad^2, the fourth in rad^2/s^2 and the fifth in m^2/s^2.

A.2.5 Process noise matrix

The power spectral density of the process noise is chosen to be

$$\mathbf{W} = 0.1^2 \times \mathbf{I}_{6\times 6} \tag{A.24}$$

The discrete process noise matrix $\mathbf{Q_k}$ was computed using the method summarized in section A.1.4.